Aus der Abt. Vaskuläre Biologie und Tumorangiogenese
der Medizinischen Fakultät Mannheim
European Center for Angioscience
(Direktor: Prof. Dr. Hellmut Augustin)

Accumulation of omega-6 derived trans, trans-2,4-decadienal promotes microvascular disease by disrupted insulin signaling

Inauguraldissertation
zur Erlangung des medizinischen Doktorgrades1
der
Medizinischen Fakultät Mannheim
der Ruprecht-Karls-Universität
zu
Heidelbergvorgelegt

vorgelegt von
Xin Qian

aus
(Jiangsu, China)
(2023)

Dekan: Prof. Dr. med. Sergij Goerdt

Referent(in): Prof. Dr. Jens Kroll

CONTENTS

Page

Abbreviations

T2D	Type 2 diabetes
DR	Diabetic retinopathy
VEGF	Vascular endothelial growth factor
T1D	Type 1 diabetes
ROS	Reactive oxygen species
PUFAs	Polyunsaturated fatty acids
RCS	Reactive carbonyl species
MDA	Malondialdehyde
4-HNE	4-hydroxy-trans-2-nonenal
ALDH	Aldehyde dehydrogenase
AKR	Aldo-keto reductase
GLO	Glyoxalase
MG	Methylglyoxal
AGEs	Advanced glycation end products
NAD(P)	Nicotinamide adenine dinucleotide (phosphate)
SD	Sprague Dawley
tt-DDE	Trans, trans-2,4-decadienal
B2M	β2 microglobulin
dpf	Days post fertilization
gRNA	Guide RNA
bp	Base pair
EGFP	Enhanced green fluorescence protein
PAS	Periodic Acid-Schiff
EM	Electron microscope
GBM	Glomerular basement membrane
BAL	Betaine aldehyde
ABAL	4-aminobutyraldehyde
4-HHE	4-hydroxyhexenal
PCA	Principal Component Analysis
KEGG	Kyoto Encyclopedia of Genes and Genomes

GSVA	Gene set variation analysis
PLS-DA	Partial least squares-discriminant analysis
INS	Insulin
INSRa/b	Insulin receptor a/b
IRS	Insulin receptor substrate
PDX1	Pancreatic and duodenal homeobox 1),
NOS2	Nitric oxide synthase 2
VEGFAa	Vascular endothelial growth factor Aa
HK1	Hexokinase 1
GCK/HK4	Glucokinase
PKLR	Pyruvate kinase L/R
G6PC1A.1	Glucose-6-phosphatase catalytic subunit 1a
FBP1a	Fructose-1,6-bisphosphatase 1a
PCK1	Phosphoenolpyruvate carboxykinase 1
UGP2a	UDP-glucose pyrophosphorylase 2a
GYS2	Glycogen synthase 2
GLUT2	Glucose transporter 2
MF	Metformin
RG	Rosiglitazone
CAR	Carnosine
PTU	1-phenyl-2-thiourea
RT-qPCR	Reverse-transcription quantitative polymerase chain reaction analysis
ISVs	Intersegmental vessels
PFA	Paraformaldehyde
ddH_2O	Double distilled water

1.INTRODUCTION

1.1 ALDH superfamily in diabetes

Aldehyde dehydrogenases (ALDHs) (EC 1.2.1.3) are a family of enzymes reliant on nicotinamide adenine dinucleotide (phosphate) (NAD(P)) for their catalytic activity, commonly featuring a molecular mass of approximately 50–60 kDa. These enzymes engage in the oxidation of a diverse array of aliphatic and aromatic aldehydes—both endogenous and exogenous—leading to the formation of corresponding carboxylic acids. Distinct in their subcellular localization, tissue distribution, and substrate preferences, ALDHs collectively contribute to a wide spectrum of biologically relevant activities, spanning across prokaryotes, eukaryotes, and Archaea. To date, human ALDH superfamily currently consists of 19 known putatively functional genes in 11 families and 4 subfamilies with distinct chromosomal locations [1].

ALDHs mainly play its role in detoxification, biosynthesis activities, antioxidant functions, as well as structural and regulatory mechanisms [2, 3]. Cells are equipped with protective mechanisms aimed at swiftly metabolizing and detoxifying lipid aldehydes, which are byproducts of lipid peroxidation. These defense strategies involve a range of processes, including the conversion of lipid aldehydes to acids, their reduction to alcohols, and their conjugation with vital cellular nucleophiles such as ascorbic acid, glutathione, and carnosine [4]. Vital to *in vivo* detoxification of lipid aldehydes are two primary enzymatic pathways: ALDH and AKR superfamilies [3]. The classic detoxification of aldehyde dependent on NAD(P)+/NAD(P)H by ALDH enzyme were shown in **Figure1**.

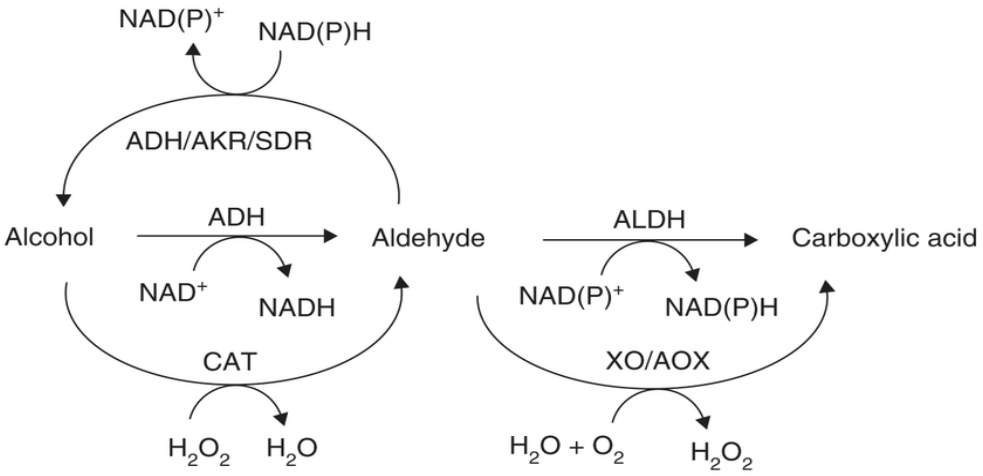

Figure1. General reaction equation of ALDH enzymes, cite[5].

ALDH9a1 is a cytosolic enzyme that catalyzes the NAD^+-dependent oxidation of a variety of aldehydes, such as betaine aldehyde (BAL) and γ-trimethylaminobutyraldehyde (TMABAL) and its highest expression was found in livers[6, 7].Besides, a comprehensive analysis conducted in the retinas of Sprague Dawley (SD) rats revealed robust mRNA expression levels ALDH9a1, implying its significant involvement in retinal physiological processes[8, 9]. One of the most extensively studied functions of ALDH9a1 is the oxidation of TMABAL to 4-N-trimethylaminobutyrate, which represents a critical step in carnitine biosynthesis [7]. Carnitine, in turn, plays a key role in the transport of long-chain fatty acids from the cytosol to the mitochondrial matrix for acyl-CoA synthesis required for β-oxidation. Due to the impermeability of the mitochondrial membrane to acyl-CoAs, fatty acids must be conjugated with carnitine to facilitate their entry into the mitochondria. Hence, ALDH9A1 indirectly contributes to β-oxidation [7].

The recent analysis of the X-ray structure of ALDH9a1 has revealed that this enzyme assembles as a tetramer [7]. Given that the functions of most ALDHs are elucidated through structural studies, this finding offers a deeper insight into the biological activities of ALDH9a1. Although current research has established associations between ALDH9a1 and certain diseases, such as single-nucleotide polymorphisms (SNPs) in renal cancer, as well as its expression in conditions like Kawasaki disease and non-alcoholic steatohepatitis without inflammation, the underlying mechanisms behind these diseases remain to be fully determined[10-12]. Many ALDHs impact physiological function by detoxifying various substrates. For instance, ALDH3a1 detoxifies 4-hydroxy-trans-2-nonenal (4-HNE) and is implicated in the progression of type 1 diabetes (T1D) [13], while ALDH2 detoxifies acetaldehyde and plays a role in disrupting glucose metabolism [14]. Similarly, ALDH9a1 has been demonstrated to possess similar detoxification capabilities toward other aldehydes, such as TMABAL [6]. In the context of zebrafish, ALDH9a1b serves as the homolog to human ALDH9a1. Our previous study showed *aldh9a1b* mRNA expression was significantly increased in *glo1*$^{-/-}$ zebrafish but the knockout of *glo1* only led to 50% increase of endogenous methylglyoxal (MG), suggesting a compensatory mechanism of *aldh9a1b* for MG detoxification [15]. Consequently, combined with its link to lipid metabolism, ALDH9a1b exhibits substantial potential for further research and therapeutic targeting. It has now become imperative to gain a comprehensive understanding of the mechanisms through which each family member contributes to proliferation disorders such as diabetes mellitus.

1.2 Reactive carbonyl species and their association with diabetes

Reactive carbonyl species (RCS) are commonly formed through the oxidation of carbohydrates, lipids, and amino acids, comprising a wide range of biological compounds characterized by one or more carbonyl groups[16]. These compounds are ubiquitously present within living organisms and are primarily recognized for their detrimental impacts [17, 18]. However, it is crucial to recognize that RCS concentrations in the body vary due to the dynamic nature of the cellular environment. Elevated levels of RCS are a primary driver of carbonyl stress, influenced by factors such as aging, diabetes, associated chronic complications, and various disorders[18]. Due to the electrophilic nature of RCS, they readily react with nucleophilic groups on macromolecules, including proteins, nucleic acids, and aminophospholipids, leading to irreversible modifications and the formation of various adducts. Unsaturated RCS are typically more reactive, and the majority of biological damage caused by RCS is associated with α, β-unsaturated aldehydes, dialdehydes, and keto-aldehydes[19]. Biomolecules' highly nucleophilic sites, such as thiol, imidazole, and hydroxyl groups, are the most susceptible targets for electrophilic attacks. Compounds like MDA, GO, MGO, 3-DG, glucosone, and ribosone, which are highly reactive α- or β-dicarbonyl compounds, exemplify this reactivity [16, 19, 20] (**Figure 2**).

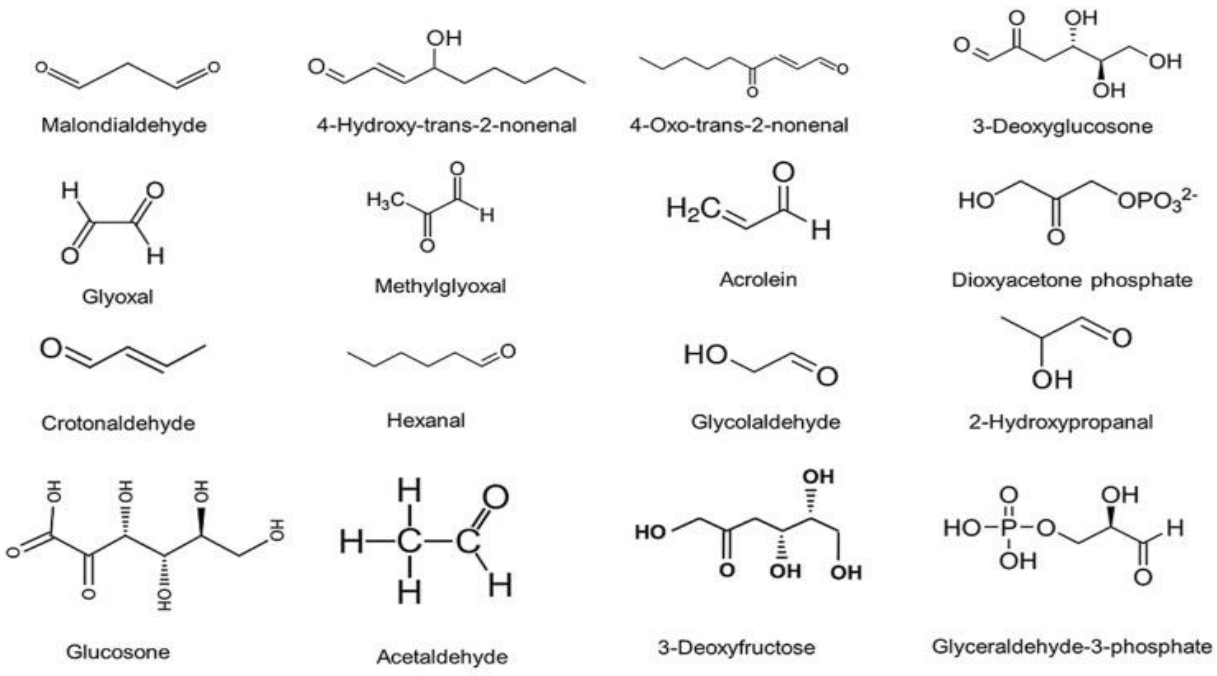

Figure 2 Common RCS in living organisms, cited [18].

The source of well-recognized biological RCS can be classified into five clusters including lipid peroxidation, nonenzymatic glycation, enzymatic polyol pathways, enzymatic glycation and amino acid oxidation [16]. Prominent among these are MDA, 4-HNE, 4-oxo-trans-2-nonenal, glyoxal, MG, acrolein, crotonaldehyde, and hexanal. Additionally, nonenzymatic glycation entails glyoxal, MG, glucosone, 3-deoxyglucosone, and acrolein. The enzymatic polyol pathway contributes to compounds like 3-deoxyglucosone and 3-deoxyfructose, while enzymatic glycation encompasses acetaldehyde, glyceraldehyde-3-phosphate, dioxyacetone phosphate, and methylglyoxal. Furthermore, the oxidation of amino acids gives rise to glyoxal, MG, acrolein, glycolaldehyde, and 2-hydroxypropanal [16, 18, 21, 22]. These diverse sources make RCS ubiquitous in the environment and commonly detected in the food and water [23]. In vitro, they can be detected in cooking fumes, automobile exhaust, flavorings and many other industrial products [24]. *In vivo*, they come from the attack of excess reactive oxygen species (ROS) on membrane-incorporated polyunsaturated fatty acids (PUFAs).

Diabetes Mellitus constitutes a cluster of metabolic disorders marked by prolonged elevated blood sugar levels. Excessive hyperglycemia stimulates an increase in an imbalance between oxidative and antioxidative statuses within cells and tissues, which leads to an increase in RCS. This metabolic irregularity arises when abnormal chemical reactions within a hyperglycemic body disrupt the customary metabolic processes, a circumstance intrinsically linked to the generation of RCS. This, in turn, amplifies the concentration of RCS, potentially leading to carbonyl-induced oxidative stress [18, 25]. For instance, hyperglycemia-induced cell damage is a consequence of increased flux through metabolic pathways [polyol pathway flux, advanced glycation-end product formation, activation of protein kinase C isoforms, and increased hexosamine pathway flux] [26]. External sources of RCS encompass products from organic pharmaceutical chemistry, tobacco smoke, food additives, and browned food [16]. These synthetic effects contribute to an increased RCS concentration, potentially inducing carbonyl-related oxidative stress and hyperglycemia can be attributed to an imbalance between cellular and tissue oxidative and antioxidative statuses [18, 27].

As described in previous section, RCS can be as substrate and detoxified by several enzyme systems, such as ALDH, AKR, and GLO [28-30]. The loss of these enzymes created a specific signature of upregulated dicarbonyls, such as MG, 4-HNE, acrolein and acetaldehyde, which were subsequently discovered to regulate glucose

homeostasis and induce microvascular complications through various pathways [13-15, 28]. MG, a precursor of advanced glycation end products (AGEs), could considerably increase insulin resistance when combined with excessive calorie consumption, while only having relatively mild effects on glucose metabolism alone [15]. 4-HNE disrupted pancreas development and caused alterations associated with T1D, while acrolein impaired insulin sensitivity and glucose homeostasis similar to T2D [13, 31]. By contrast, acetaldehyde decreased glucose production and brought on hypoglycemia by inhibiting glucose-6-phosphatase activity [14]. In conclusion, the data identified the crucial role of RCS in glucose homeostasis and a screening and understanding of RCSs and their function will be of great benefit in preventing, treating and delaying the onset of diabetes.

1.3 Diabetes mellitus and diabetes related microvascular disease

Over the past decades, the prevalence of diabetes has increased incredibly, from 108 million in 1980 to 463 million in 2019 and is projected to reach 700 million by 2045, with type 2 diabetes (T2D) accounting for approximately 95% of cases[32, 33]. The most substantial increments are expected in rapidly developing regions, which undergoes economic shifts from low-income to middle-income status [34]. The rising prevalence and surge in diabetes cases have imposed significant societal and financial challenges on nearly every healthcare system worldwide and contributed markedly to the global burden of mortality and disability. For instance, the Global Burden of Disease Study 2013 recognized diabetes mellitus (all forms included) as the leading contributor to reduced life expectancy [33, 35]. In 2010, diabetes mellitus was estimated to be responsible for 3.96 million deaths among 20–79 years-old-adults, accounting for 6.8% of global mortality [36]. This estimation was subsequently revised to 5.0 million deaths by the International Diabetes Federation report and indicated one death every six seconds [33, 37].

Diabetes mellitus was classically divided into two primary types. T1D is characterized by dysfunction of beta cells in pancreas, resulting in insufficient insulin production and secretion. On the other hand, T2D typically manifests later in life and is believed to be influenced by both genetic and environmental factors. Since T2D has a high heterogeneity, a recent study reported a novel classification to stratify diabetes into five groups based on six variables (glutamate decarboxylase antibodies, age at diagnosis, BMI, HbA1c, and homoeostatic model assessment 2 estimates of β-cell function and insulin resistance) [38]. Recent research has identified the substantial heterogeneity

within the T2D population and introduced a novel classification system. This system stratifies diabetes into five distinct clusters based on six key variables: glutamate decarboxylase antibodies, age at diagnosis, body mass index (BMI), HbA1c levels, and estimates of β-cell function and insulin resistance using the homeostatic model assessment 2 (HOMA2) [38]. Cluster 1, termed 'severe autoimmune diabetes,' carries the highest risk of ketoacidosis. Cluster 2, referred to as 'severe insulin-deficient diabetes,' exhibits the most frequent symptoms of diabetic retinopathy. Cluster 3, labeled 'severe insulin-resistant diabetes,' is associated with a higher risk of diabetic kidney disease. Clusters 4 and 5 are categorized as 'mild obesity-related diabetes' and 'mild age-related diabetes,' respectively[38]. This new classification system has proven instrumental in revealing distinct risk profiles for diabetic complications and disease progression among different T2D patient clusters. It offers a powerful tool for tailoring treatment regimens to individual patients and for identifying individuals with an elevated risk of complications at the time of diagnosis.

Diabetes related complications, especially vascular complications, are the leading causes of disability and death in diabetic patients. The prevalence of disability attributed to diabetes mellitus has shown marked escalation since 1990, particularly among the demographic of individuals aged 15 to 69 years [39].Diabetic vascular complications have been categorized into macrovascular complications (such as, heart attack) and microvascular complications (including kidney, retinal, and nervous system complications). Notably, microvascular complications have a high prevalence in T2D patients with 38% chronic kidney disease, nearly 30% retinopathy (DR), and >30% peripheral neuropathy [40-43].

DR constitutes roughly 1% of the overall diabetes-affected population[44]. In the early stages of DR, various processes come into play, including an increase in pericyte loss, apoptosis of endothelial cells, permeability of retinal capillary endothelial cells and accumulation of advanced glycation end products[45, 46]. As the disease progresses, the occlusion of retinal capillaries and arterioles leads to retinal ischemia, triggering an increase in the intraocular production of vascular endothelial growth factor (VEGF). Consequently, there is a subsequent release of blood from delicate neo-proliferative blood vessels. As a result of this, there is a loss of retinal astrocytes and photoreceptors due to microglial fibrosis, ultimately leading to the impairment of vision[45, 46]. While anti-VEGF therapy is the most common therapeutic approach, it may not be effective for all

DR patients, thus prompting ongoing investigations into alternative drugs, some of which are currently in clinical trials [47].

Diabetic nephropathy main pathogenesis of the end-stage renal disease. The diverse array of cell populations within the kidney and the various physiological roles of this vital organ make diabetic nephropathy extremely complex [48]. The popular hypothesis for diabetic nephropathy was 'hyperfiltration'. Elevated glucose levels induce specific cellular responses that affect numerous resident kidney cells, including endothelial cells, smooth muscle cells, mesangial cells, podocytes, cells of the tubular and collecting duct system, as well as inflammatory cells and myofibroblasts[48]. Hemodynamic changes, which manifest as alterations in blood pressure both systemically and within the kidney, are reported to occur early in diabetes, resulting in glomerular hyperfiltration and disrupts glomerular filtration barrier[48]. The most widely employed interventions target the renin-angiotensin-aldosterone system (RAAS), which includes the use of angiotensin-converting enzyme (ACE) inhibitors. Additionally, addressing oxidative stress through reactive oxygen and carbonyl species, as well as managing inflammatory processes, may offer new promising opportunities[49].

Diabetic neuropathy is a syndrome that affects both the somatic and autonomic divisions of the peripheral nervous system. The traditional clinical characterization of disease progression in neuropathy has often focused on the development of vascular abnormalities. These abnormalities include capillary basement membrane thickening and endothelial hyperplasia, which lead to a subsequent decrease in oxygen tension and the occurrence of hypoxia. In clinical practice, the use of inhibitors of the renin-angiotensin system and α1-antagonists has shown improvements in nerve conduction velocities. This improvement is postulated to be a result of increased blood flow to the neurons[48].

While the precise mechanisms of hyperglycemia-induced vascular damage are both complex and not fully understood, it is thought that high levels of intracellular glucose increase the production of reactive oxygen species altering a series of critical downstream pathways, including polyol pathway flux, advanced glycation end product formation and activation, protein kinase C activation, and hexosamine pathway flux[50, 51].However, in contrast to T1D, the underlying factors contributing to T2D form a complex network involving genetic, epigenetic, and lifestyle elements. These components interplay within the broader physical and sociocultural context, underscoring the significant role of environmental factors in the onset of diabetes [33].

To date, the well acknowledged risk factors remain limited, commonly obesity and physical inactivity. Therefore, more efforts should be made to find out the hidden threats in our normal life.

1.4 Omega fatty acids and their roles in diabetes

Dietary lipids constitute essential constituents of all living cells, playing a significant role in preserving the structural integrity of bilipid cell membranes, serving as sources of energy, and serving as precursors for numerous biologically active compounds that influence a wide range of cellular and immune responses [52]. In contrast to animals, which lack Δ-15 or Δ-12 desaturase enzymes, humans are unable to biosynthesize n-3 or n-6 fatty acids [53].

Omega-3 (n-3) PUFAs are characterized by a double bond at the n-3 position. The three most critical ω-3 fatty acids are Alpha-linolenic acid (ALA), Eicosapentaenoic acid (EPA), and Docosahexaenoic Acid (DHA). EPA and DHA, often referred to as marine ω-3 fatty acids, are plentiful in fish, fish oil, and some types of algae, while ALA, categorized as a vegetable ω-3 fatty acid and the parent fatty acid of the ω-3 family, is primarily sourced from walnuts, flaxseed, and rapeseed oils [54]. Diverging from ALA, EPA and DHA are considered as conditional essential fatty acids because they can be synthesized from ALA through desaturation, elongation, and oxidation processes [53, 55, 56]. EPA and DHA are associated with numerous health benefits and play a vital role in modulating membrane viscosity and anti-inflammatory properties [54]. Both EPA and DHA are indispensable for fetal development, contributing to enhanced brain and visual development in developing fetuses, as well as a reduced risk of cardiovascular disease, obesity, metabolic syndrome, diabetes, arthritis, and cognitive decline [54]. In the context of diabetes, they sensitize insulin receptors, reduce hepatic fat storage through increased synthesis and release of adipocytokines, and exert anti-inflammatory effects [54, 57, 58]. However, the benefits of ALA remain equivocal [59-61]. A meta-analysis of Omega-3 polyunsaturated fatty acid biomarkers and disease outcomes found no reduction in cardiovascular events associated with ALA levels [60]. Another extensive systematic review indicated limited or no effect on HbA1c and fasting glucose levels, while it might increase fasting insulin levels, suggesting impaired insulin sensitivity [61].

Omega-6 fatty acids have a double bond at the n-6 position and mainly comprise linoleic acid (LA) and Arachidonic acid (AA). Similar to ALA, AA can be synthesized

from LA, designating LA as an essential fatty acid[62]. Sources of LA primarily come from vegetable oils, with smaller amounts found in animal fats, eggs, cereals, and whole-grain bread. Linoleic acid (LA; 18:2 n-6) represents the principal PUFAs in most Western diets [63]. Dietary guidelines for cardiovascular health advocate for the replacement of saturated fatty acids with foods rich in linoleic acid[64-67]. Nevertheless, changing dietary patterns have coincided with a remarkable increase in obesity and type 2 diabetes [63]. While no conclusive evidence supports a direct association between linoleic acid and type 2 diabetes, it is worth noting that ω-6 PUFA-rich vegetable oils, such as soybean and canola oils, are widely utilized in households and restaurants worldwide. The precise relationship between these oils and diabetes remains unclear, warranting further research to contribute to the treatment, prevention, and delay of the onset of type 2 diabetes mellitus.

1.5 Trans, trans-2,4-decadienal in vascular disease

Trans, trans-2,4-decadienal (tt-DDE), a mid-chain, moderately polar unsaturated aldehyde, primarily arises from the oxidation of omega-6 fatty acids, specifically linoleic acid and arachidonic acid [68, 69]. In the context of linoleic acid, tt-DDE is formed through the breakdown of 9-hydroperoxide, while in the arachidonic acid system, it is synthesized from 1-hydroperoxyicosatetraenoic acid [70, 71]. During the deep-frying of omega-6 fatty acids, lipid peroxidation products known as RCS is generated [72]. Among these RCS compounds, tt-DDE is the most abundant and was suggested to be detoxified by ALDH enzyme into 2,4-decadienoic acid, while the exact ALDH enzyme was still not charaterized[73, 74]. tt-DDE was suggested to be detectable in substantial quantities in heated edible oils and emissions from cooking environments, indicating widespread human exposure [68, 75-77]. Besides, this aldehyde also serves as a food additive [73]. Moreover, it is readily absorbed upon ingestion, disseminating across various organs and tissues [78].

Emerging evidence highlights the potential adverse impacts of tt-DDE on human health, particularly in the realm of cardiovascular disease [79-82]. Notably, tt-DDE has been linked to the promotion of hypertension, atherosclerosis, and arrhythmogenesis, acting through the modulation of autophagy, inflammation, and apoptosis. Comparative evaluations involving diverse unsaturated aldehydes, including acrolein, crotonaldehyde, trans-2-pentenal, trans, trans-2,4-heptadienal, tt-DDE, and 4-HNE, have identified tt-DDE as the most detrimental to human umbilical vein endothelial cell viability [80]. Furthermore, observations from SD rats exposed to tt-DDE-rich diets have

indicated elevated fasting blood glucose levels, suggesting a potential role of tt-DDE in diabetes pathogenesis [81]. However, the mechanisms underlying tt-DDE detoxification and the implications of impaired detoxification, particularly in metabolic conditions like diabetes and hyperlipidemia-driven atherosclerosis, remain elusive.

1.6 Aim of the thesis

Acknowledging the potential importance of ALDH9a1b and tt-DDE in diabetes research, our study focused on examining the pathological and metabolic impacts of *aldh9a1b* gene deletion in zebrafish. To explore these aspects, we developed an *aldh9a1b* knockout zebrafish line. With the availability of transgenic lines of zebrafish, our research focus on consequences of *aldh9a1b* loss on vascular development, renal function, and metabolic processes. The investigation aimed to address several key questions:

1. Does the loss of ALDH9a1b result in vascular alterations in zebrafish during their developmental phase? Are there any changes in trunk versus retinal vasculature?
2. What is the impact of Aldh9a1b loss on zebrafish kidney functionality during adulthood?
3. What is the interplay between ALDH9a1b and tt-DDE? How is tt-DDE metabolized in zebrafish, and could it potentially be a triggering substrate for phenotypes associated with ALDH9a1b deficiency?
4. What mechanisms underlie vascular modifications? In what ways are ALDH9a1b and tt-DDE implicated in glucose metabolism?
5. Are there effective treatments available to rescue the detrimental effects caused by the loss of ALDH9a1b or exposure to tt-DDE?

2. Materials and Methods

2.1 Materials

2.1.1 Equipment

Product	Company
Quantstudio 3 qPCR system	Applied Biosystems
Quantstudio 5 qPCR system	Applied Biosystems
Agarose gel chamber	Peqlab Biotechnologie GmbH
Electronic Balance	Kern
Hamilton syringe (Glastight® #1705)	Hamilton
PCR cycler	BioRad
Western Blot system	BioRad
Leica DM6000 B confocal Microscope	Leica
Bench top centrifuge (Rotina 420R)	Hettich
Electrophoresis power supply	Consort
Heating/Shaking block	HLC
pH-meter ProfiLine 197i	WTW ProfiLine
Chemi – Smart 5000	PeqLab
Dry cabinet Memmert UNB 300	Memmert
UV Transilluminator	INTAS
Glucometer Freedom Lite	Abbott
Vertical Micropipette Puller P30	Sutter Instruments
Pipettes	Eppendorf
Jun-Air 3-4 Quiet Running Compressor	Jun-Air
Table centrifuge	Carl Roth GmbH
Dry bath incubator	Major Science
See-saw rocker	Stuart
Water Bath	Seelbach
Leica RM2235 microtome	Leica
T100TM Thermal Cycler	BioRad

2.1.2 Chemicals

All the chemicals used in this project were purchased from following companies if not indicated specifically.

Sigma Aldrich Chemie GmbH

Cell Signaling Technology Europe B.V.

AppliChem GmbH

Diagnostics GmbH

Carl Roth GmbH

Thermo Fisher Scientific Inc.

Merck AG Roche

2.1.3 Consumables

Product	**Company**
Whatman filter paper	Sigma Aldrich
PCR tubes (0.2 ml)	Star Labs
Safe-Lock tubes (0.5, 1.5 and 2.0 ml)	Eppendorf
Pipette tips (1000, 200, 10 µl)	TipOne Star Labs
Pipette filter tips (1000, 100, 20 and 10 µl)	Nerbe plus GmbH
Conical tubes (15 ml, 50 ml)	Falcon
Needle 20G – 30G x1 ½”	BD Microlance
Syringes (1 mL)	BD Plastipak
6-, 24- and 96- well plates	Greiner
Petri disches (5 cm, 10 cm; quadratic)	Greiner
Quantitative PCR 96-well reaction plates	Life Technologies
Quantitative PCR 384-well reaction plates	Life Technologies
Nitrocellulose membrane 0.22 µm	Whatman
Dumont Tweezers	NeoLabs
Adhesive Optical Film	Biozym

pH-Fix 0-14	Macherey-Nagel
Pasteur Pipettes	Hirschmann
Nitrile Gloves	BioWorld
Cover slips (22x22 mm)	Menzel Gläser
Disposable scalpel	NeoLabs
Blood glucose test-stripes (Lite)	FreeStyle Lite
Stainless steel beeds (5 mm)	Qiagen
pH-Fix 0-14	Macherey-Nagel
Superfrost ultra plus® microscope slides	Thermo Scientific

2.1.4 Buffers and Solutions

Solution	**Components**
Tricaine	400 mg Tricaine powder
	~2.1 mL 1 M Tris (pH 9)
	97.9 mL MilliQ water
	Ad to pH ~7 and 100 mL MilliQ water
5x PTU	304 g PTU
	ad 1L MilliQ water
10x ERM	20 g NaCl
	0.6 g KCl
	0.54 g CaCl2*6H2O
	3.2 g MgSO4*7H2O
	0.01 g Methylene blue
	Ad 1 L MilliQ water
50x TAE	242 g TrisBase
	57.1 mL conc. acetic acid
	100 mL 0.5 M EDTA pH 8.6
	ad 1 L MilliQ water
10x PBS	400 g NaCL
	72,09 g Na2HPO4 * H2O
	10 g KCl
	10 g KH2PO4
	ad 5 L MilliQ water

5x Laemmli	5 g SDS
	0.25 g bromophenol blue
	8.34 mL Tris/HCl, pH 6.8
	25 mL glycerol
	3.45 g DTT
	ad 50 mL MilliQ water
4% PFA	4 g PFA
	10 mL 10x PBS
	80 mL MilliQ water
	ad 100 mL MilliQ water
Lysis buffer	60 µL Glycerol
	40 µL 0.5 M EDTA
	133 µL of 1.5 M Tris/HCl, pH8
	60 µL Tween
	ad 20 mL MilliQ water
1%-Periodic Acid Solution	1 g Periodic acid
	ad 100 mL MilliQ water
Sulfurous water	30 mL 1 M HCl
	600 mL MilliQ water
	36 mL 10% Sodium metasulphite (Na2S2O5)
10x blotting buffer	30.28 g Tris
	106.6 g Glycine
	ad 1 L MilliQ water
NP40 lysis buffer	5 mL 1M Tris/HCl, pH 7.4
	1 bottle Proteinase inhibitor cocktail
	0.87 g NaCl
	1.8 mL 0.5 M Na2EDTA, pH 8
	10 mL Glycerol
	10 mL 10% Nonidet P40 solution
	ad 100 ml MilliQ water
DPX mounting medium	Thermo Fisher Scientific
Mayer’s hemalum solution	Millipore
Horseradish Peroxides substrate	SupersignalTM Thermo Scientific

2.1.5 Oligonucleotides

Oligonucleotides were purchased from Sigma Aldrich.

CRISPR-construct name	**Primer sequence (5‘ to 3‘)**
Aldh9a1b-CRISPR-for	GGGCCTGTTCAATGTGGTTC
Aldh9a1b-CRISPR-rev	GAACCACATTGAACAGGCCC
Aldh3b1-CRISPR-for	GGAGGGCCAGAAGCAGG
Aldh3b1-CRISPR-rev	CCTGCTTCTGGCCCTCC

Genotyping primer name	**Primer sequence (5‘ to 3‘)**
9a1b_genotyping_forward	CCTGCCATCGCTTGTGGTAT
9a1b_genotyping_reverse	TCTTTCCTGTGGGCACACTTC

qPCR primer name	**Primer sequence (5‘ to 3‘)**
9a1b_qpcr_forward	CTATGGTGTTCAAGCCGTCTC
9a1b_qpcr_reverse	C ACCGAAGGGTGAAGACAGAG
b2m_qpcr_forward	GCAACGCTCTTTGTGAGGTG
b2m_qpcr_reverse	AACCACTGAACACGGACCTC
ins_qpcr_forward	GCCCAACAGGCTTCTTCTACAAC
ins_qpcr_reverse	GCAGATTTAGGAGGAAGGAAACCC
insra_qpcr_forward	AGAGGCCAGCGAGCTCTAC
insra_qpcr_reverse	CACTTGTGTGGGGGCTCT
insrb_qpcr_forward	GCCTCTGCGGATCACTACAT
insrb_qpcr_reverse	CTCCTGCGTGGTCTTGAAC
irs1_qpcr_forward	ACTACTCTTTGCCCCGCTCA
irs1_qpcr_reverse	TCGTCCGTTGGTTACTGTCG
hk1_qpcr_forward	ATGATAGCGGCACAGCTTCT
hk1_qpcr_reverse	GTTGGTGTCTCGTGCCAATC
gck_qpcr_forward	AATCACCGCTGACCTGCTAT
gck_qpcr_reverse	GCCACTTCACATACGCAATG
pklr_qpcr_forward	CAAAGGACACTTCCCTGTAGAG
pklr_qpcr_reverse	GGACAACGAGGACGATAACG
g6pc1a.1_qpcr_forward	GCTGCACCATACGAGATGGA
g6pc1a.1_qpcr_reverse	TCACCAAACAGCACCCACTT

fbp1a_qpcr_forward	CATCTGTATGGGATTGCTGG
fbp1a_qpcr_reverse	TTACCCCGTCTATCTGGCTC
pck1_qpcr_forward	GTGAACTGAACCGAGACCTG
pck1_qpcr_reverse	AGCACTTGAGAGCAAACGAT
ugp2a_qpcr_forward	CTGACGGGAGAGAATGAGGA
ugp2a_qpcr_reverse	GTCTTGGGGTTGACAATGAT
gys2 _qpcr_forward	AAATCTTCCCCTGGCGACTA
gys2 _qpcr_reverse	AAAGTTGTTGGTTTTGGCGG
glut2_qpcr_forward	GCAGAAGAACCCTCACTC
glut2_qpcr_reverse	TCTCCGCCACAATAAACC
pdx1_qpcr_forward	ACACGCACGCATGGAAAGGACA
pdx1_qpcr_reverse	GCGGGCGCGAGATGTATTTGTT
NOS2a_qpcr_forward	TGCCGTCATTCACAGCTATC
NOS2a_qpcr_reverse	ACCAGCCAGACCCAATCC
NOS2b_qpcr_forward	AACGGCATCATGAACTGTTG
NOS2b_qpcr_reverse	TACATTGTAGTCCTCCATGCAAA

2.1.6 Kits and Reagents

Product	**Company**
Fluoromount-G™	eBioscience/Invitrogen/Thermo Fishe
RNeasy Mini Kit	Qiagen
TetraMin fish flake food	Tetra
Great Salt Lake artemia cysts	Sanders
Paraplast Plus® (=Paraffin)	Sigma
MAK263-1KT Glucose Assay Kit	Sigma Aldrich
PowerSybr Green PCR Master Mix	Thermo Fischer Scientific
Pierce™ BCA Protein Assay Kit	Thermo Fischer Scientific
Maxima First strand cDNA Kit	Thermo Fischer Scientific
MEGAshortscriptTM T7	invitrogen by Thermo Fisher Scientific
Gene Ruler DNA ladder mix	Thermo Fisher Scientific
mMESSAGE mMachineTM T7	invitrogen by Thermo Fisher Scientific
Tissue-Clear®	Tissue-Tek®, Sakura Finetek
Quick-hardening mounting medium	Sigma-Aldrich

DAB Peroxidase (HRP) Substrate Kit (with Nickel)	vector laboratories
QIAquick PCR Purification Kit	QIAGEN

2.1.7 Antibodies

Products	Company
Anti-β-actin antibody	Santa Cruz Biotechnology, sc-47778
Anti-AKT antibody	CST, 9272S
Anti-P-AKT antibody	CST, 4060P
Anti-mouse IgG, HRP-linked Antibody	DAKO, P0260
Anti-rabbit IgG, HRP-linked Antibody	Dako, P0448

2.1.8 Zebrafish transgenic lines

transgenic zebrafish line Tg(fli1:EGFP) was used for all the zebrafish (Danio rerio) experiments.

2.2 Methods

2.2.1 Study approval

Experimental procedures on animals were conducted in compliance with approved guidelines and received ethical approval from the local government authority Regierungsprasidium - Karlsruhe and the Medical Faculty Mannheim, with license numbers G-98/15 and I-19/02, respectively.

2.2.2 Zebrafish husbandry

The zebrafish line *Tg(fli1: EGFP)* was utilized and raised under standard husbandry conditions [83]. Embryos and larvae up to 5dpf were maintained in egg water at a temperature of 28.5°C, with or without 0.003% 1-phenyl-2-thiourea (PTU) (Sigma) to inhibit pigmentation. Larvae older than 5 dpf and adult fish were subjected to a 13-hour light/11-hour dark cycle and fed twice daily with freshly hatched Artemia Salina in the morning and fish flake food in the afternoon.

2.2.3 Mutant Generation

The *aldh9a1b* knockout CRISPR zebrafish line was generated as previously described [13]. Specifically, gRNA targeting *aldh9a1b* exon 6 was designed using ZiFiT Targeter

4.2 and cloned into a T7-driven promoter expression vector (pT7-gRNA; Addgene). The pT3TSnCas9n vector (Addgene) was used for in vitro transcription and synthesis of Cas9 mRNA after linearization with xbal (Biolab) [84]. The gRNA and Cas9 mRNA were obtained using the T7 mMessage mMachine Kit (Invitrogen) and T3 MEGAshortscript Kit (Invitrogen), respectively, following the manufacturer's protocols. At the one-cell stage, a mixture containing 200 pg/nL of gRNA and 200 pg/nL of Cas9 mRNA in 0.1 M KCl solution was injected into the embryo. The generated F0 fish were screened for germline transmission and crossed with *Tg(fli1: EGFP)* fish. Genotyping was performed using Sanger sequencing and gel electrophoretic separation of PCR products. The genome and amino acid sequence analyses were conducted using benchling (benchling.com) [85].

2.2.4 Reverse-transcription quantitative polymerase chain reaction analysis (RT-qPCR)

For each sample, 20 larvae at 5 dpf or one organ from an adult fish were collected. Total RNA was extracted using the RNeasy Mini Kit (Qiagen) according to the manufacturer's instructions. Subsequently, 1 µg of RNA was used for cDNA synthesis with the Maxima First Strand cDNA Synthesis Kit (Thermo Fisher Scientific). Primers were designed using NCBI primer blast. RT-qPCR was performed using the Power SYBR™ Green PCR Master Mix Kit (Thermo Fisher Scientific) in 96 or 384 reaction plates and analyzed using the QuantStudio™ 3 or QuantStudio™ 5 Real-Time PCR System (Thermo Fisher Scientific).

2.2.5 Microscopy and Analysis of Vascular Alterations in Larvae and Adults

To visualize zebrafish trunk vasculature in vivo, *aldh9a1b* larvae were incubated with PTU from day 1. At 4 dpf, larvae were anesthetized using 0.0003% tricaine and placed in individual wells of a 96-well plate. Confocal microscopy images were acquired using a Leica TCS SP5 DS scanner attached to a confocal microscope (DM6000 B). The imaging settings included a resolution of 1024 × 1024 pixels, 0.8 µm z-steps, and a 20x water immersion objective. A total of 10 pairs of trunk vasculature were examined in this study, specifically focusing on the first five intersegmental vessels (ISVs). Within the observed vasculature, newly formed small vessels were identified as "hyperbranches." Conversely, vessels displaying aberrant characteristics such as

incorrect direction, lack of connection, excessively thin or thick morphology were classified as abnormal ISVs.

For imaging of zebrafish hyaloid vasculature in vivo, *aldh9a1b* larvae were anesthetized with 0.003% tricaine and then fixed in 4% paraformaldehyde (PFA) overnight at 5 dpf. Fixed larvae were washed three times with double distilled water (ddH2O) for 10 minutes each. Subsequently, the larvae were incubated in a solution of 0.3% Trypsin/EDTA buffered with TRIS HCl (1.5 M, pH 7.8) for 90 minutes at 37°C. After the incubation, the larvae were washed three times and dissected to obtain the hyaloid. The hyaloid was then placed in ddH2O for visualization. Confocal microscopy images were acquired using the same confocal microscope setup described earlier, with a resolution of 1024 × 1024 pixels, 0.6 µm z-steps, and a 20x/3 objective.

For imaging of zebrafish retina vasculature in vivo, a similar method as described in a previous study was used[86]. Heads from adult zebrafish were fixed in PFA and placed on an agarose platform covered with cold 1x PBS. The retina was carefully detached from the eyes and washed three times. The detached retina was then transferred to a slide and immersed in mounting media before being covered with a cover slide. The confocal microscope with the same specifications mentioned earlier was used for imaging. The settings for imaging the retina vasculature included a resolution of 1024 × 1024 pixels, 1.5 µm z-steps, and a 20x/1 objective. GIMP and ImageJ software were utilized for quantifying the sprouts and branches within squares measuring 350 × 350 µm².

2.2.6 Analysis of Kidney Morphology

In the context of the PAS staining technique, the kidneys of adult zebrafish were first detached and subsequently fixed in 4% PFA. The fixed kidneys were then embedded in paraffin and sectioned into 4 µm thick slices using a Leica RM2235 microtome. These sections were placed onto slides and subjected to a deparaffinization process. Subsequently, the sections were immersed in a 1% periodic acid solution for a duration of 10 minutes. Following this, the sections underwent three washes with ddH2O and were then treated with Schiff's reagent for a period of 20 minutes. To remove excess reagent, the sections were rinsed three times with SO2 water for 2 minutes each. The sections were further washed using running tap water and subsequently stained with hematoxylin solution. Following staining, the sections were dehydrated using a series of ethanol solutions and mounted using a suitable mounting medium. Brightfield

imaging was performed using a Zeiss Axio Scan.Z1 scanner. The evaluation of glomerular structure was carried out according to a previously described methodology [87].

For the electron microscopic assessment of the GBM, imaging and analysis were conducted in collaboration with the Institute of Pathology IPH at Heidelberg University Hospital. Briefly, the kidneys of adult zebrafish were detached and fixed in a 3% glutaraldehyde solution in cacodylate buffer (0.1 M, pH 7.4). The kidneys were then sectioned into 1 mm^3 pieces, washed in buffer, and subsequently post-fixed in a 1% aqueous osmium tetroxide solution for a duration of 1 hour. Following a water rinse, the specimens were dehydrated using a series of ethanol solutions, transferred into propylene oxide, and embedded in epoxy resin (glycidether 100). Semithin sections with a thickness of 1 µm and ultrathin sections ranging from 60 to 80 nm were obtained using an ultramicrotome (Reichert Ultracut E). The semithin sections were stained with methylene blue and examined under a light microscope (Olympus). The ultrathin sections were stained with uranyl acetate and lead citrate, and imaging was performed using a transmission electron microscope (JEM 1400) equipped with a 2k TVIPS CCD camera (TemCam F216) at magnifications ranging from ×3,000 to ×10,000.

2.2.7 Enzyme Activity Assay

At 5 dpf, a total of 120 larvae were subjected to anesthesia using 0.003% tricaine, after which they were immediately frozen in liquid nitrogen for subsequent analysis. The measurement of total ALDH activity was performed at 25 °C. The assay was conducted in a buffer solution consisting of 75 mM Tris-HCl (pH 9.5), supplemented with 10 mM DL-2-amino-1propanol, 0.5 mM NAD, and 5mM AA 10mM ABAL, 10mM BAL, 2mM MG, 10mM MDA, 4mM 4HNE, 10mM (2E)-2-Hexadecenal and 10mM tt-DDE. The ALDH activity was from Michalis-mention kinetics, as previously described [88].

2.2.8 Pharmacological Treatment of Zebrafish Embryos/Larvae

Fertilized eggs were carefully transferred into individual wells of a 6-well plate, with each well containing 30 eggs and 5 mL of egg water. At 24 hours post-fertilization (hpf), the chorion surrounding the embryos was delicately removed using tweezers. Subsequently, the embryos were immersed in various substrates and rescue medicines for further treatment. Specifically, a range of concentrations was prepared for each of the following substances: tt-DDE (W313505, Sigma-Aldrich) at concentrations ranging from 0 to 20 µmol, ABAL (A44150, Sigma-Aldrich) at

concentrations ranging from 0 to 200 µmol, BAL (B3650, Sigma-Aldrich) at concentrations ranging from 0 to 400 µmol, and L-Carnosine (C9625; Sigma-Aldrich) at a fixed concentration of 10 mmol, all dissolved in egg water. The culture medium containing the treatments was refreshed on a daily basis to maintain the appropriate conditions for the embryos.

2.2.9 RNA-seq Analysis

Total RNA was extracted from larvae treated with 8 µmol tt-DDE at 5 dpf derived from *aldh9a1b*$^{+/+}$, *aldh9a1b*$^{-/-}$, and *aldh9a1b*$^{+/+}$ groups. The isolation of RNA was carried out using established protocols. Subsequently, library construction and sequencing were performed using the BGISEQ-500 platform, which is available through the Beijing Genomic Institution (BGI, www.bgi.com). Gene expression analysis was conducted by the Core-Lab for microarray analysis at the Center for Medical Research (ZMF). Sequencing data analysis was conducted following previously described methods [13]. The RNA-Seq datasets generated as part of this study have been deposited in the Gene Expression Omnibus (GEO, NIH) database under the accession number: (https://www.ncbi.nlm.nih.gov/geo/query/acc.cgi?acc=GSE223340).

2.2.10 Western Blot Analysis

For western blot analysis, a total of 20 larvae or one adult organ sample were utilized. To inhibit phosphatases, the samples were incubated for 10 minutes on ice with 2 mM Natrium-Vanadate in 1× PBS. Subsequently, the fish samples were homogenized and lysed using NP40 lysis buffer containing 150 mmol L−1 NaCl, 50 mmol L−1 Tris-HCl (pH 7.4), 1% NP40, 10 mmol L−1 EDTA, 10% glycerol, and protease inhibitors. The lysate was kept on ice for 30 minutes with intermittent shaking. The lysate was then diluted with 5x Laemmli buffer and boiled at 95 °C for 5 minutes. SDS-PAGE was employed for electrophoresis, while a 0.2 µM supported nitrocellulose membrane (Amersham) was used for the transblotting process. The membranes were blocked using a 5% BSA solution and subsequently incubated with primary antibodies at a dilution of 1:1000. The primary antibodies used were anti-Actin (Santa Cruz Biotechnology, sc-47778), AKT (CST, 9272S), and P-AKT (CST, 4060P). Following primary antibody incubation, the membranes were incubated with secondary HRP-conjugated antibodies at a dilution of 1:1000. Specifically, for β-actin, a rabbit anti-mouse antibody (DAKO, P0260) was used, while for P-AKT and AKT, a goat anti-rabbit antibody (Dako, P0448) was utilized. Visualization of the protein bands was achieved

using enhanced chemiluminescence (ECL) with the Western Lightning Plus ECL reagent (PerkinElmer) on a Vilber Fusion Solo S imaging system.

2.2.11 Blood Glucose Measurement

For whole-Body Glucose Determination in Zebrafish Larvae, a total of 20 zebrafish larvae at 5dpf were collected and considered as one sample. The larvae were immediately snap-frozen in liquid nitrogen to preserve their metabolic state. To prepare the samples for analysis, the larvae were homogenized using a 20 G syringe in an assay buffer. A glucose assay kit (MAK263, Sigma-Aldrich) was employed to measure the glucose levels following the manufacturer's instructions. The fluorometric intensity, which corresponds to the glucose concentration, was detected using a plate reader (Tecan Infinite M200).

For fasting glucose measurement, adult zebrafish were individually transferred to separate containers and fasted overnight. After the fasting period, the fish were euthanized by submerging them in ice water for 2 minutes. Blood samples were collected from the caudal vessels, and the glucose levels were measured using a glucometer (Freestyle Abbott) [25].

For the 2-hour postprandial glucose measurement, the fish were fed with 0.5 g of flake food and the water was changed after 1 hour to simulate a post-meal state. Following the 2-hour post-feeding period, blood samples were extracted and the glucose levels were measured using the same method described above.

2.2.12 Metabolomic Analysis

A total of 100 zebrafish larvae and one organ per fish were collected as a sample for metabolomics analysis. The analysis was conducted in collaboration with the Metabolomics Core Technology Platform (MCTP) of the Center for Organismal Studies (COS) at Heidelberg University. Gas chromatography-mass spectrometry (GC/MS) was employed for the detection of metabolites [89, 90].

The generated GC/MS data underwent preprocessing using ChromaTof v5.50 software (LECO Corporation, Michigan). This involved converting the signal peak area to signal intensity per sample amount. Ribitol was used for data adjustment, and fatty acids were normalized to C17:0. To assess the quality of the data, partial least squares-discriminant analysis (PLS-DA) and correlation maps were generated using R software.

Differential metabolites were identified through fold change analysis with a threshold of 1.5. For further analysis related to functional interpretation or pathway analysis, the Kyoto Encyclopedia of Genes and Genomes (KEGG) database was utilized. The advanced analysis was performed using MetaboAnalyst 5.0, following the suggested protocol [91].

2.2.13 Molecular Docking Analysis

To analyze the binding affinities and modes of interaction between tt-DDE and insulin receptor, Autodock Vina v.1.1.2, a computational tool, was used for protein-ligand docking [92, 93]. The molecular structure of tt-DDE and linsitinib was obtained from the PubChem Compound database (https://pubchem.ncbi.nlm.nih.gov/). 3D coordinates of the insulin receptor (with PDB ID, 1irk and resolution, 2.1 Å) were sourced from the Protein Data Bank (http://www.rcsb.org/pdb/home/home.do).

2.2.14 TT-DDE determination

Zebrafish larvae (40 pooled larvae/sample; around 15 mg), liver and muscle samples were extracted for target quantification the following way: 20 x the volume of ice-cold Methanol/H2O (80/20; v/v) containing 0.1 % formic acid and 10 µM of 4-hydroxy Nonenal-d3 as internal standard were added to pregrounded samples. Samples were shortly vortexed, sonicated for 30 sec on ice (2-5 x) and incubated on ice for 10 min. After centrifugation at 14 000 rpm for 10 min at 4°C, the supernatant was transferred to a new tube. The methanol part was evaporated with N2-gas, the remaining water part was shock-frozen in liquid nitrogen and freeze-dried to complete dryness. Dried samples were reconstituted in 30 µl of H2O containing 0.1 % formic acid, centrifuged as above, transferred to MS-vials and ready to be analyzed.

For target identification and relative quantification, 15 µl per sample were injected into an Infinity II Bio liquid chromatography system coupled to a 6495C triple quadrupole mass spectrometer (Agilent Technologies). Metabolites were separated on an AtlantisTM T3 column (2.1 x 150 mm, 3 µm; Waters) by using the solvent system and gradient as described previously[74]. The gas temperature of the mass spectrometer was set to 290 °C and the gas flow to 20 L/min. The nebulizer was set to 45 psi. The sheath gas flow was set to 11 L/min, with a temperature of 400 °C. The capillary voltage was set to 5000 V with a nozzle voltage of 500 V (both positive mode). The MS analysis was performed in positive ionization mode. All metabolites were screened by their mass-to-charge ratio, retention time and fragmentation pattern (five fragments each,

Fig. S4). For the latter four, no standards are available. Cys-conjugated 2,4-decen-1-ol was identified as described in Pan KL. et al[74]. tt-DDE was CE-optimized by using an authentic standard. The fragmentation pattern of the remaining metabolites was developed according to mentioned paper and CE-optimized by test injections with sample material.

2.2.15 Statistical Analysis

All data presented in this study were obtained from at least three independent biological replicates and are expressed as the mean ± standard deviation (SD). Statistical comparisons between two groups were performed using the unpaired Student's t-test. For comparisons involving multiple groups and one or two variables, one-way or two-way analysis of variance (ANOVA) was utilized. The survival rates were analyzed using the chi-square test. All statistical analyses were conducted using GraphPad Prism 8 software. The significance level was set at *$p < 0.05$, **$p < 0.01$, ***$p < 0.001$, and ****$p < 0.0001$ to denote statistical significance.

3.Results

The data presented in the result section have recently been accepted for publication in *Advanced Science* (2023) and have been originally written by myself:

Impaired detoxification of trans, trans-2,4-decadienal, an oxidation product from omega-6 fatty acids, alters insulin signaling, gluconeogenesis and promotes microvascular disease. Advanced Science 2023, in press.

Xin Qian, Stephan Klatt, Katrin Bennewitz, David Philipp Wohlfart, Bowen Lou, Ye Meng, Michael Buettner, Gernot Poschet, Jakob Morgenstern, Thomas Fleming, Carsten Sticht, Ingrid Hausser, Ingrid Fleming, Julia Szendroedi, Peter Paul Nawroth, Jens Kroll.

3.1 Generation and validation of *aldh9a1b* knockout zebrafish

The primary objective of this study was to explore the involvement of ALDH9a1b and its interplay with RCSs within the framework of diabetes mellitus. Leveraging the advantageous characteristics of zebrafish as a model organism, we harnessed its suitability to investigate microvascular complications associated with diabetes [94]. To facilitate our investigation, we engineered a zebrafish line in which the *aldh9a1b* gene was intentionally knocked out. This genetically modified zebrafish line served as a pivotal tool for conducting our research.

3.1.1 Evolutionary relationship of ALDH9a1 among representative vertebrates

ALDH9a1 has three distinct isoforms in zebrafish, namely ALDH9a1a.1, ALDH9a1a.2, and ALDH9a1b. To clarify their evolutionary relationship among representative vertebrates, a comprehensive phylogenetic analysis of ALDH9a1 amino acid sequences were performed. The resulting Neighbor-joining phylogenetic bootstrap tree revealed that ALDH9a1b exhibited a closer relationship with ALDH9a1 **(Figure 3A)**. Furthermore, through an amino acid alignment of ALDH9a1, it became apparent that zebrafish, human, and mouse share a high degree of similarity, including identical active sites and NAD binding sites, showing a remarkable level of conservation among the three species **(Figure.3B)**. Collectively, these findings strongly support the rationale for employing zebrafish as a suitable model organism for investigating the functional characteristics of ALDH9a1b.

Figure 3 Evolutionary relationship of ALDH9a1 among representative vertebrates. (A) Neighbor-joining phylogenetic bootstrap tree of ALDH9a1 amino sequence elucidates the inferred evolutionary associations among representative vertebrates. (B) Amino acid alignment of ALDH9a1 showed high similarity, same NAD binding site (blue frame) and active site (red frame) between

3.1.2 Distribution of *aldh9a1b* in zebrafish organs and developmental stages

To investigate *aldh9a1b* role in the growth and development of zebrafish, *aldh9a1b* mRNA expression was determined first. Throughout the larval stages, the fluctuation in the expression of *aldh9a1b* was not significantly observable from 1day post fertilization(dpf) to 5dpf (**Figure.4A**). In the context of adult zebrafish, the expression of *aldh9a1b* mRNA was mostly expressed in livers and brains, while least expressed in spleens (**Figure.4B**). These data suggested a broad distribution of *aldh9a1b* across varying stages and organs, underscoring its critical role in the development and physiological functionality of zebrafish.

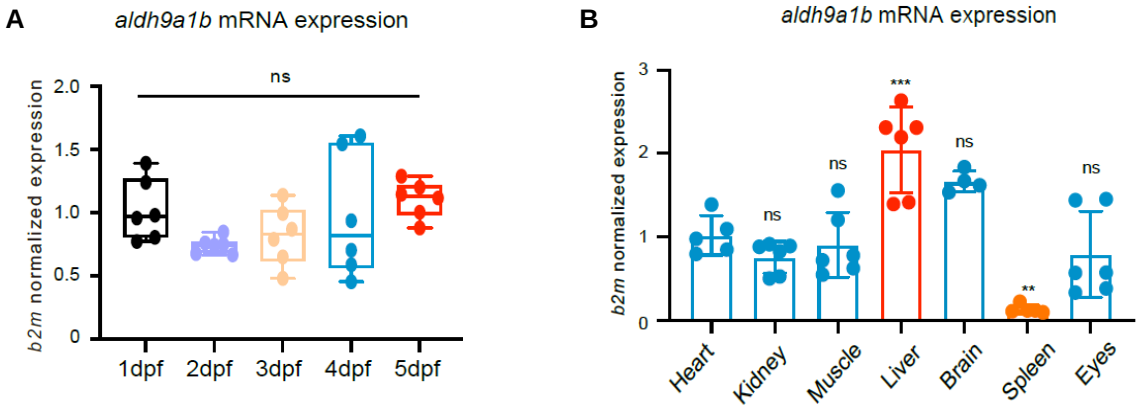

Figure 4 Distribution of *aldh9a1b* in zebrafish organs and developmental stages. (A) The expression of *aldh9a1b* mRNA didn't show a significant trend from 1dpf to 5dpf. n=6. (B) *aldh9a1b* mRNA expression was mostly expressed in the livers, while least in the spleen of adult zebrafish. n=5 and 6. The quantification of mRNA expression was conducted through RT-qPCR and subsequently standardized against b2m. Each data point illustrated corresponded to either 20 larvae or a single adult fish. The bars indicate mean ± SD values. Statistical analysis was performed by one-way ANOVA and Student's t-test. ns = not significant, **p < 0.01, ***p < 0.001. b2m, β2 microglobulin; dpf, days post fertilization.

3.1.3 Generation of *aldh9a1b* knockout zebrafish with CRISPR/Cas9 technology

To explore the role of ALDH9a1b in zebrafish, a knockout model (*aldh9a1b*$^{-/-}$) was established using CRISPR/Cas9 technology in collaboration with Dr. Bowen Lou. The CRISPR guide RNA (gRNA) was meticulously designed to target exon 6 of ALDH9a1b. This gRNA, along with Cas9 mRNA, was introduced into zebrafish embryos at the one-cell stage of *TG(fli1:EGFP)* strain. Subsequent analysis was conducted on the resulting F0 generation through Sanger sequencing. Evaluation of the genomic DNA sequencing of *aldh9a1b*$^{-/-}$ zebrafish unveiled a frameshift mutation arising from a 10-base pair (bp) deletion. This deletion consequently induced a premature stop codon within the amino acid sequence **(Figure 5).**

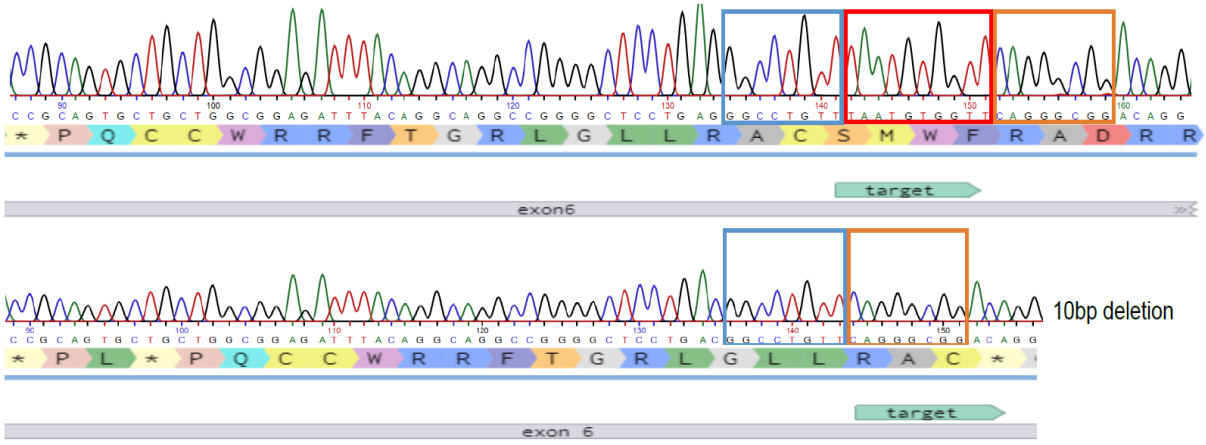

Figure 5 Establishment of *aldh9a1b* knockout zebrafish line. DNA sequencing displayed 10bp deletion (red frame) and resulted early stop codon in the amino acid sequence. The genotypes were analyzed using sanger sequencing chromatograms of PCR-amplified *aldh9a1b* region containing the target sites.

3.1.4 Validation of *aldh9a1b* knockout zebrafish line

In order to verify the successful establishment of the *aldh9a1b*$^{-/-}$ zebrafish line, several validation tests were conducted, including assessments on genomic DNA, mRNA and various functional levels. Genotyping-PCR gel clearly distinguished *aldh9a1b*$^{+/+}$, *aldh9a1b*$^{+/-}$ and *aldh9a1b*$^{-/-}$ zebrafish using genomic DNA (**Figure 6A**). On mRNA level, a significant decrease in *aldh9a1b* expression was observed in the larvae, livers and muscles of *aldh9a1b*$^{-/-}$ zebrafish (**Figure 6B-C**). Furthermore, total Aldh activity was evaluated by utilizing acetaldehyde as a substrate, indicating a substantial decrease in *aldh9a1b*$^{-/-}$ larvae (**Figure 6D**).

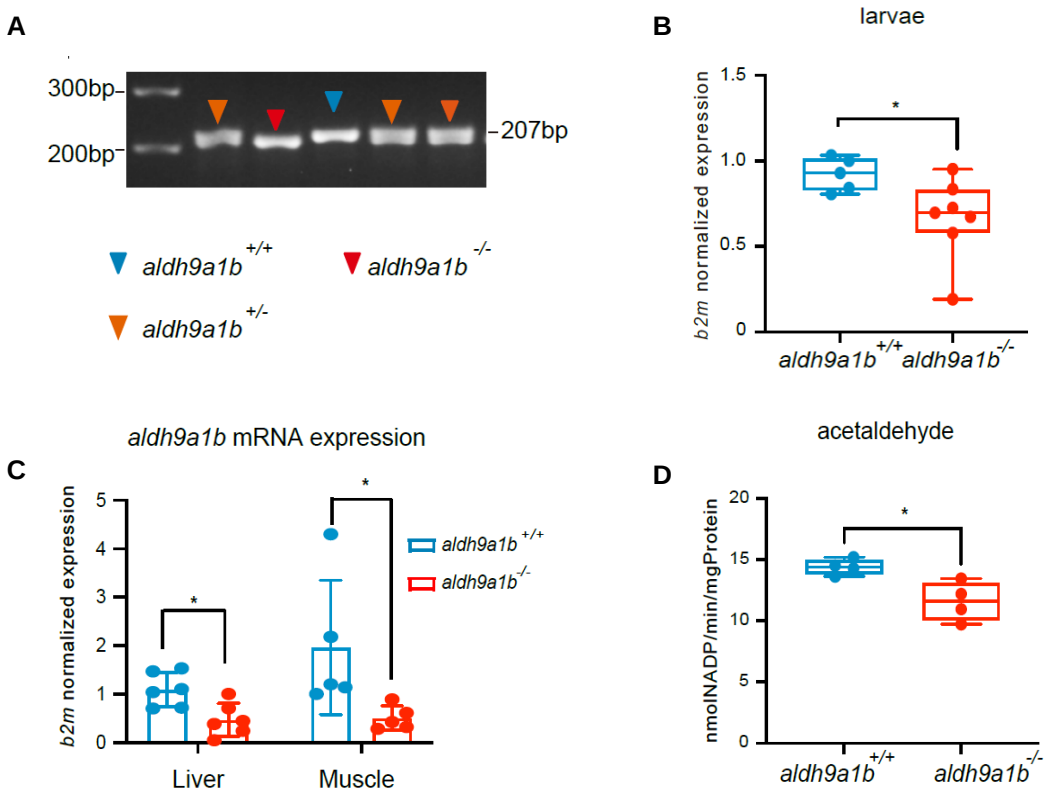

Figure 6 Validation of *aldh9a1b* knockout zebrafish line. (A) Zebrafish with genotypes of *aldh9a1b*$^{+/+}$, *aldh9a1b*$^{+/-}$, and *aldh9a1b*$^{-/-}$ can be differentiated through a genotyping-PCR gel. The PCR products of cDNA from *aldh9a1b*$^{+/+}$, *aldh9a1b*$^{+/-}$, and *aldh9a1b*$^{-/-}$ zebrafish are marked by blue, red, and yellow arrows respectively. (B) The expression of *aldh9a1b* mRNA exhibited a significant reduction in *aldh9a1b*$^{-/-}$ larvae. n=5 and 7. (C) *aldh9a1b* mRNA levels were significantly decreased in livers and muscles of *aldh9a1b*$^{-/-}$ adult fish, n=6 and 5. (D) Total ALDH enzyme activity was decreased with the substrate acetaldehyde at 5dpf, n = 4. The quantification of mRNA expression was conducted through RT-qPCR and subsequently standardized against b2m. Each data point illustrated corresponded to either 20 larvae or a single adult fish. The bars indicate mean ± SD values. Statistical analysis was performed by Student's t-test and one-way ANOVA. *p < 0.05.

3.1.5 The effect of *aldh9a1b* loss on the development of zebrafish

Since *aldh9a1b* wide distribution in larvae and zebrafish, the effect of its loss on zebrafish development was analyzed from 1 to 15 months of age. The gross morphology of adult zebrafish was equivalent in *aldh9a1b*$^{+/+}$ and *aldh9a1b*$^{-/-}$**(Figure 7A)**. Further investigations revealed that the absence of *aldh9a1b* did not impact the survival rate of adult zebrafish aged between 1 to 15 months **(Figure 7B)**. The adult body length and weight remained unaffected in *aldh9a1b*$^{-/-}$ mutants **(Figure 7C-D)**. Moreover, genotype analysis post-heterozygous incrosses demonstrated a distribution pattern consistent with Mendelian inheritance among *aldh9a1b* larvae (**Figure 7E**). Collectively, these findings confirm the successful establishment of the *aldh9a1b* knockout zebrafish.

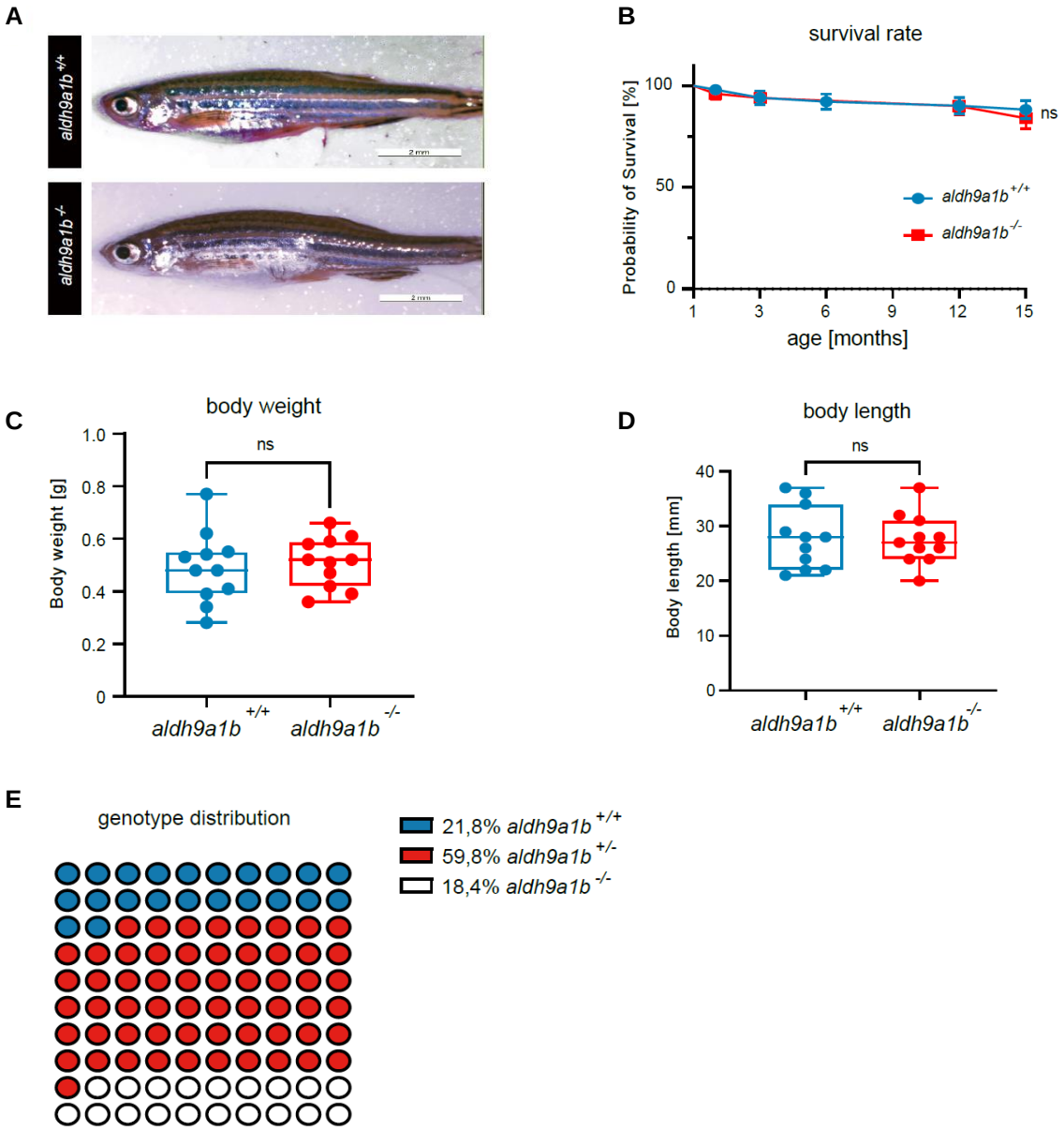

Figure 7 *aldh9a1b* knockout caused no effect of zebrafish development. (A) *aldh9a1b*$^{-/-}$ showed normal morphology compared to *aldh9a1b*$^{+/+}$ adult zebrafish. (B) The survival rate exhibited no notable difference between *aldh9a1b*$^{+/+}$ and *aldh9a1b*$^{-/-}$. n=51 and 53. (C and D) Adult *aldh9a1b*$^{-/-}$ showed equivalent body weight (C) and body length (D) to *aldh9a1b*$^{+/+}$ zebrafish. n=11 (D) The distribution of zebrafish across different genotypes conformed to Mendelian inheritance patterns in the first generation (F2). *aldh9a1b*$^{+/+}$ = 52, *aldh9a1b*$^{+/-}$ = 143, *aldh9a1b*$^{-/-}$ = 44. The quantification of mRNA expression was conducted through RT-qPCR and subsequently standardized against b2m. Each data point illustrated corresponded to a single adult fish. Statistical analysis was performed by Student's t-test and chi-square test. ns, not significant.

3.2 Vascular related phenotypes of *aldh9a1b*$^{-/-}$ zebrafish

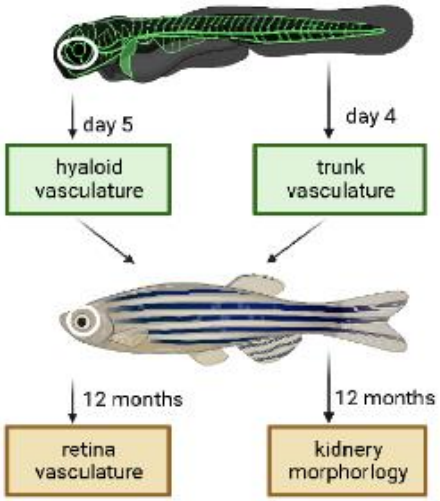

Figure 8 Workflow of vascular phenotypes exploration into *aldh9a1b*$^{-/-}$ zebrafish.

Diabetic nephropathy and diabetic retinopathy are prevalent microvascular complications that significantly impair the quality and longevity of life for patients with diabetes[95]. Moreover, MG is strongly associated with the progression of diabetes and its vascular complications[96]. Given zebrafish characteristics as a valuable animal model for investigating RCS detoxification enzyme systems' microvascular complications, it was utilized to explore the effects of the loss *aldh9a1b* loss on vascular phenotypes (**Figure 8**). For the larval stage, we conducted analyses of trunk vasculature and hyaloid vasculature at 4dpf and 5dpf separately. For adult zebrafish, vascular phenotyping was conducted on fish aged over one year, aiming to replicate the chronic vascular damage caused by diabetes.

3.2.1 Zebrafish larvae vascular phenotypes

Due to expressed enhanced green fluorescence protein (EGFP) in endothelial cells, *Tg(fli1:EGFP)* reporter line was used to analyze the vascular structures under confocal microscope. At 4dpf, *aldh9a1b*$^{-/-}$ larvae did not showed significantly changed trunk vasculature (**Figure 9A-B**). At 5dpf, the branches and sprouts of hyaloid vasculature displayed a significantly increase in *aldh9a1b*$^{-/-}$ larvae (**Figure 9C-D**). These data

suggested the damage of *aldh9a1b* knockout on microvasculature compared to macrovasculature.

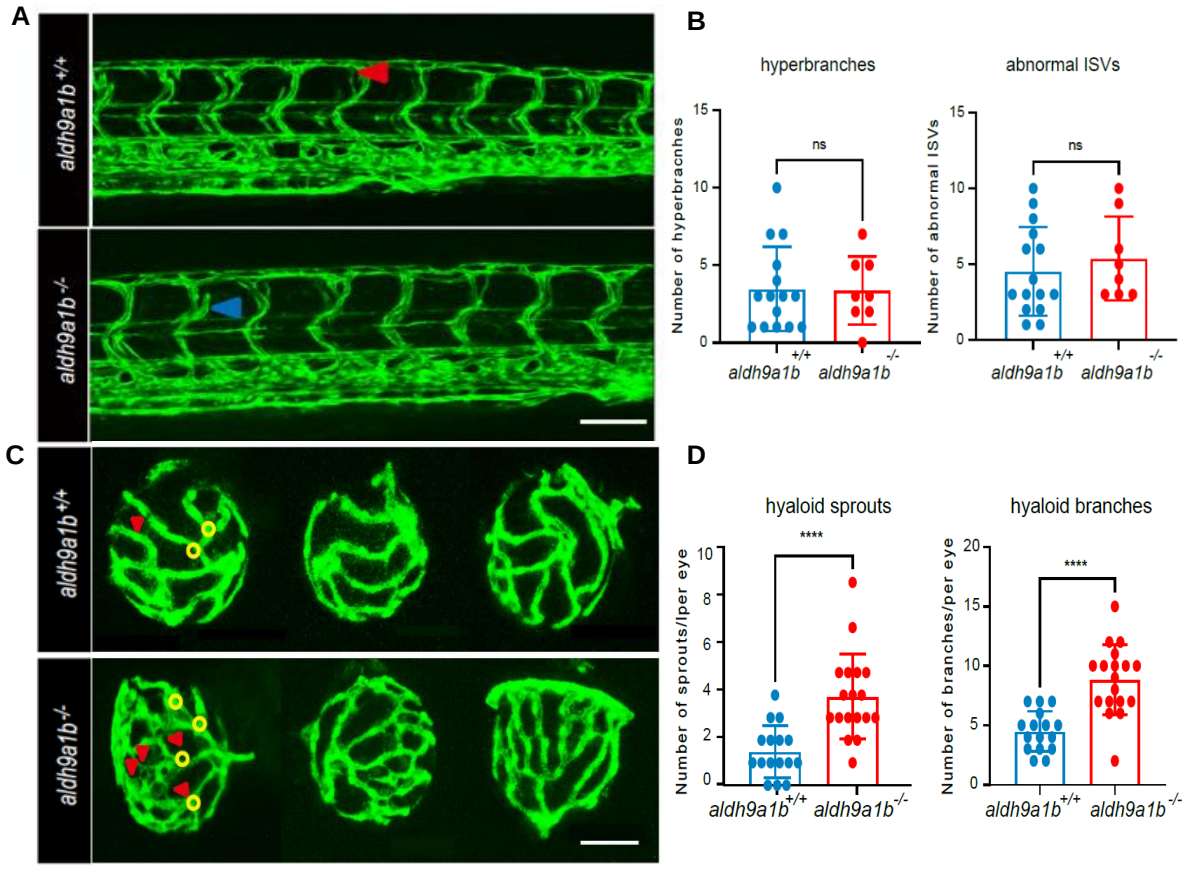

Figure 9 Vascular alterations in *aldh9a1b*$^{-/-}$ larvae. (A) The confocal image showed unaltered trunk vasculature of *aldh9a1b*$^{-/-}$ larvae at 4dpf. Hyperbranches are indicated by red arrows, while ISVs are marked by blue arrows. The white scale bar = 100 μm. (B) The quantification of hyperbranches and abnormal ISVs indicated no significant differences in the trunk vasculature between *aldh9a1b*$^{+/+}$ and *aldh9a1b*$^{-/-}$ larvae at 4dpf. Each datapoint represented one larva, n=15 and 8. (C) The confocal image showed increased hyaloid vasculature of *aldh9a1b*$^{-/-}$ larvae at 5dpf. Yellow circle=branches, red arrows=sprouts. The white scale bar = 50 μm. (D) The quantification of hyaloid branchpoints and sprouts formation displayed significantly increased vasculature in *aldh9a1b*$^{-/-}$ larvae at 5dpf. Each datapoint represented one larva, n=16 and 18. zebrafish. Statistical analysis was performed by Student's t-test. ns, not significant, ****p < 0.0001.

3.2.2 Zebrafish adult vascular phenotypes

Therefore, adult retina vasculature was further analzed to evaluate the microvascular damage caused by *aldh9a1b* knockout. A visualization and quantification of over one-year old zebrafish retina displayed preceding angiogenesis as hyaloid vasculature, confirming a permanent phenotype in *aldh9a1b*$^{-/-}$ zebrafish (**Figure 10A-B**).

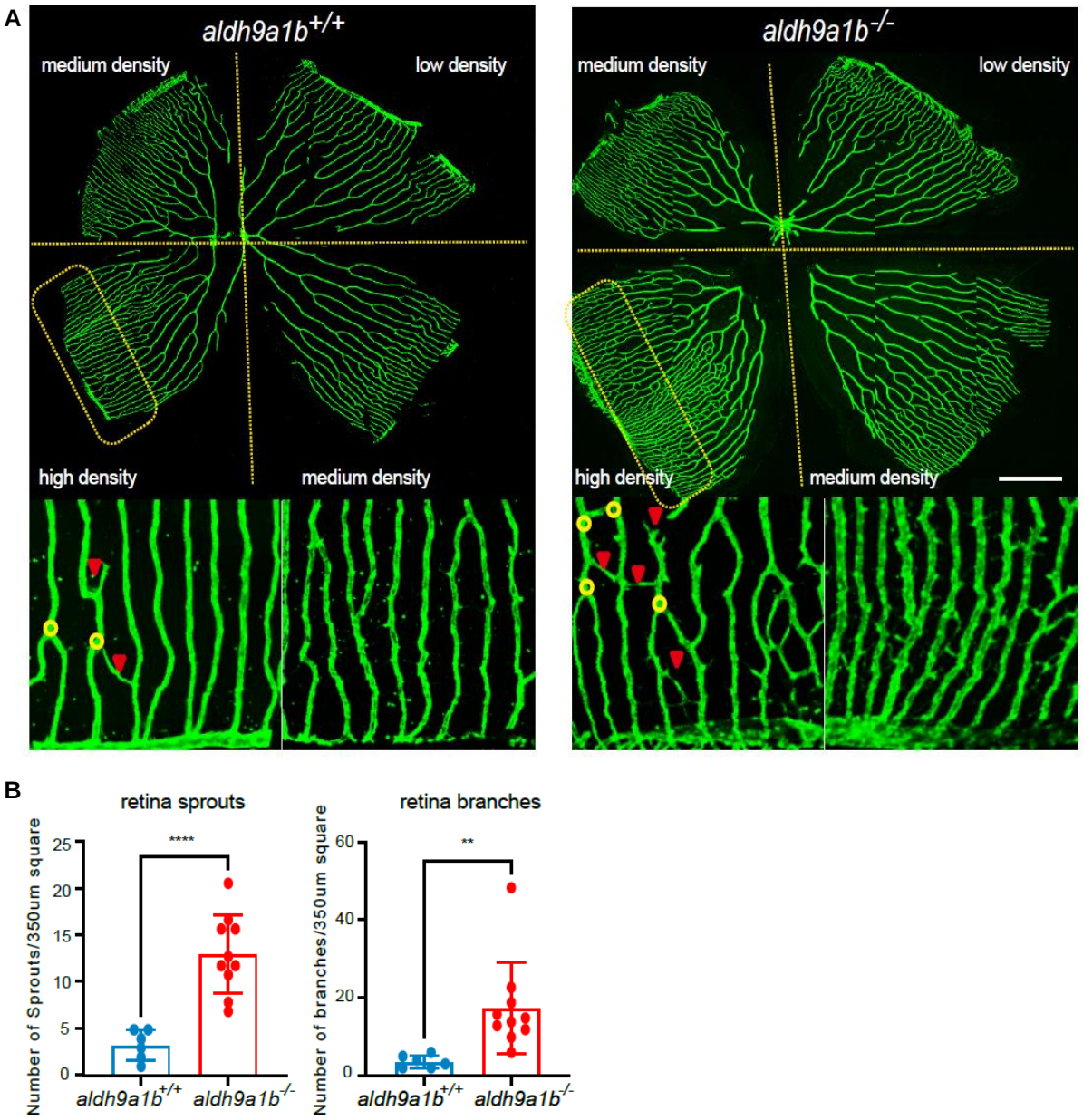

Figure 10 Vascular alterations in *aldh9a1b*$^{-/-}$ adults. (A) The confocal image showed retina vasculature of *aldh9a1b*$^{-/-}$ adult zebrafish at 12mpf. Branches are indicated by yellow circles, while sprouts are marked by red arrows. The white scale bar = 500 μm. (B) The quantification of branches and spouts showed significantly increase in *aldh9a1b*$^{-/-}$ adults at 12mpf. Each datapoint represented one 350 μm2 square in high-density retina, n=8 and 10. The bars indicate mean ± SD values. Statistical analysis was performed by Student's t-test, **p < 0.01, ****p < 0.0001.

3.2.3 Zebrafish adult kidney phenotypes

Moreover, kidney development was also analyzed by Periodic Acid-Schiff (PAS) staning (**Figure 11A**) and electron microscope (EM) (**Figure 11B-C**) to further evaluate the effect of *aldh9a1b* loss. Both the morphology and glomerular basement membrane (GBM) thickness did not show significant change between *aldh9a1b*$^{+/+}$ and *aldh9a1b*$^{-/-}$

kidneys, indicating *aldh9a1b* loss did not cause diabetic nephropathy in zebrafish.

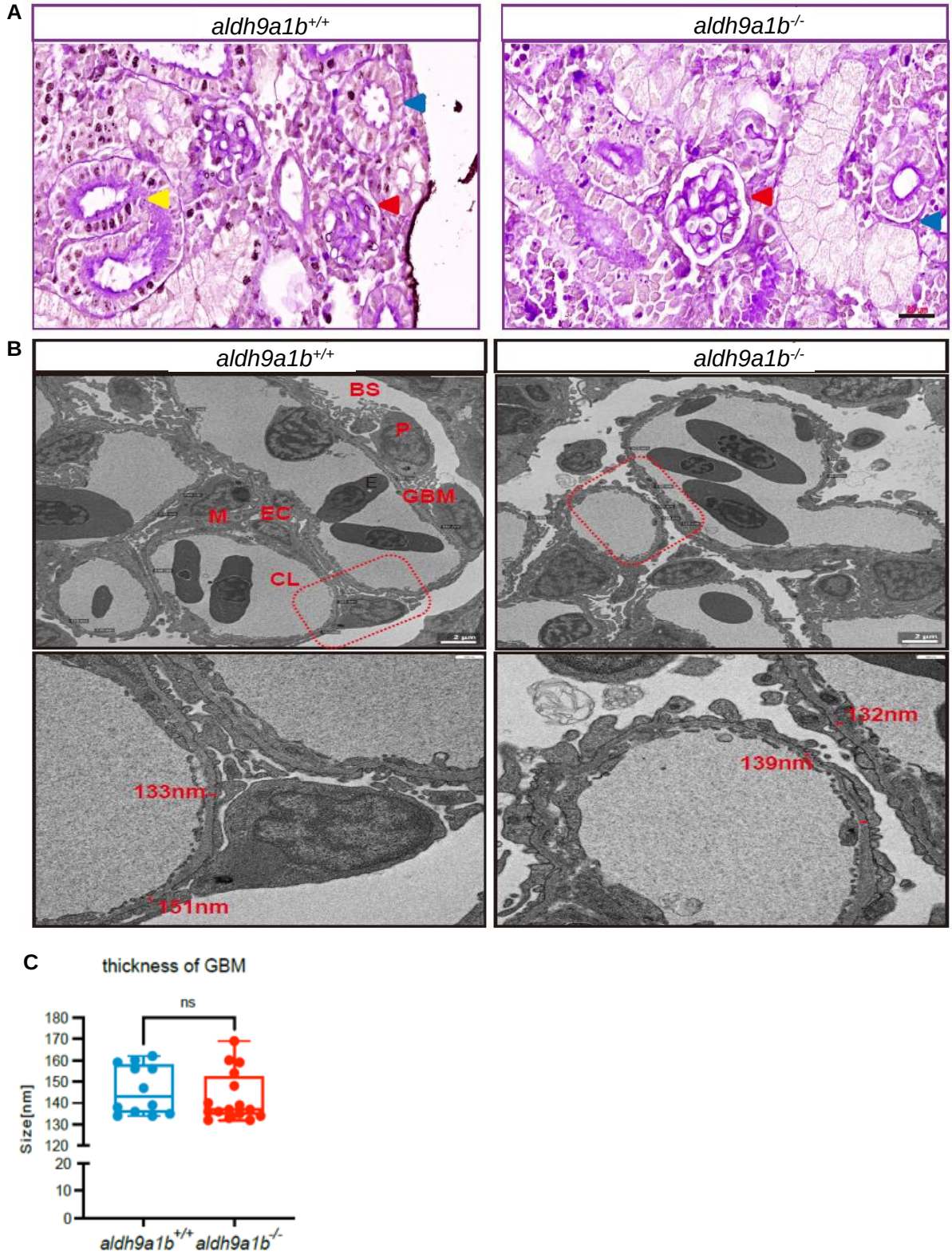

Figure 11 *aldh9a1b*$^{-/-}$ did not cause kidney phenotypes in zebrafish. (A) *aldh9a1b*$^{-/-}$ showed normal kidneys structure compared to *aldh9a1b*$^{+/+}$ by PAS staining. Yellow arrow=PAS-positive hyaline droplets; blue arrow=renal tubule; red arrow=glomeruli. Black scale bar=20μm. (B) Representative glomeruli morphology of *aldh9a1b*$^{-/-}$ and *aldh9a1b*$^{+/+}$ zebrafish under electron microscope. Scale bar, 2 μm and 500nm. (C) The thickness of GBM didn't change significantly in *aldh9a1b*$^{-/-}$ glomeruli. The bars indicate

mean ± SD values. Statistical analysis was performed by Student's t-test. ns, not significant. CL, capillary lumen; BS,bowman space; M, mesangium; GBM, glomerular basement membrane; P, podocyte EC, endothelial cell; E, erythrocyte.

3.3 tt-DDE acted as a substrate for ALDH9a1b

ALDH enzyme has displayed a wide range of spectrum of aldehydes[2]. Since zebrafish ALDH9a1b were not studied and it shared same active site with human ALDH9a1, the specific substrate Betaine aldehyde (BAL) and 4-aminobutyraldehyde (ABAL) for ALDH9a1 were also considered as candidates for ALDH9a1b[6, 7]. Besides, the oxidation of a broad range of aldehydes is facilitated by ALDH enzymes. Malfunctioning of these enzymes results in the build-up of harmful aldehydes and the development of serious ailments[2]. Therefore, aligned with our phenotype, MDA, (2E)-2-Hexadecenal, 4-hydroxyhexenal (4-HHE), MG and tt-DDE were partially identified as reactive carbonyls responsible for vascular alterations, they were also included in the study [14, 81, 87, 97, 98].

3.3.1 tt-DDE was preferred substrate for ALDH9a1b

Total enzyme activity was measured using Michalis-mention kinetics with the following substrates, 10mM ABAL, 10mM BAL, 2mM MG, 10mM MDA, 4mM 4HHE, 10mM (2E)-2-Hexadecenal and 10mM tt-DDE. *aldh9a1b*$^{-/-}$ mutants exhibited the most reduction of ALDH activity with the chemical tt-DDE, suggesting tt-DDE as more suitable substrate for ALDH9a1b (**Figure 12A-G**).

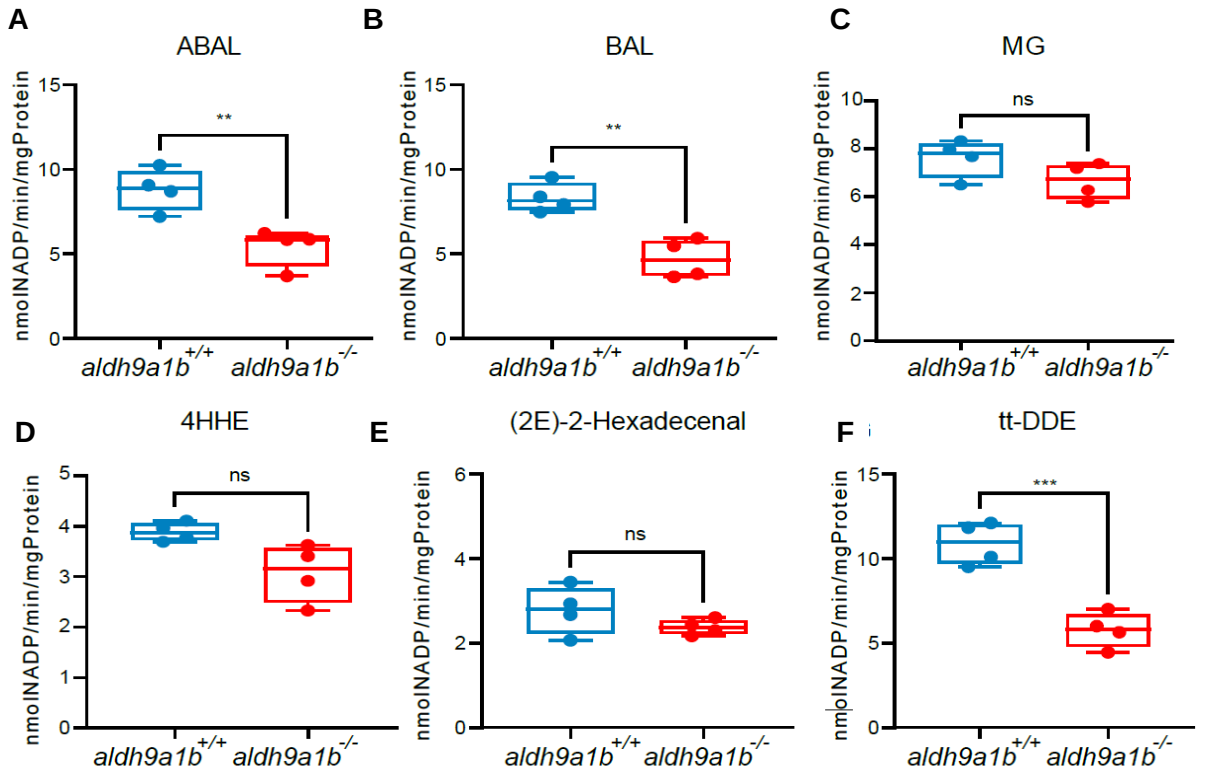

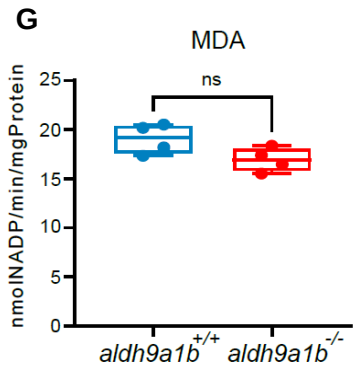

Figure 12 tt-DDE acted as a potential substrate for ALDH9a1b. (A-G) Aldh enzyme activity was significantly decreased using substrate ABAL (A), BAL (B) and tt-DDE (F), but unaltered with substrate MG (C), 4HHE (D), 2(E)-2-hexadecenal (E) and MDA (G) in *aldh9a1b*$^{-/-}$ larvae at 5dpf. Each datapoint meant 120 larvae per clutch, n=4. The bars represented mean ± SD values. Statistical analysis was performed by Student's t-test analysis.

3.3.2 tt-DDE effect on hyaloid vasculature

To validate tt-DDE responsible for *aldh9a1b*$^{-/-}$ vascular phenotype, *aldh9a1b*$^{+/+}$ was used to incubated with multiple concentrations of tt-DDE. The zebrafish exposed to 20 µmol of tt-DDE exhibited a significantly higher mortality rate, while those exposed to 10 µmol of tt-DDE displayed noticeable morphological changes (**Figure 13A-D**). As a result, concentrations of tt-DDE up to 8 µmol were determined to be safe for zebrafish. Subsequent analysis and quantification of the hyaloid vasculature revealed an increase in branchpoints and sprout formation in tt-DDE-treated larvae, resembling the microvascular phenotype observed in *aldh9a1b*$^{-/-}$ larvae (**Figure 13E-F**).

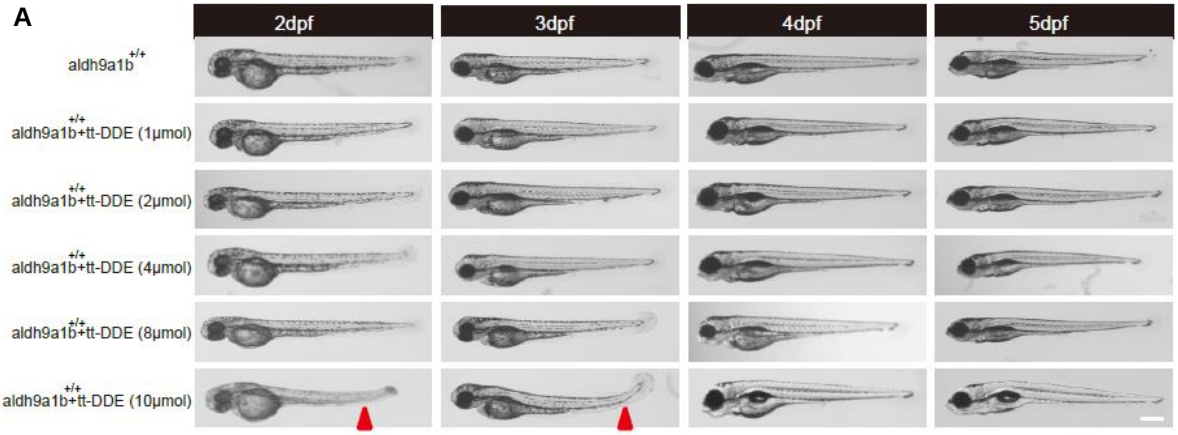

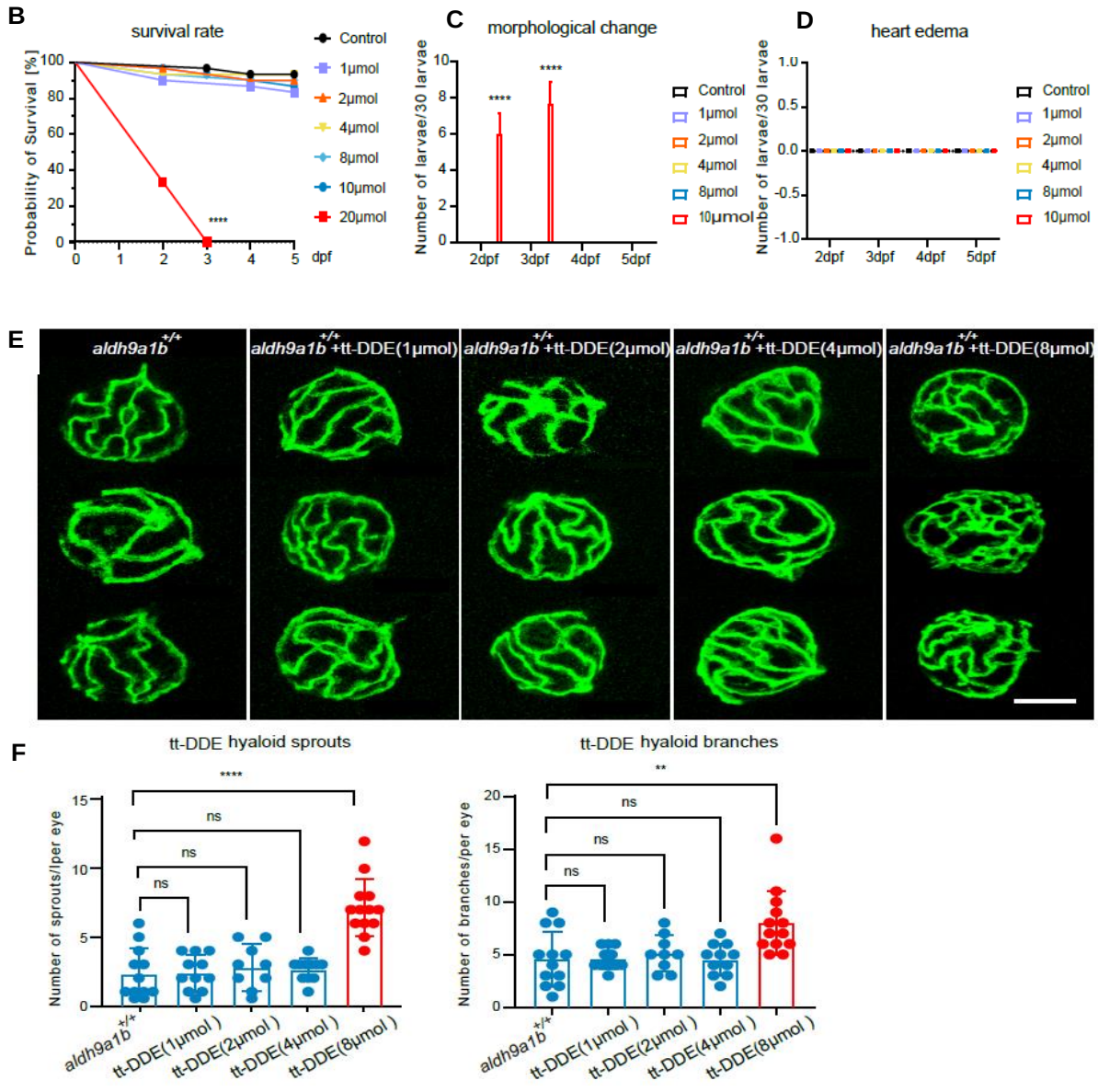

Figure 13 The effect of tt-DDE incubation on hyaloid vasculature. (A) Morphological images depicting zebrafish larvae aged between 2 dpf and 5 dpf with 0 – 10 µmol tt-DDE treatment. Noteworthy morphological changes are indicated by red arrows.White bar, 200 µm. (B) Zebrafish larvae treated with 20 µmol tt-DDE exhibited elevated mortality. (C) Quantification of morphological change showed malformed spine in the 2dpf and 3dpf larvae treated with 10 µmol tt-DDE. (D Cardiac development remained unaffected across different tt-DDE treatment groups. (E) onfocal images showcasing alterations in hyaloid vasculature in *aldh9a1b*$^{+/+}$ larvae treated with 0-8 µmol tt-DDE at 5dpf. White scale bar = 50 µm. (F) Quantification of increased hyaloid branchpoints and sprouts formation in 8µmol tt-DDE treated *aldh9a1b*$^{+/+}$ zebrafish larvae. No significant changes were observed in treatments with 1 µmol, 2 µmol, and 4 µmol tt-DDE. Each data point corresponds to one hyaloid structure per larva. Error bars represent mean ± SD values. Statistical analysis was performed by Student's t-test and one-way ANOVA, two-way ANOVA and logrank test. ns = not significant, **p < 0.01, ****p < 0.0001.

3.3.3 Impact of *aldh9a1b* knockout and tt-DDE exposure on tt-DDE metabolites

Previous study has suggested tt-DDE can metabolized via two pathways: (i) tt-DDE may be oxidized to 2,4-decadienoic acid by ALDHs or AOX1. (ii) glutathione (GHS) conjugation, GSH breakdown, and aldehyde reduction, which generate cysteine-conjugated 2,4-decadien-1-ol[74]. To confirm the detoxification of ALDH9a1b for tt-DDE and the successful establishment of vivo tt-DDE exposure model, we collaborated with researchers from Frankfurt University in Germany and successfully developed a Liquid Chromatography–Mass Spectrometry-based approach for detecting tt-DDE exposure, as detailed in a recent publication[74].

The fragmentation of representative metabolites was illustrated in **Figure 14A.** PCA analyzed the differentiation between different groups (**Figure 14B**). Each organ displayed their distinct metabolites pattern. Larvae exhibited higher levels of cyscon2-cyscon6, the liver was notably enriched in -con-1, and GSH-DDE, while muscle predominantly contained cys-con-2 and cys-con-3(**Figure 14C**). In larvae and muscle, tt-DDE incubation significantly increased the concentrations of cys-con and GSH-DDE, indicating higher exposure in tt-DDE incubated group (**Figure 14D-E**). In liver, which showed highest expression of *aldh9a1b,* elevated tt-DDE levels also found in *aldh9a1b* knockout group as well as in muscles, which strongly aligned with our cited paper and confirmed Aldh9a1b system responsible for tt-DDE detoxification (**Figure 14F**).

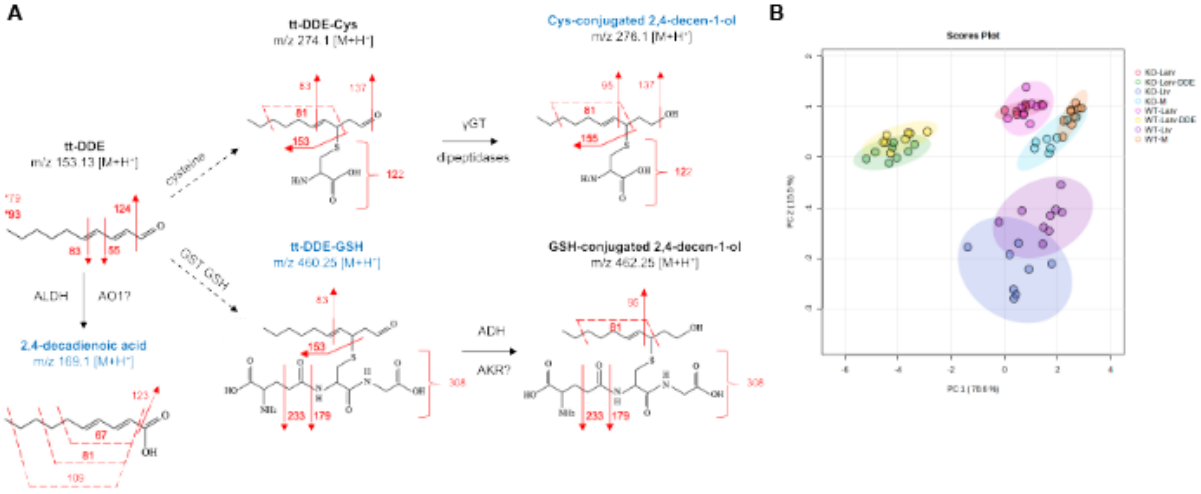

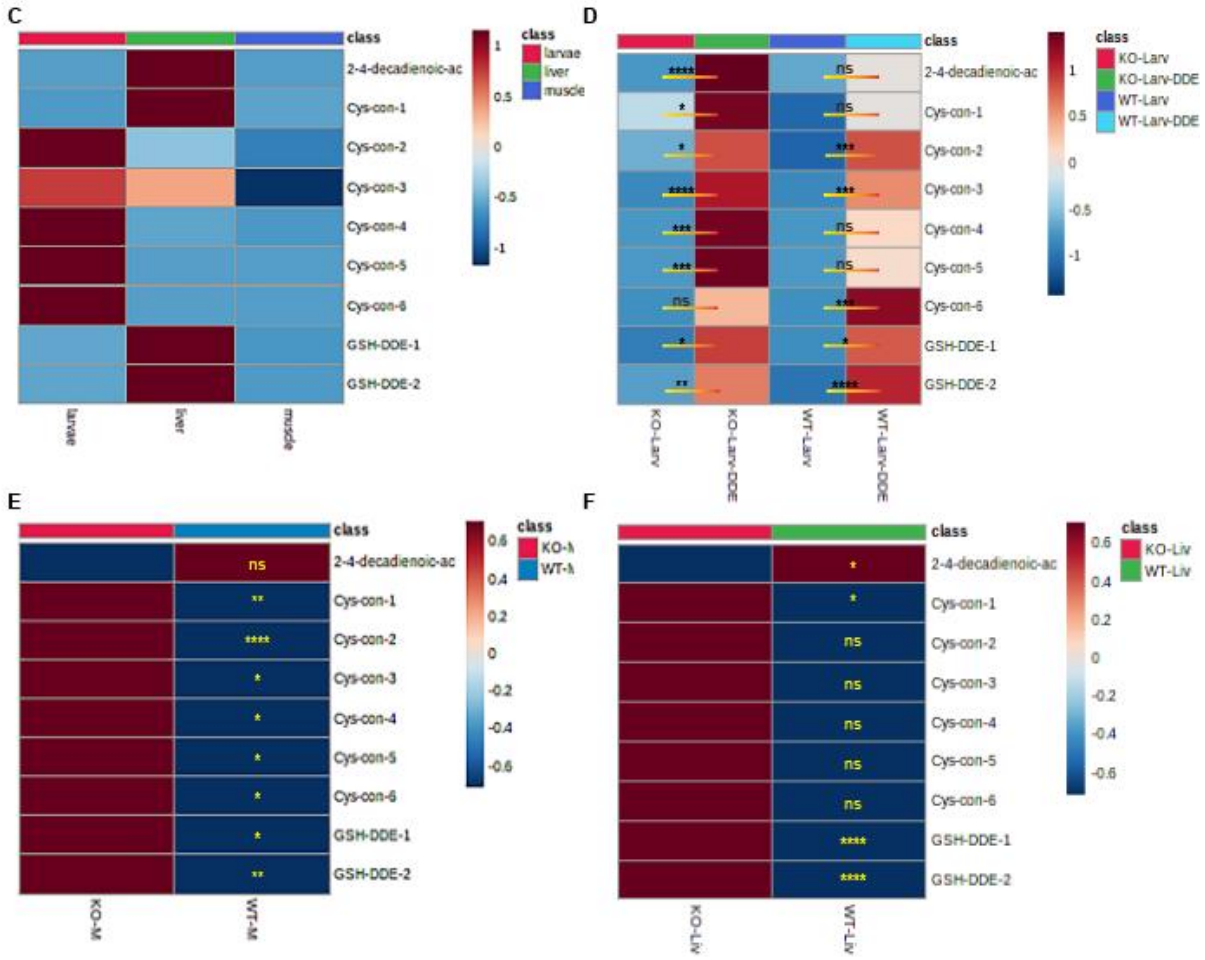

Figure 14 Impact of aldh9a1b knockout and tt-DDE exposure on tt-DDE metabolites. (A) The fragmentation pattern/selected fragments which were identified via HPLC/MS are shown (*unknown fragment location). The fragmentation pattern of tt-DDE was CE-optimized on the 6495C QQQ with the use of an authentic standard. (B) PCA analysis was conducted to visualize the differentiation among the analyzed groups. (C) A heatmap illustrates the abundance level of tt-DDE metabolites in different organs. Larvae exhibited higher levels of cyscon2-cyscon6, the liver was notably enriched in cys-con-1 and GSH-DDE, while muscle predominantly contained cys-con-2 and cys-con-3. Each group contains all the respective samples with n=17 in liver and muscles, and n=31 in the larvae group. (D-F) tt-DDE metabolites were significantly changed induced by aldh9a1b knockout and tt-DDE treatment. n=9/8 in liver and muscle, n=8/7 in larvae. Statistical analysis was performed by Student's t-test and one-way ANOVA. ns = not significant, *p < 0.05, **p < 0.01, ***p < 0.001, ****p < 0.0001. MS, Mass spectrometry; tt-DDE, trans, trans-2,4-decadienal; CYS-con2, Cys-conjugated 2,4-decen-1-ol; WT, *aldh9a1b*$^{+/+}$; KO, *aldh9a1b*$^{-/-}$; Liv, liver; M, muscles.

3.3.4 ABAL effect on hyaloid vasculature

ABAL was considered to be specific substrate for human ALDH9a1 and was suggested to be substrate for zebrafish Aldh9a1b by enzyme activity experiment. Therefore, its effect on hyaloid vasculature was also determined to explore whether ABAL is also

responsible for *aldh9a1b*$^{-/-}$ hyaloid phenotypes. Combined with survival rate, morphology and heat development, its safe concentration was regarded as 0-100 μmol **(Figure 15A-D).** But, none of above any ABAL concentrations caused significantly changed hyaloid vasculature **(Figure 15E-F).**

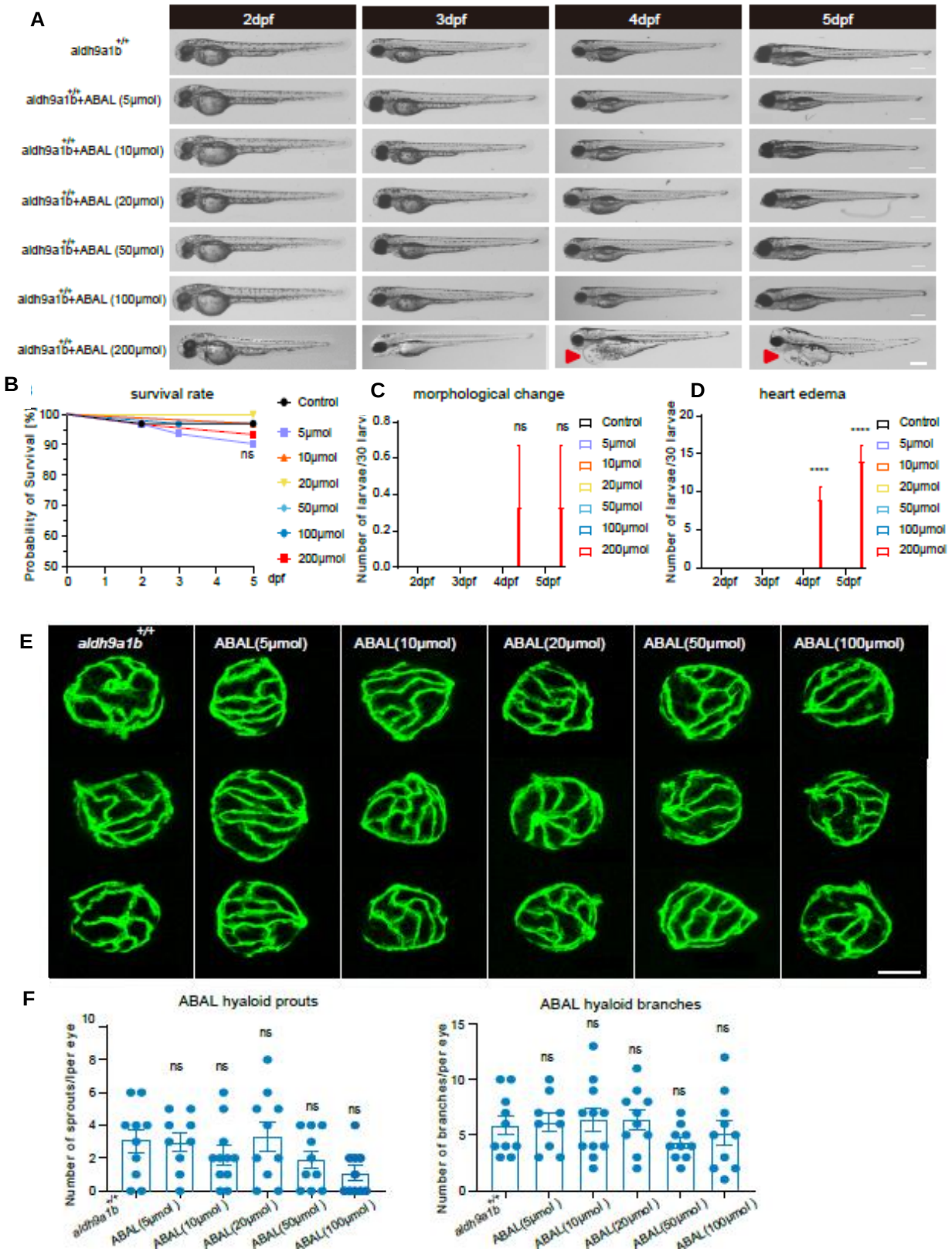

Figure 15 The effect of ABAL incubation on hyaloid vasculature. (A) Morphological images depicting zebrafish larvae aged between 2 dpf and 5 dpf with 0 – 200 µmol ABAL treatment. Noteworthy morphological changes are indicated by red arrows. White bar, 200 µm. (B) 0-200 µmol ABAL didn't significantly affect survival rate of zebrafish larvae. (C) 0-200 µmol ABAL didn't significantly change zebrafish morphology in the 2-5 dpf larvae. (D) Quantitative analysis of cardiac edema revealed significant increase in *aldh9a1b*$^{+/+}$ larvae at 4 dpf and 5 dpf with 200 µmol ABAL treatment. (E) Confocal images showcasing alterations in hyaloid vasculature in *aldh9a1b*$^{+/+}$ zebrafish larvae treated with 0 – 200 µmol ABAL at 5dpf. White scale bar = 50 µm. (F) Hyaloid branchpoints and sprouts formation in 0-200µmol ABAL treated *aldh9a1b*$^{+/+}$ zebrafish larvae were not significantly changed. Each data point corresponds to one hyaloid structure per larva. Error bars represent ± SD values. Statistical analysis was performed by Student's t-test and one-way ANOVA, two-way ANOVA and logrank test. ns = not significant, **p < 0.01, ****p < 0.0001.

3.3.5 BAL effect on hyaloid vasculature

Comparable to ABAL, BAL also shared same characteristics to be explored its hyaloid phenotype. 400µmol BAL caused half of total tested larvae dead, so hyaloid vasculature was detected in 0-200µmol BAL incubation (**Figure 16A-D**). Intriguingly, BAL also did not induce similar hyaloid changed to *aldh9a1b*$^{-/-}$, indicating tt-DDE important role in *aldh9a1b*$^{-/-}$ hyaloid phenotype (**Figure 16E-F**).

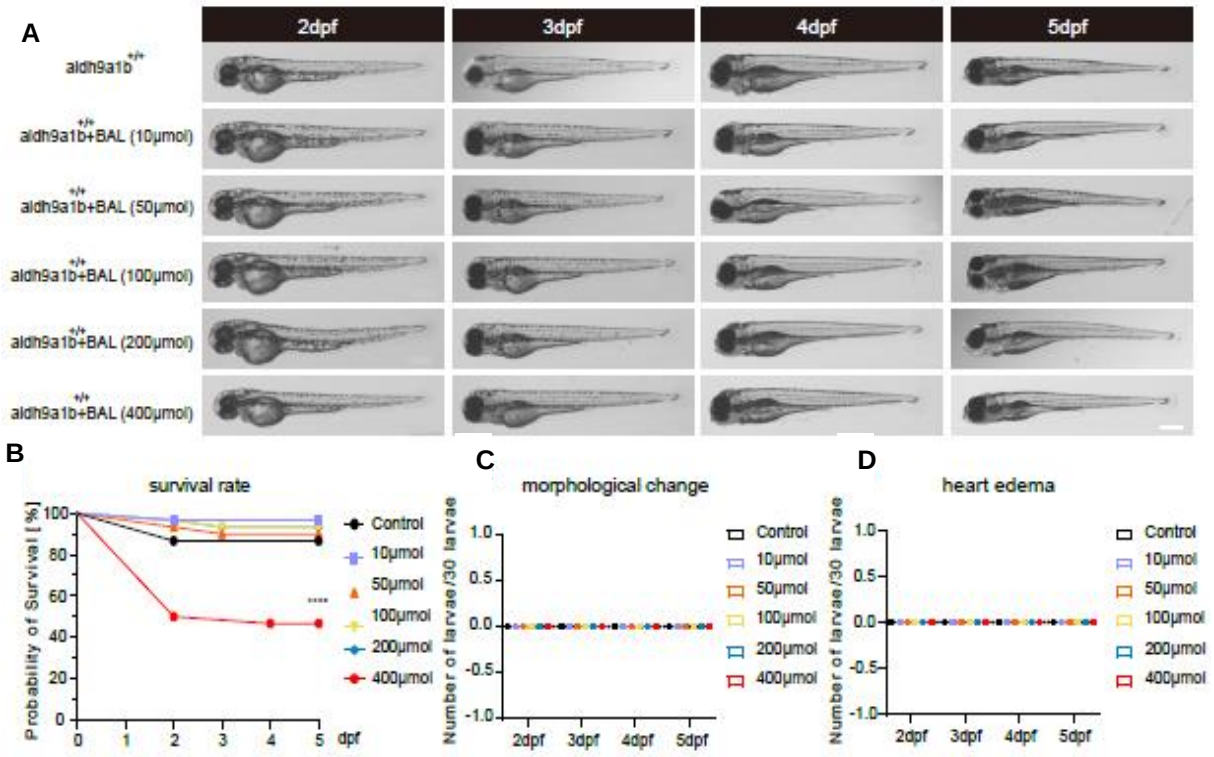

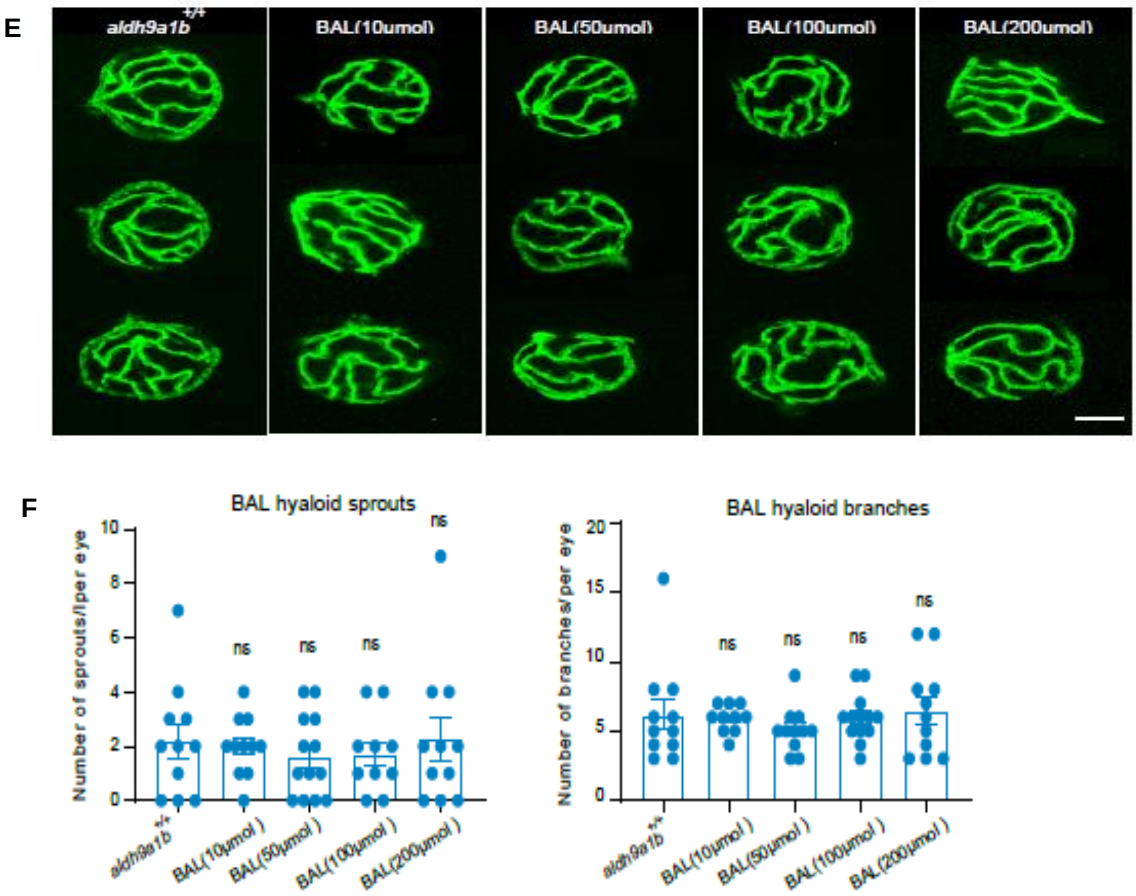

Figure 16 The effect of BAL incubation on hyaloid vasculature. (A) Morphological illustrations of zebrafish larvae aged between 2 dpf and 5 dpf with 0 – 400 µmol BAL treatment. Noteworthy morphological changes are indicated by red arrows. White bar, 200 µm. (B) A 400 µmol BAL treatment resulted in a 50% mortality rate among zebrafish larvae. (C Morphology of zebrafish larvae aged 2-5 dpf remained largely unaffected by BAL treatments ranging from 0 to 400 µmol. (D) Quantification of heart edema showed normal cardiac development in *aldh9a1b*$^{+/+}$ larvae subjected to BAL treatments spanning 0 to 400 µmol. (E) Representative confocal images of hyaloid vasculature showed vascular alterations in *aldh9a1b*$^{+/+}$ zebrafish larvae treated with 0 – 400 µmol BAL at 5dpf. White scale bar = 50 µm. (F) Neither hyaloid branchpoints nor sprout formation were significantly impacted by BAL treatments spanning 0 to 400 µmol in *aldh9a1b*$^{+/+}$ larvae. Each data point corresponds to one hyaloid structure per larva. Error bars represent mean ± SD values. Statistical analysis was performed by Student's t-test and one-way ANOVA, two-way ANOVA and logrank test. ns = not significant, **p < 0.01, ****p < 0.0001.

3.4 Analysis of transcriptomics

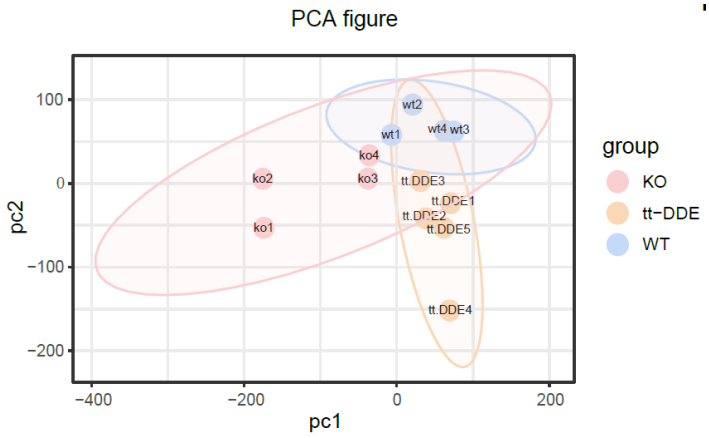

Figure 17 PCA displayed the difference of components among all the groups.

To investigate the fundamental mechanisms contributing to the changes in vasculature of *aldh9a1b*$^{-/-}$ and tt-DDE treated zebrafish, an exploration of gene enrichment patterns was conducted using RNA-Seq analysis in *aldh9a1b*$^{-/-}$ and tt-DDE treated larvae at 5dpf. The utilization of Principal Component Analysis (PCA) enabled the differentiation of each sample's components, enabling distinct clustering from other experimental groups (**Figure 17**).

3.4.1 Enrichment analysis of differential genes

With limma package, A total of 940 genes exhibited differential expression in *aldh9a1b*$^{-/-}$ zebrafish, while 239 genes demonstrated differential expression within the tt-DDE-treated group, as compared to *aldh9a1b*$^{+/+}$ controls. Pathway enrichment analysis utilizing the Kyoto Encyclopedia of Genes and Genomes (KEGG) database was performed on these differentially expressed genes, highlighting the predominant modified pathways across the distinct experimental groups. In *aldh9a1b*$^{-/-}$ mutants, a significant alteration was observed in the pathways associated with omega-6 fatty acid metabolism, encompassing arachidonic acid and linoleic acid metabolism, which can be attributed to the fact that omega-6 fatty acids serve as the principal source of tt-DDE (**Figure 18A-B**). Conversely, in the tt-DDE treated group, pathways linked to insulin signaling and its associated cascades constituted more than half of the pathways that displayed alterations (**Figure 18C-D**).

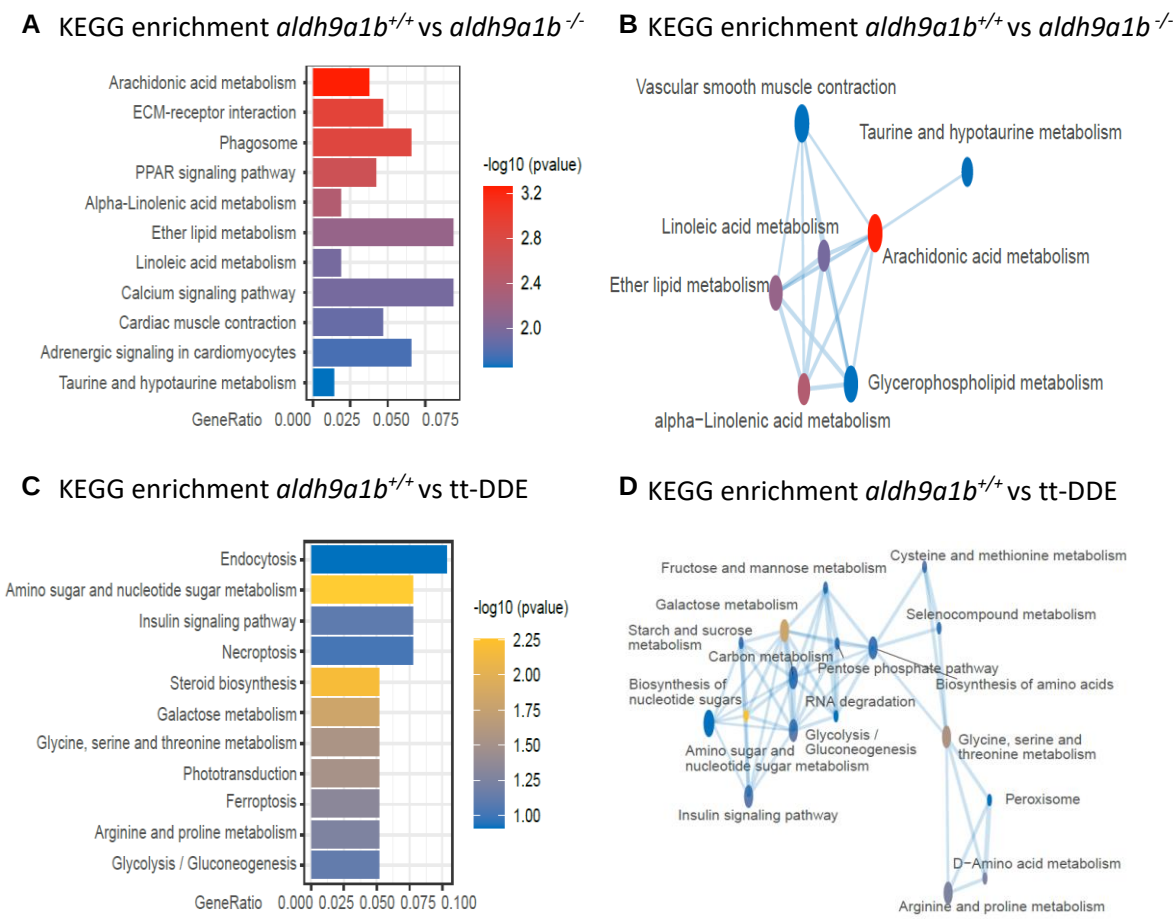

Figure 18 Enrichment analysis of differential genes. (A)KEGG enrichment analysis of differential genes showed top altered pathways in *aldh9a1b-/-* compared to *aldh9a1b*+/+. (B)Emapplot of KEGG enrichment analysis showed the interaction of altered pathways in *aldh9a1b-/-* mutants. (C) KEGG enrichment analysis of differential genes showed top altered pathways in tt-DDE treated *aldh9a1b*+/+ larvae compared to *aldh9a1b*+/+ larvae. (D) Emapplot of KEGG enrichment analysis showed the interaction of altered pathways in the tt-DDE
treated group.

3.4.2 GSVA analysis

As both fatty acid metabolism and glucose metabolism can be associated with carbon metabolism and are regulated by the insulin pathway, we performed Gene set variation analysis (GSVA) to further investigate their relationship. Among various comparisons, top 10 altered pathways were identified that exhibited alterations relevant to carbon metabolism and insulin signaling. Intriguingly, the modification of insulin signaling and its downstream pathways, namely MAPK and MTOR signaling, consistently emerged across both experimental groups. This consistent pattern strongly suggests that an altered insulin signaling pathway serves as an inducer of vascular alterations in tt-DDE treated and in *aldh9a1b*$^{-/-}$ zebrafish (**Figure 19A-B**).

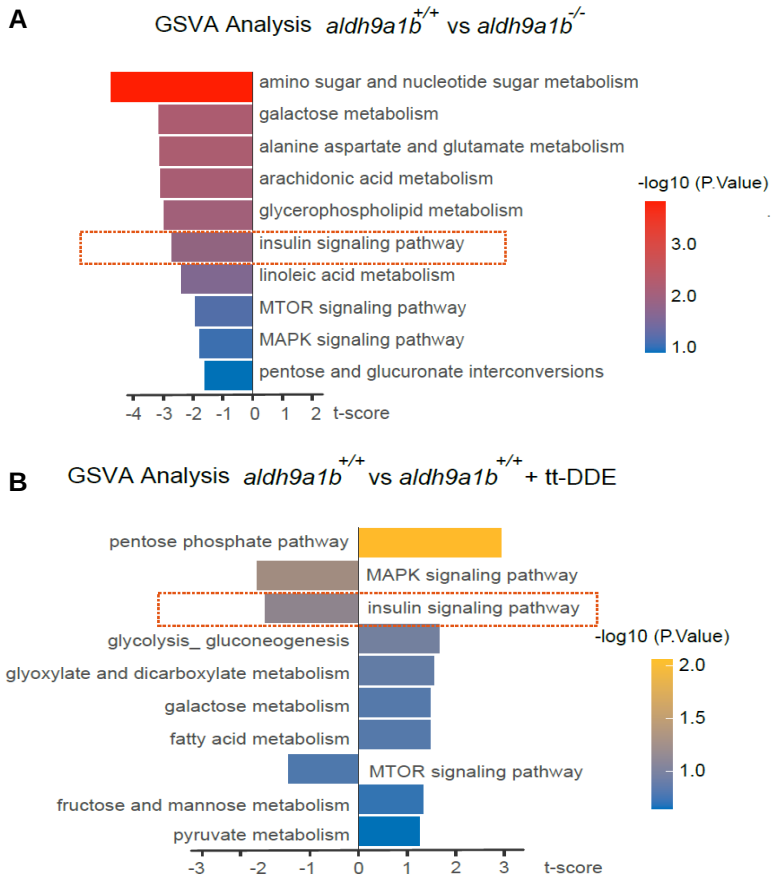

Figure 19 GSVA analysis showed downregulated insulin receptor signaling pathway in *aldh9a1b*$^{-/-}$ and in tt-DDE treated zebrafish. (A) GSVA analysis of RNA-seq exhibited top pathways associated with insulin receptor signaling and carbon metabolism in *aldh9a1b*$^{-/-}$ larvae compared to *aldh9a1b*$^{+/+}$ larvae at 5 dpf. Left, downregulated pathways; right; upregulated pathways. (B) GSVA analysis of RNA-seq data illustrated the leading 10 pathways related to insulin receptor signaling and carbon metabolism in tt-DDE treated *aldh9a1b*$^{+/+}$ larvae compared to *aldh9a1b*$^{+/+}$ controls. Left, downregulated pathways; right; upregulated pathways.

3.5 Metabolomics analysis

To elucidate the precise downstream effects of insulin signaling induced by *aldh9a1b*$^{-/-}$ and tt-DDE, a comprehensive screening of glucose-related metabolites, encompassing fatty acids and carbohydrates, was conducted using GC/MS in both larval and adult zebrafish organs. The application of Partial Least Squares-Discriminant Analysis (PLS-DA) yielded distinct separation of groups by contrasting their compositional components. This separation strongly indicated significant differences among the various experimental groups (**Figure 20A-C**). Consequently, a fold change analysis was executed to pinpoint the metabolites exhibiting differential expression.

Remarkably, nearly half of all the analyzed metabolites within the larvae, as well as the livers and muscles of adult zebrafish, underwent significant changes due to the loss of aldh9a1b and tt-DDE treatment (**Figure 20D-G)**. Moreover, enrichment analysis conducted on the screened metabolites revealed a convergence of pathways that are intricately linked to both fatty acid metabolism and glucose metabolism across all four experimental groups. This concurrence not only mirrors the findings from the RNA-seq analysis but also fortifies the notion that *aldh9a1b*$^{-/-}$ and tt-DDE treatments contribute to the alteration of glucose metabolism (**Figure 21A-D**).

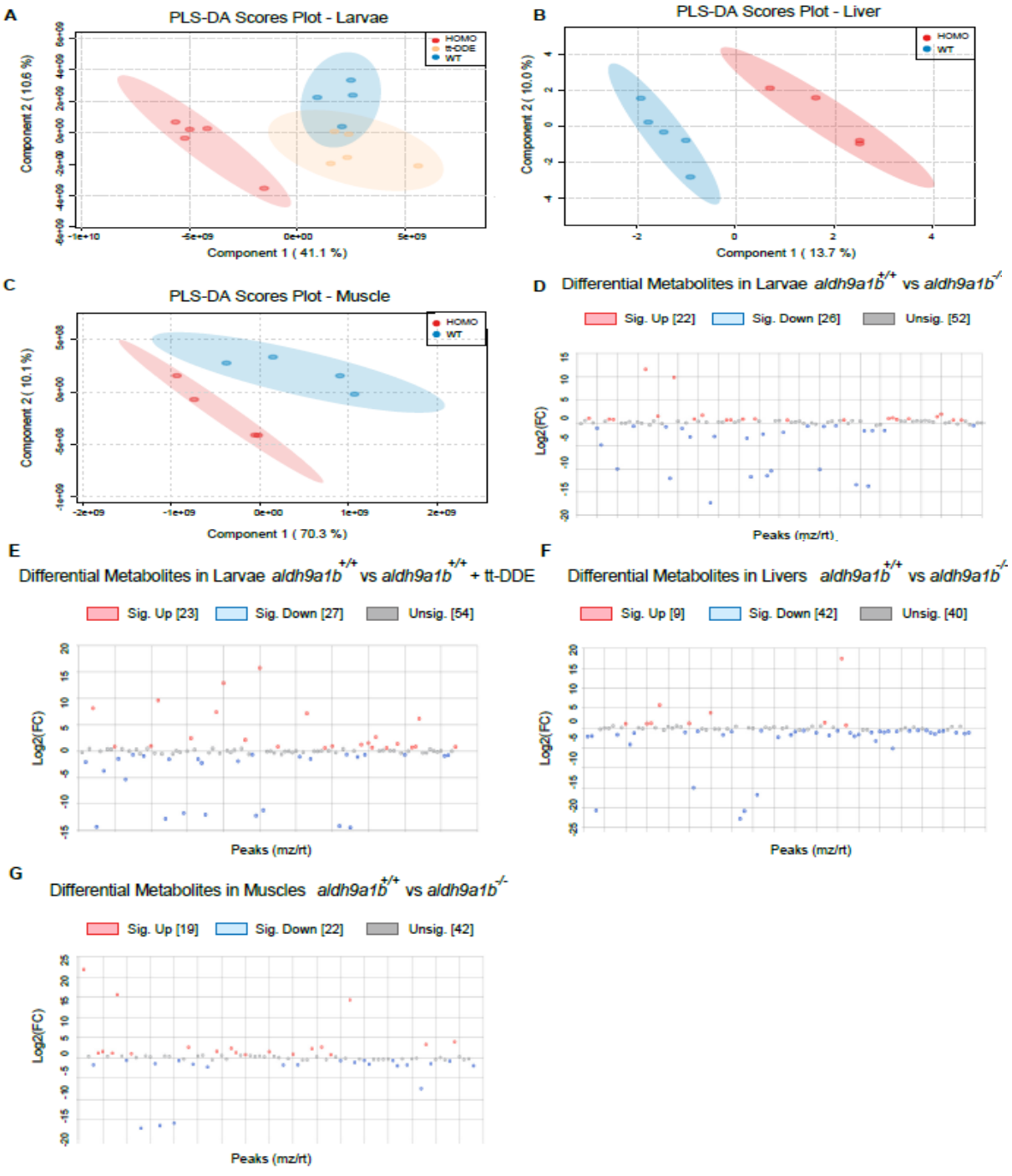

Figure 20. Altered glucose metabolism in *aldh9a1b-/-* and tt-DDE treated zebrafish (A-C) PLS-DA scores plot showed different groups in the larvae (A), livers (B) and muscles (C) of adult zebrafish. (D-G) Fold change analysis displayed differential metabolites induced by *aldh9a1b*$^{-/-}$ or tt-DDE by comparison to *aldh9ab*$^{+/+}$.

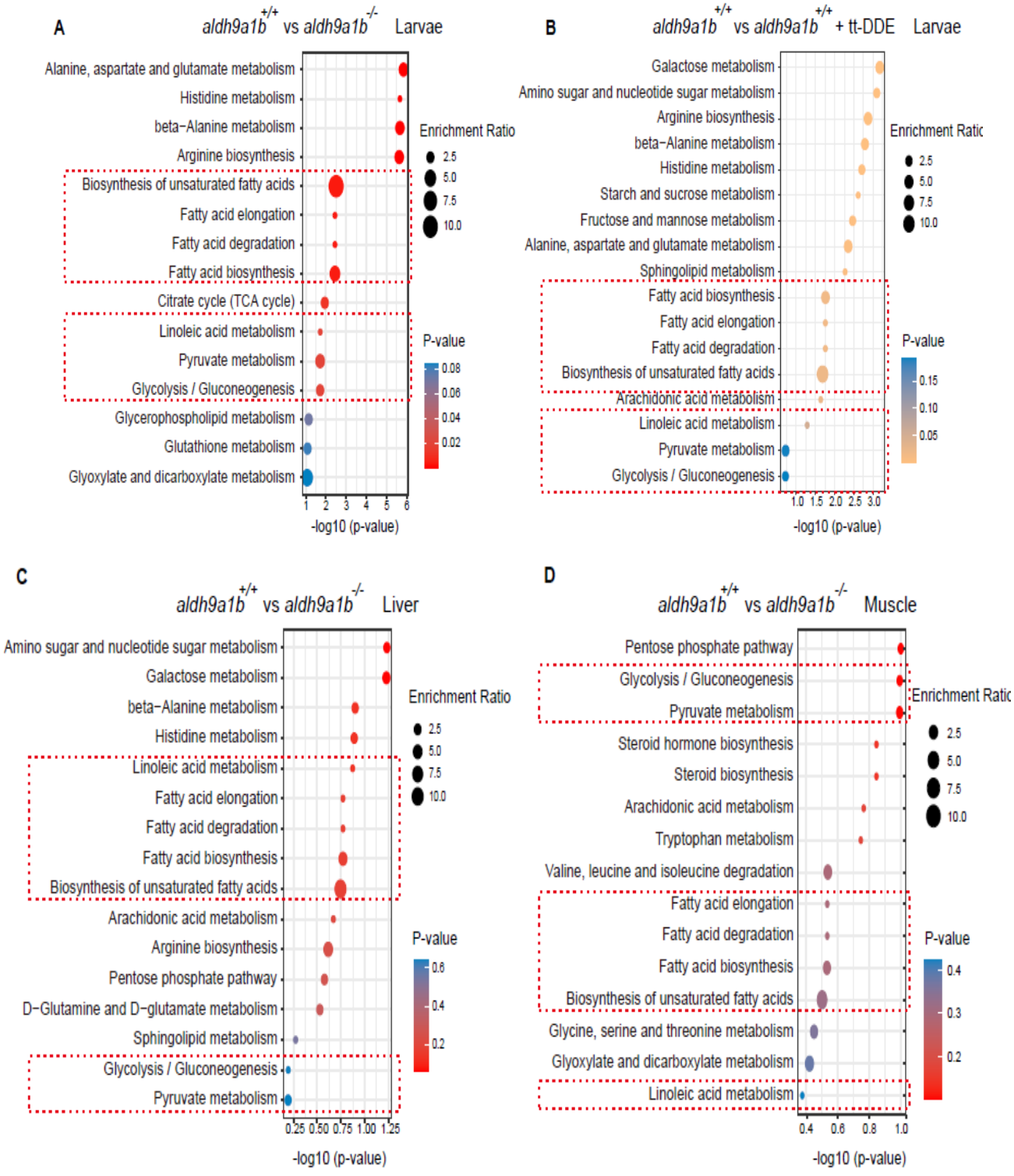

Figure 21. Altered glucose metabolism in *aldh9a1b*$^{-/-}$ and tt-DDE treated zebrafish (A) Enrichment analysis of targeted metabolomics revealed the primary carbon metabolic pathways that were altered in

aldh9a1b$^{-/-}$ larvae in comparison to *aldh9a1b*$^{+/+}$ larvae at 5 dpf. (B) Enrichment analysis of targeted metabolomics showed top carbon metabolic pathways in tt-DDE treated *aldh9a1b*$^{+/+}$ larvae compared to *aldh9a1b*$^{+/+}$ controls. (C-D) Enrichment analysis of targeted metabolomics displayed top carbon metabolic pathways in *aldh9a1b*$^{-/-}$ livers (C) and muscles (D) compared to *aldh9a1b*$^{+/+}$. Red frame represented over-lapped altered pathways among four comparisons.

3.6 *aldh9a1b* knockout and tt-DDE induced insulin resistance and disordered glucose metabolism

Integrative analysis has indicated impaired insulin signaling was underlying mechanism behind altered microvascular phenotype induced by *aldh9a1b* knockout and tt-DDE. To validate this hypothesis, the changed of insulin signaling was examined by molecular biology experiment in its important targeted organs, like muscle and liver. Moreover, glucose intolerance, as the most important consequences of impaired insulin signaling was also determined in *aldh9a1b*$^{-/-}$ adult zebrafish.

3.6.1 *aldh9a1b* knockout and tt-DDE caused insulin resistance

Insulin resistance characterizes by decreased insulin receptor, altered or unaltered insulin secretion and impaired glucose metabolism [99]. To investigate this, the expression and activity of key insulin signaling molecules such as *insulin* (*ins*), *insulin receptor* (*insr*), *insulin receptor substrate* (*irs*) and AKT were evaluated by qPCR and Western blot.

The mRNA expression of *insulin* demonstrated a notable decrease in tt-DDE treated zebrafish, whereas it remained unchanged in *aldh9a1b*$^{-/-}$ zebrafish (**Figure 22A**). The reduced *insulin* expression in tt-DDE treated larvae implies potential harm to pancreatic development, although the expression of *pdx1* (*pancreatic and duodenal homeobox 1*), a key gene in pancreatic development, remained relatively unaffected (**Figure 22B**). Additionally, *insra*, *insrb* and *irs1* exhibited a similar decline in both *aldh9a1b*$^{-/-}$ zebrafish and in tt-DDE treated larvae (**Figure 22C**). Notably, Akt phosphorylation, a critical downstream mediator of insulin signaling, displayed a significant reduction in both experimental groups (**Figure 22D-E**).

Given that liver and muscle are pivotal insulin target organs, and considering the liver's high expression of *aldh9a1b*, *ins* expression was further examined in these organs. Although *ins* mRNA level remained relatively unchanged, the expressions of *insra*,

insrb, *irs1* and also Akt phosphorylation resembled the findings in the larvae, exhibiting a substantial decrease (**Figure 23A-F**).

Lastly, *nos2b*, acting as a homologue of human endothelial nitric oxide synthase (eNOS) and regulating endothelial function, displayed decreased expression in both *aldh9a1b*$^{-/-}$ zebrafish and tt-DDE treated larvae [100] (**Figure 24A-C**). Yet, VEGF, an angiogenic factor, did not exhibit a significant increase in the *aldh9a1b*$^{-/-}$ mutants (**Figure 24D**).

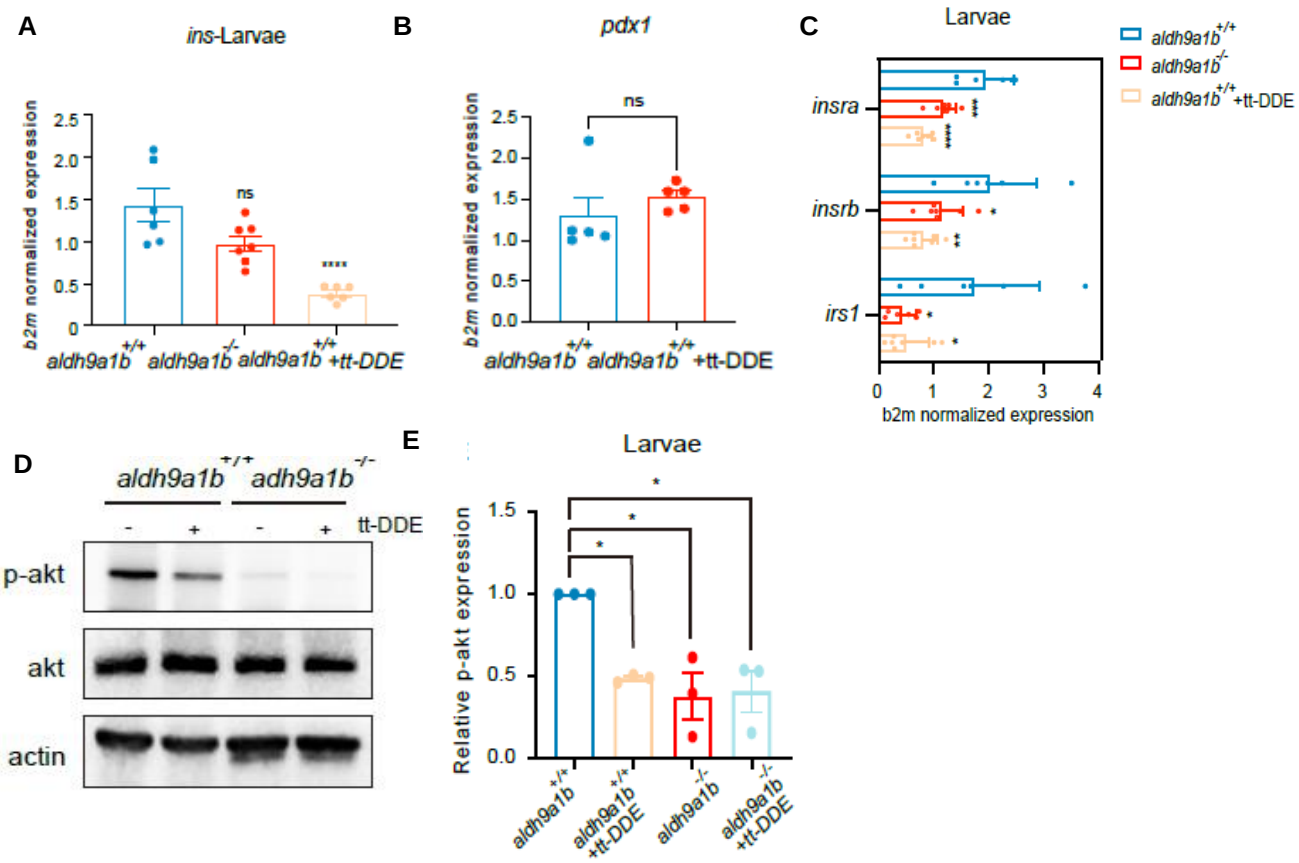

Figure 22. Impaired insulin signaling in *aldh9a1b*$^{-/-}$ and tt-DDE treated larvae (A) The expression of *ins* mRNA was significantly decreased in tt-DDE treated *aldh9a1b*$^{+/+}$ with a slight reduction observed in *aldh9a1b*$^{-/-}$ larvae, n=6 and 7. (B) The mRNA expression of *pdx1* remained unaltered in tt-DDE treated *aldh9a1b*$^{+/+}$ compared to *aldh9a1b*$^{+/+}$ larvae, n=5. (C) mRNA expression of *insra*, *insrb* and *irs1* displayed significant decreases in both *aldh9a1b*$^{-/-}$ larvae and tt-DDE treatments at 5dpf, n=6 and 7. (D-E) Representative Western blot (D) and corresponding quantification (E) indicated reduced p-AKT activation in both *aldh9a1b*$^{-/-}$ larvae and tt-DDE treatments at 5dpf. Total Akt protein was utilized as a loading control, n=3 Error bars represent ± SD values. Statistical analysis was performed by Student's t-test and one-way ANOVA, *p < 0.05, **p < 0.01, ***p < 0.001, ****p < 0.0001.

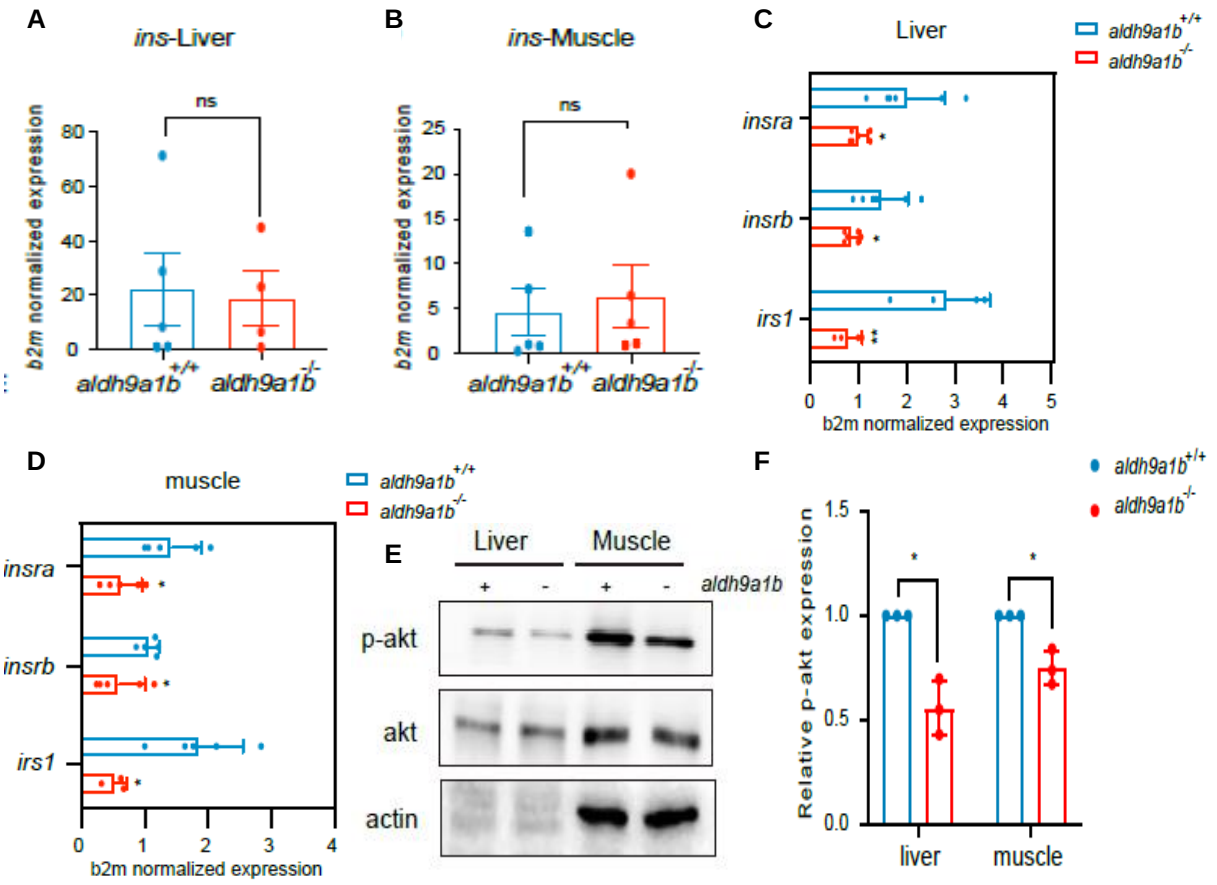

Figure 23. Impaired insulin signaling in *aldh9a1b*$^{-/-}$ adult zebrafish. (A-B) Expression of *ins* mRNA remained unchanged in the livers (A) and muscles (B) of *aldh9a1b*$^{-/-}$ zebrafish, n=5. (C-D) mRNA expression of *insra*, *insrb* and *irs1* significantly decreased in both livers (C) and muscles (D) of *aldh9a1b*$^{-/-}$ adult zebrafish, n=6 and 5. (E-F) Representative Western blot and corresponding quantification revealed reduced p-AKT phosphorylation in *aldh9a1b*$^{-/-}$ in livers and muscles. Total Akt protein served as a loading control, n=3. Error bars represent mean ± SD values. Statistical analysis was performed by Student's t-test and one-way ANOVA, *p < 0.05, **p < 0.01, ***p < 0.001, ****p < 0.0001.

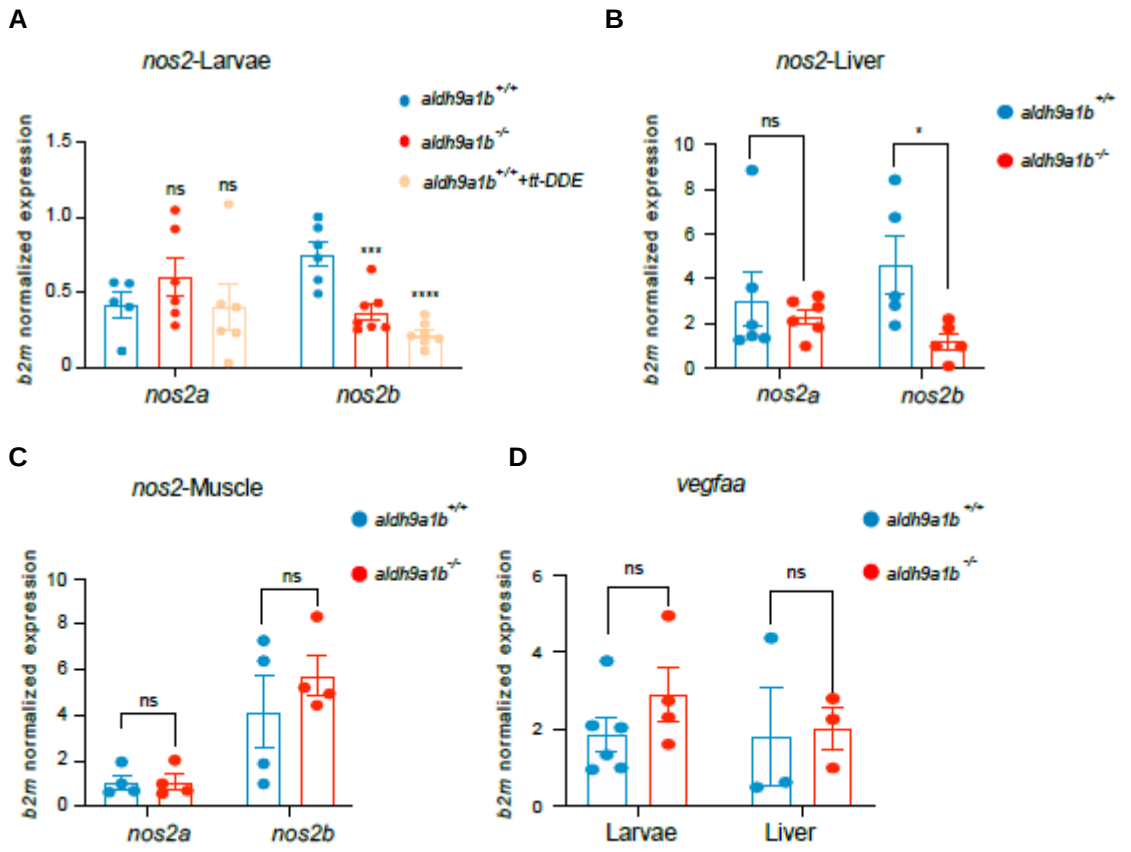

Figure 24. Modified downstream insulin signaling in *aldh9a1b*$^{-/-}$ zebrafish. (A) The *nos2a* mRNA level demonstrated no significant change among the three groups, while *nos2b* displayed a significant decrease in both *aldh9a1b*$^{-/-}$ and tt-DDE treated larvae, n=6 and 7. (B-C) neither *nos2a* nor *nos2b* exhibited significant alterations in the livers and muscles of *aldh9a1b*$^{-/-}$ zebrafish, n=6 and 4. (D) mRNA expression of *vegfaa* remained unchanged in the larvae and livers of *aldh9a1b*$^{-/-}$ zebrafish, n=6 and 4. mRNA Expression was quantified by RT-qPCR and normalized to b2m. Each datapoint in this figure represented 20 larvae or one fish. Error bars represent mean ± SEM values. Statistical analysis was performed by Student's t-test, one-way ANOVA. ns, not significant; ****p < 0.0001.

3.6.2 tt-DDE modified insulin receptor tyrosine kinase domain

Furthermore, to investigate the regulatory mechanism of tt-DDE on the insulin receptor, we performed docking analysis using AutoDock Vina. Linsitinib (OSI-906), a classic nonpeptide small molecule, inhibits the tyrosine kinase activity of the insulin receptor and was used as a positive control in this analysis [101]. The docking model revealed that tt-DDE shared same binding pocket with linsitinib and bound to the insulin receptor with a low binding energy of -4.8 kcal/mol and formed three visible hydrogen bonds with PHE1151, GLY1152, and MET1153, indicating a highly stable binding between tt-DDE and the insulin receptor **(Figure 25).**

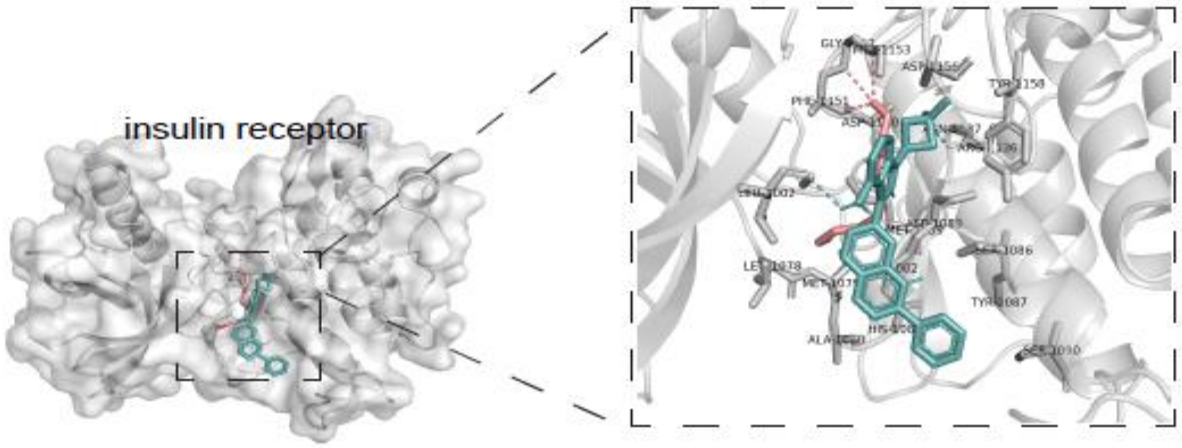

Figure 25. tt-DDE modified insulin receptor. Docking analysis showed tt-DDE bound to PHE1151, GLY1152 and MET1153 of insulin receptor.

3.6.3 *aldh9a1b* knockout and tt-DDE increased glucose level

Disordered glucose level is most important signature of diabetes. To study the effect of *aldh9a1b* knockout and tt-DDE on glucose level, both fasting glucose and 2-hour postprandial glucose level were detected in zebrafish adults and larvae. The whole-body glucose in larvae exhibited an increasing trend in both *aldh9a1b*$^{-/-}$ mutants and in tt-DDE treated animals, but a significant increase was observed only in tt-DDE treated larvae **(Figure 26A).** Yet, in adult *aldh9a1b*$^{-/-}$ zebrafish, an increase in postprandial blood glucose levels was noted. Interestingly, overnight-fasted *aldh9a1b*$^{-/-}$ zebrafish did not display significant alterations in blood glucose levels, indicating impaired glucose homeostasis in adult *aldh9a1b*$^{-/-}$ zebrafish and in tt-DDE treated larvae **(Figure 26B).**

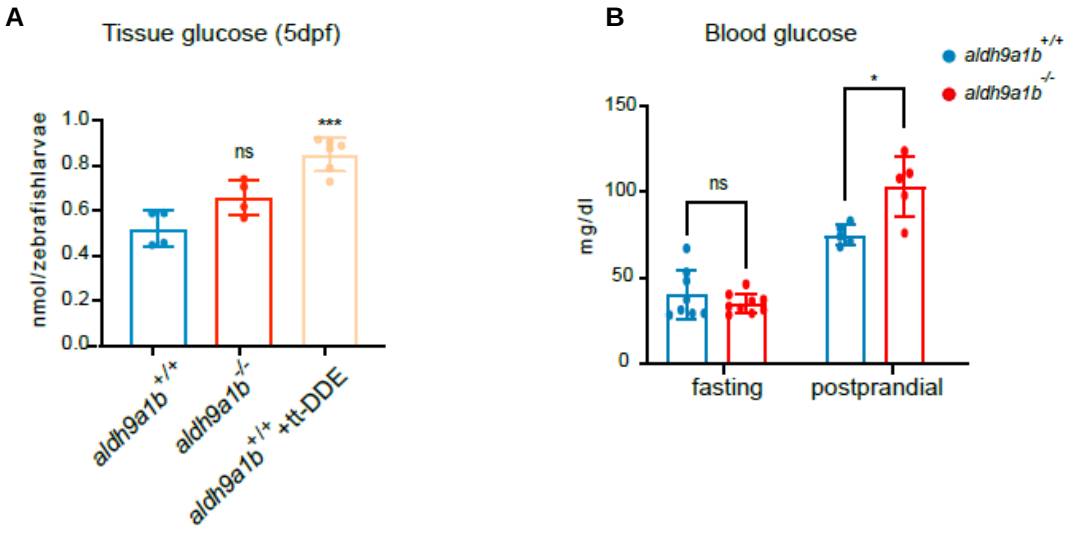

Figure 26 Impaired glucose tolerance induced by *aldh9a1b* knockout. (A) Whole-body glucose levels in larvae exhibited an increased trend in tt-DDE treated *aldh9a1b*$^{+/+}$ larvae at 5 dpf. In *aldh9a1b*$^{-/-}$ larvae, whole-body glucose was also increased, but not significantly, n=4 and 6. (B) Blood glucose of *aldh9a1b*$^{-/-}$ adults did not show any alteration in fasting state but was significantly increased in the 2-hour postprandial state. Each datapoint in this figure represented 20 larvae or one fish. The bars indicate mean ± SD values. Statistical analysis was performed by Student's t-test and one-way ANOVA, **p < 0.01, ***p < 0.001.

3.6.4 *aldh9a1b* knockout and tt-DDE impaired gluconeogenesis

The glucose balance mainly regulated by glycolysis, gluconeogenesis and glycogenesis. To further analyze the glucose metabolism in *aldh9a1b*$^{-/-}$ zebrafish, expression of key enzymes of the glucose metabolism were investigated. The rate limiting enzymes for glycolysis are *hexokinase 1 (hk1)*, *glucokinase* (*gck*, also termed *hk4*) and *pyruvate kinase L/R* (*pklr*); for gluconeogenesis are *glucose-6-phosphatase catalytic subunit 1a* (*g6pc1a.1*), *fructose-1,6-bisphosphatase 1a* (*fbp1a*) and *phosphoenolpyruvate carboxykinase 1* (*pck1*); for glycogenesis are *UDP-glucose pyrophosphorylase 2a* (*ugp2a*) and *glycogen synthase 2* (*gys2*) (**Figure 27A**). *aldh9a1b*$^{-/-}$ larvae exhibited notable increase in the expression of *g6pc1a.1* and *pck1*, while manifesting a reduction in the expression of *ugp2a*. These alterations signify an elevation in gluconeogenic activity and a concurrent decline in glycogenic processes. Additionally, the collected data revealed a rise in glucose production coupled with a decrease in glucose utilization. This phenomenon provides an explaination for the observed hyperglycemia in *aldh9a1b*$^{-/-}$ mutants and in tt-DDE treated larvae (**Figure 27B**). Moreover, a considerable increase in the levels of *glucose transporter 2* (*GLUT2*), an insulin-independent glucose transporter, as detected. This could be interpreted as a plausible response to the hyperglycemic conditions in *aldh9a1b*$^{-/-}$ zebrafish and in the tt-DDE group (**Figure 27B**). In the context of adult *aldh9a1b*$^{-/-}$ zebrafish, the liver, which serves as the pivotal organ for regulating glucose, demonstrated similar modifications in gluconeogenic activity as observed in larvae (**Figure 27C**). Conversely, within the muscle tissue, substantial alterations were noted in glycolytic processes (**Figure 27D**).

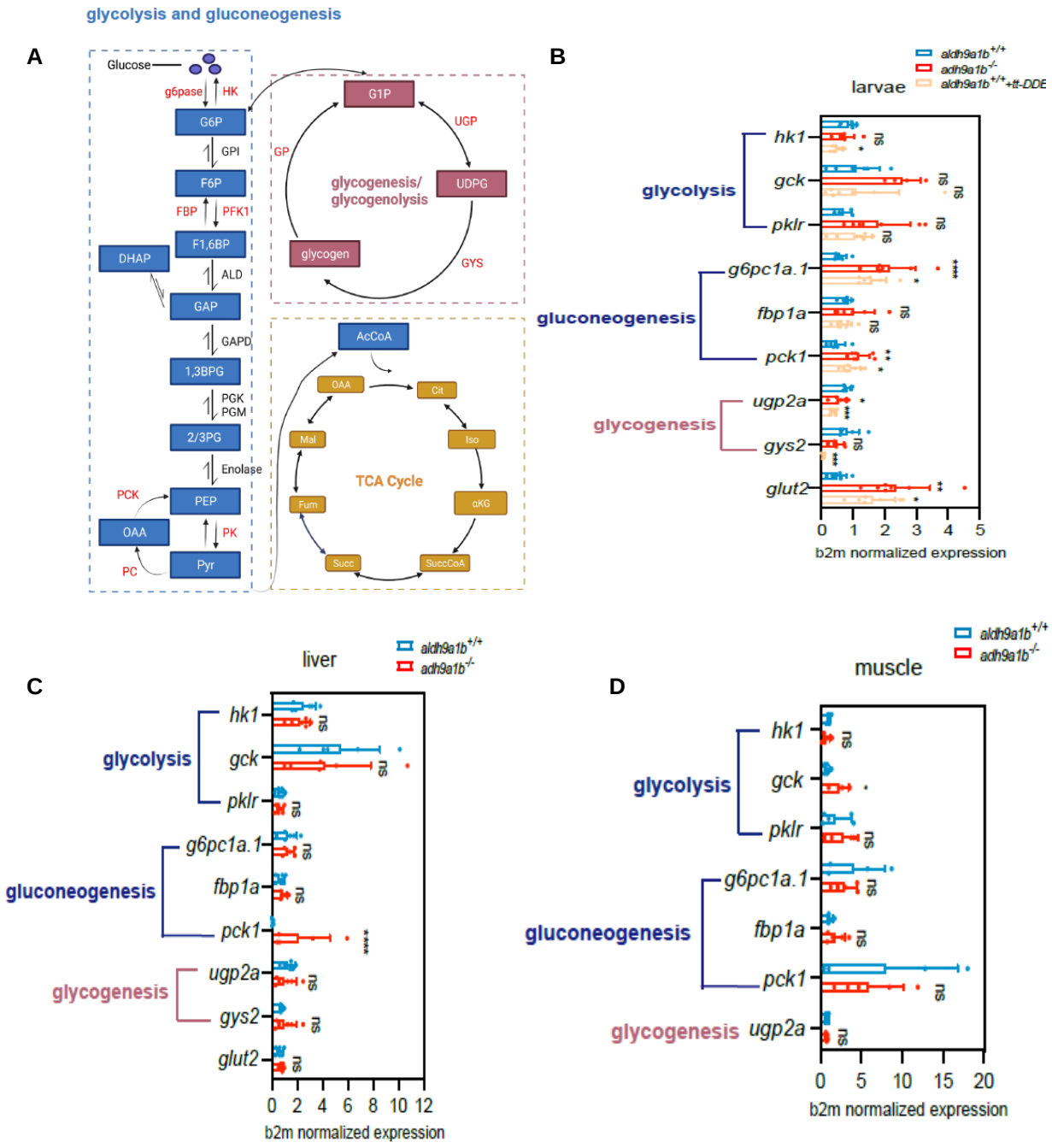

Figure 27 *aldh9a1b* knockout and tt-DDE altered gluconeogenesis in the larvae and adults. (A) Graphical overview of key biological processes in glucose metabolism. (B) Alterations in mRNA levels of critical enzymes related to glycolysis, gluconeogenesis, and glycogenesis. These changes were evident in both *aldh9a1b*$^{-/-}$ and in tt-DDE treated *aldh9a1b*$^{+/+}$ larvae at 5dpf, n=6 and 7. (C-D) Alterations in mRNA levels of critical enzymes related to glycolysis, gluconeogenesis, and glycogenesis in the livers (C) and muscles (D) of *aldh9a1b*$^{-/-}$ zebrafish, n=6 and 5. mRNA Expression was quantified by RT-qPCR and normalized to b2m. Each datapoint in this figure represented 20 larvae or one fish. The bars indicate mean ± SD values. Statistical analysis was performed by Student's t-test and one-way ANOVA, *p < 0.05, **p < 0.01, ***p < 0.001, ****p <0.0001.

3.7 Pharmacological rescue study in *aldh9a1b*$^{-/-}$ and tt-DDE treated zebrafish

All the above data has demonstrated downregulated insulin signaling and impaired glucose metabolism could be responsible for the increased retina vasculature in *aldh9a1b*$^{-/-}$ zebrafish and in tt-DDE treated animals. To validate the results further, several anti-diabetic drugs were used to perform rescue experiments.

Metformin and rosiglitazone are first-line insulin receptor sensitizer in type 2 diabetes. Besides, previous studies suggested 10 µmol metformin and 1µmol rosiglitazone could rescue hyperglycemia in zebrafish [102-104]. Thus, up to 50 µmol metformin and 10 µmol rosiglitazone were selected to confirm the effective concentrations for rescue experiments. The safe dose was analyzed based on their effect on survival rate and development of *aldh9a1b*$^{+/+}$ zebrafish. Metformin concentrations between 0 and 50 µmol didn't have any toxic effects, and 10 µmol showed the best reversal of the tt-DDE-induced changes to the hyaloid vasculature (**Figures 28**). Zebrafish development was also unaffected by up to 10 µmol rosiglitazone and 1 µmol rosiglitazone also caused strong improvement of numbers of sprouts and branches in the hyaloid vasculature (**Figures 29**).

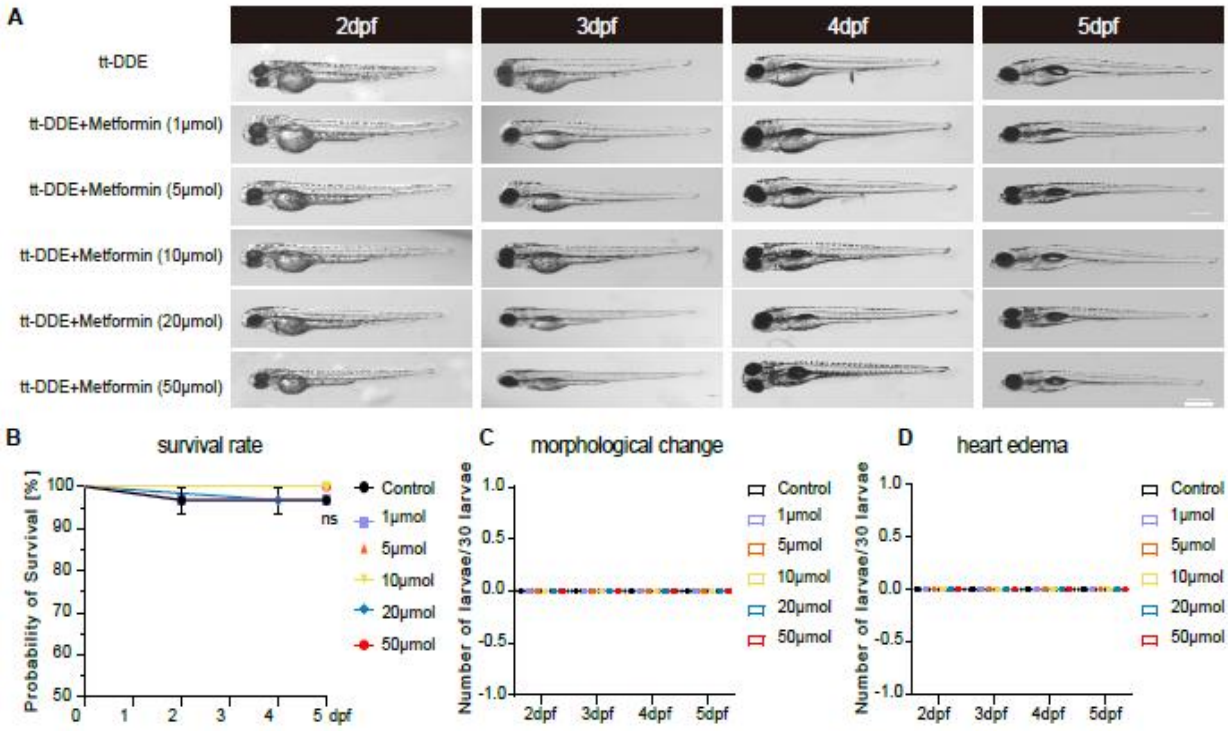

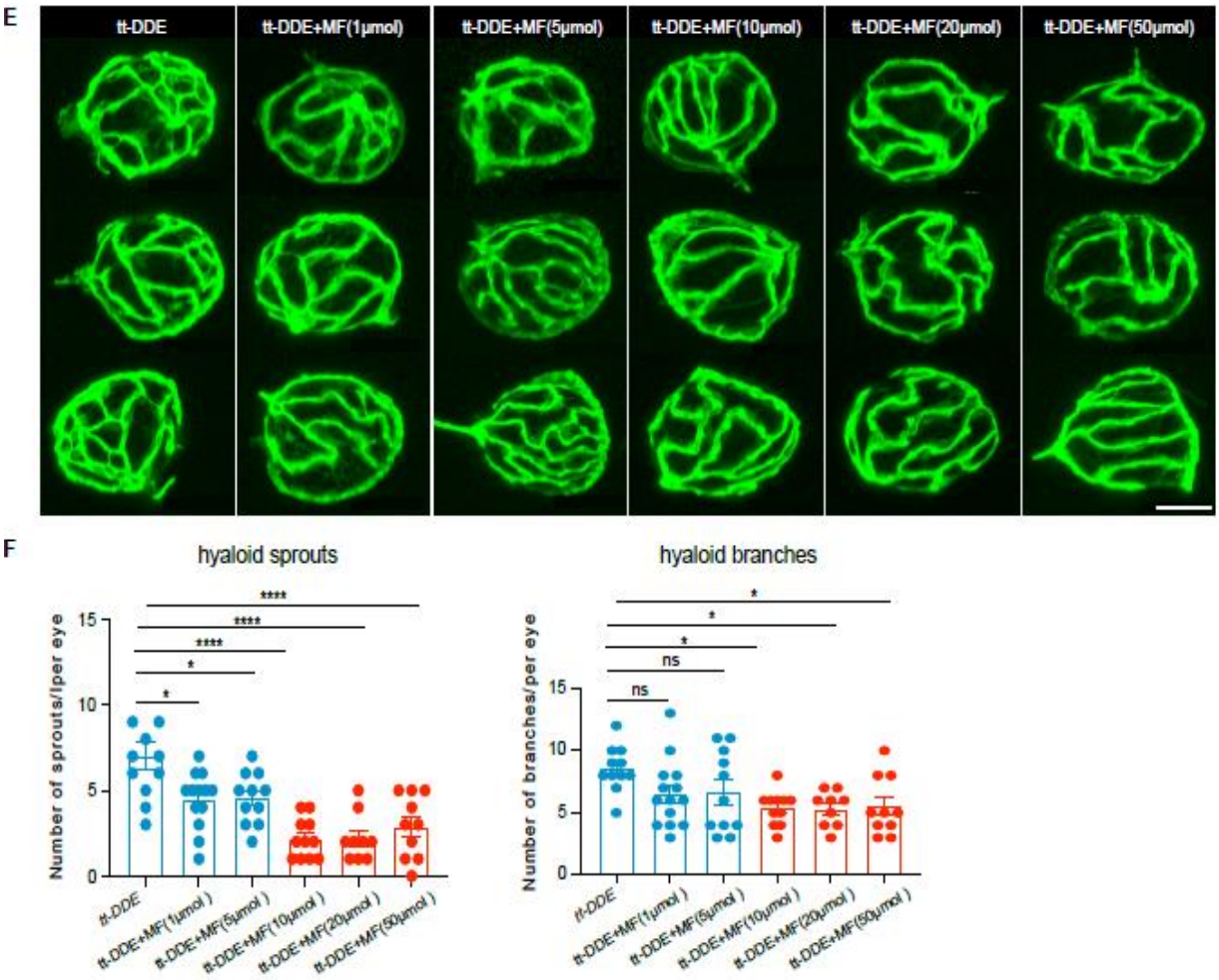

Figure 28 Morphological and hyaloid vascular rescue in *aldh9a1b*$^{+/+}$ larvae co-treated with tt-DDE and metformin (A) Representative microscopic images of zebrafish larvae between 2 dpf and 5 dpf co-treated with 8 µmol tt-DDE and 0-50 µmol MF. White bar, 200 µm. (B) Quantification of survival rates across the different experimental groups revealed no significant alterations. (C) Quantification of morphology change showed normal morphology between different groups. (D) Quantification of cardiac edema showed normal heart development across all the groups. (E) Representative confocal images of hyaloid vasculature showed beneficial effects in zebrafish larvae co-treated with 8 µmol tt-DDE and 0-50 µmol MF at 5dpf. White scale bar =50 µm. (F) Quantification of hyaloid branchpoints and sprouts formation showed increased angiogenic vasculature caused by tt-DDE treatment, which can be rescued by 1-50 µmol MF. One datapoint means one hyaloid per larva. The bars indicate mean ± SEM values. Statistical analysis was performed by one-way ANOVA, two-way ANOVA and logrank test. ns = not significant, *p < 0.05. MF, metformin.

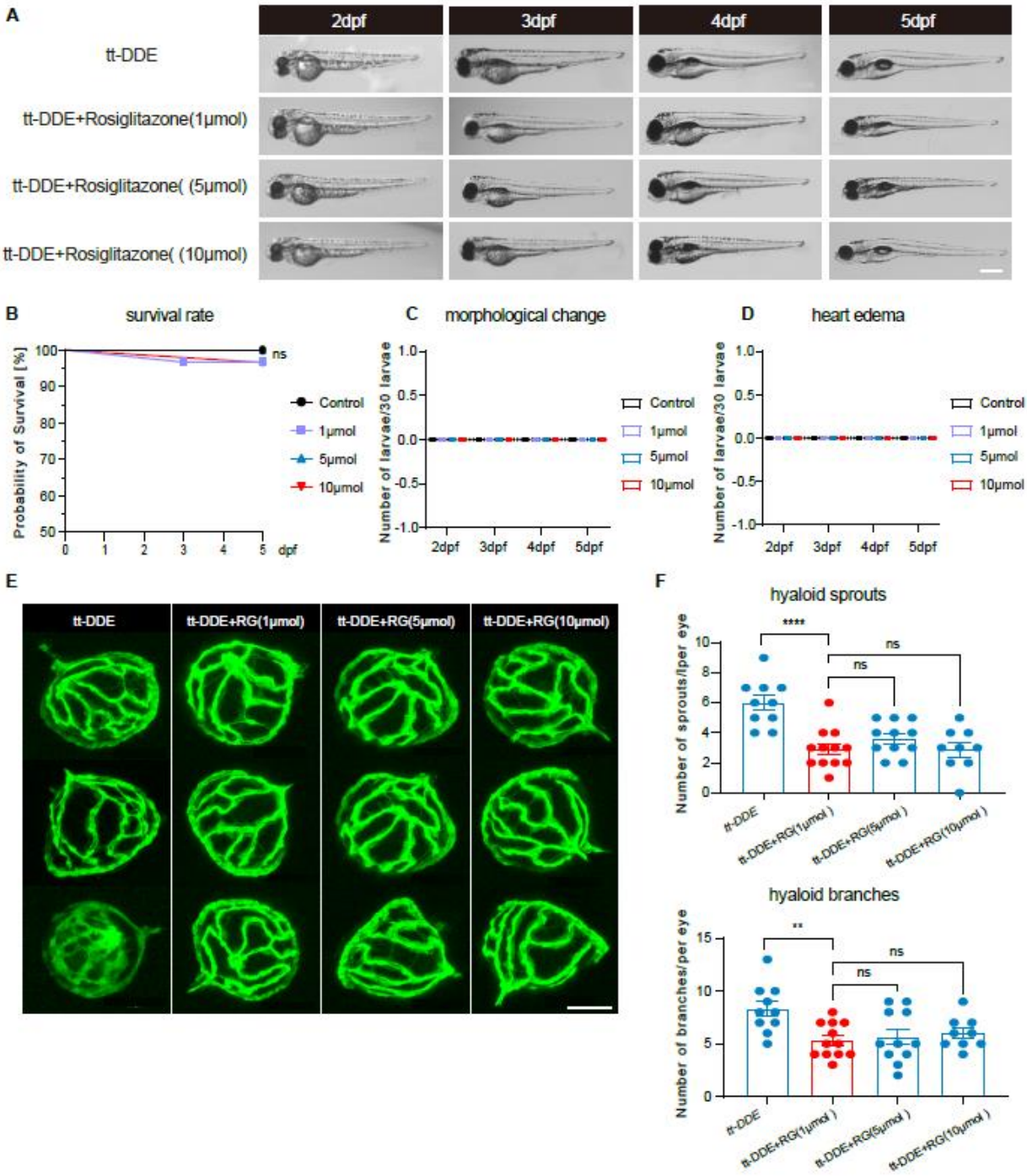

Figure 29 Morphological and hyaloid vascular rescue in *aldh9a1b*$^{+/+}$ larvae co-treated with tt-DDE and rosiglitazone (A) Representative microscopic images of zebrafish larvae between 2 dpf and 5 dpf co-treated with 8 μmol tt-DDE and 0-10 μmol RG. White bar, 200 μm. (B) Quantification of survival rates showed no significant change between these groups. (C) Quantification of morphology change showed no significant alterations across all the groups. (D) Quantification of heat edema showed normal heart morphology between different groups. (E) Representative confocal images of hyaloid vasculature showed rescue of vascular alterations in zebrafish larvae co-treated with 8 μmol tt-DDE and 0-10 μmol RG at 5dpf. White scale bar = 50 μm. (F) Quantification of hyaloid branchpoints and sprouts formation showed increased angiogenic vasculature caused by tt-DDE, which can be rescued by 1-10 μmol rosiglitazone. One datapoint means one hyaloid per larva. The bars indicate mean ± SEM values.

Statistical analysis was performed by one-way ANOVA, two-way ANOVA and logrank test. ns = not significant, **p < 0.01, ****p < 0.0001. RG, rosiglitazone.

3.7.1 Increased hyaloid vasculature induced by *aldh9a1b*$^{-/-}$ can be rescued by metformin, rosiglitazone and carnosine

Lastly. carnosine, a naturally anti-oxidant dipeptide, which can protect against the formation of advanced glycation and lipoxidation end-products, were applied because it can rescue glucose-induced microvascular alteration in zebrafish [13, 31, 105]. Therefore, we incubated *aldh9a1b*$^{-/-}$ larvae and tt-DDE treated *aldh9a1b*$^{+/+}$ zebrafish larvae with 10 µmol metformin, 1 µmol rosiglitazone, and 10 mmol carnosine. In *aldh9a1b*$^{-/-}$ zebrafish, the altered hyaloid alterations were successfully reversed by metformin, rosiglitazone, and carnosine, while metformin and rosiglitazone provided the strongest rescue effects. (**Figure 30A-B)**.

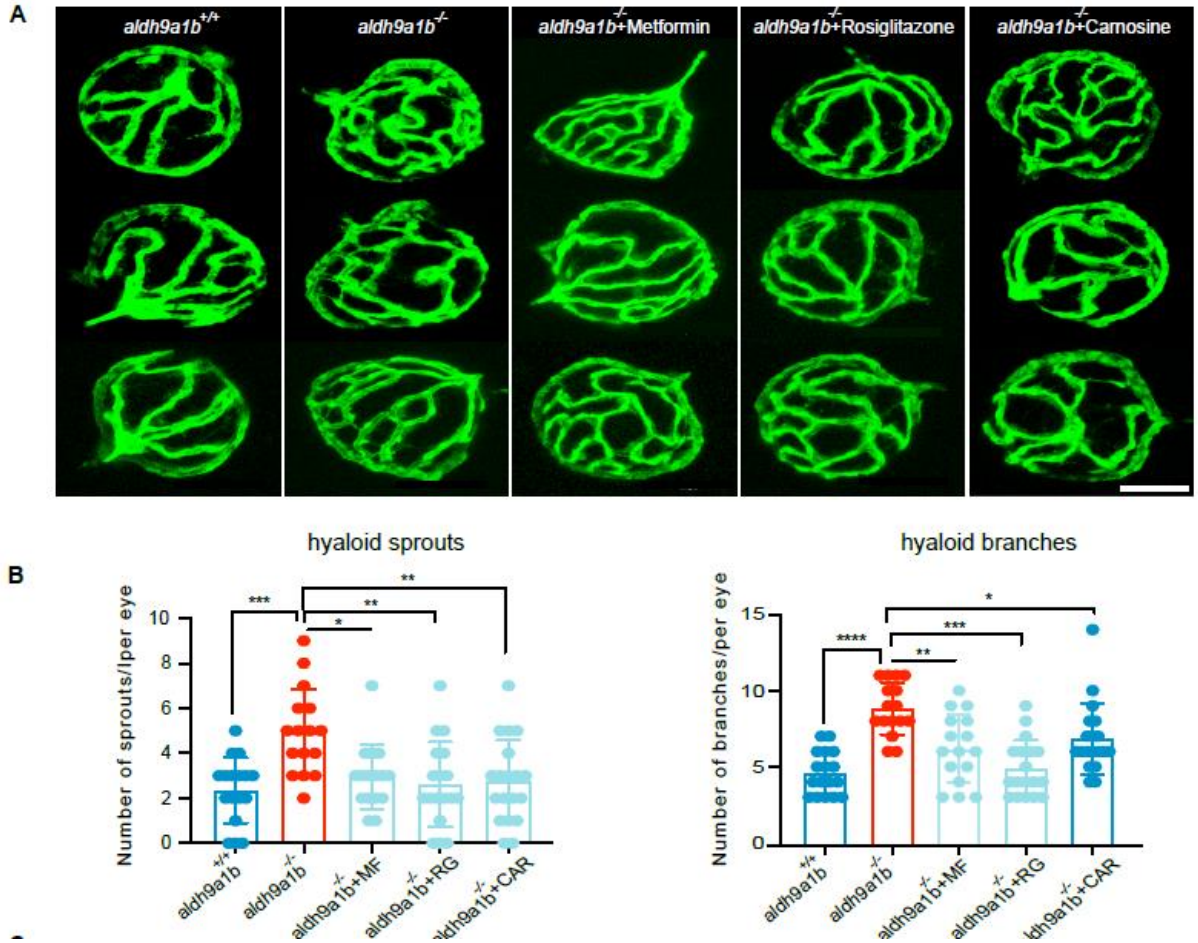

Figure 30. Altered angiogenic hyaloid vasculature caused by *aldh9a1b* knockout can be rescued by metformin, rosiglitazone and carnosine (A) Representative confocal images of hyaloid vasculature showed vascular alterations and beneficial effects in *aldh9a1b-/-* zebrafish larvae treated with MF, RG,

and CAR. White scale bar = 50 µm. (B) Quantification of hyaloid branchpoints and sprouts formation showed increased angiogenic vasculature in *aldh9a1b-/-* can be rescued by metformin, rosiglitazone and carnosine. One datapoint means one hyaloid per larva. One datapoint means one hyaloid per larva. The bars indicate mean ± SD values. Statistical analysis was performed by one-way ANOVA. *p < 0.05, **p < 0.01, ***p < 0.001, ****p < 0.0001. MF, metformin; RG, rosiglitazone; CAR, carnosine.

3.7.2 Increased hyaloid vasculature induced by tt-DDE can be rescued by metformin, rosiglitazone and carnosine

In tt-DDE treated larvae, abnormal hyaloid vasculature could also be reversed by metformin, rosiglitazone and carnosine, while metformin worked most effectively among them on the whole (**Figures 31A-B)**. In conclusion, the successful rescue effects of the anti-hyperglycemic drugs validated further that the increased angiogenic vasculature in *aldh9a1b*$^{-/-}$ mutants and in tt-DDE animals is caused by insulin resistance.

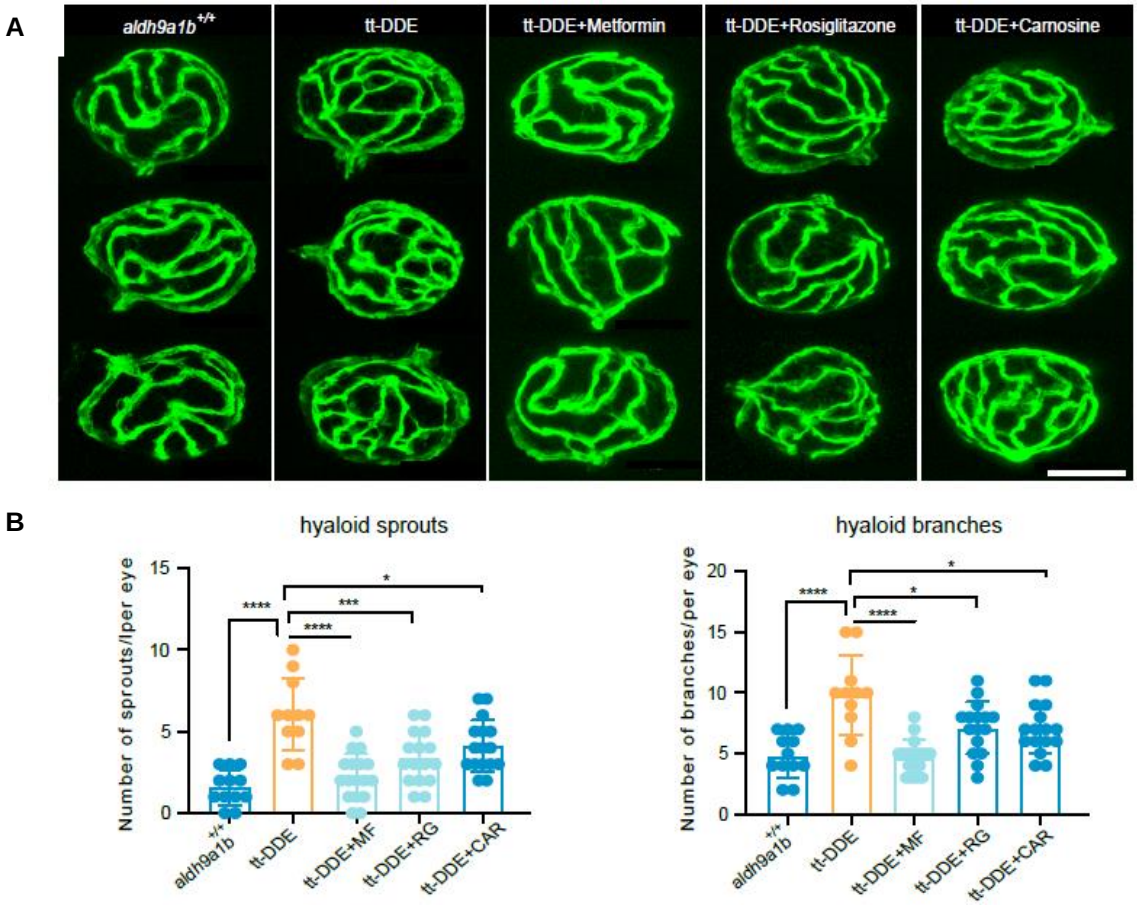

Figure 31. Altered angiogenic hyaloid vasculature caused by tt-DDE treatment can be rescued by metformin, rosiglitazone and carnosine (A) Representative confocal images of hyaloid vasculature showed vascular alterations and beneficial effects in *aldh9a1b+/+* larvae co-incubated with tt-DDE and MF, RG, and CAR. White scale bar = 50 µm. (B) Quantification of hyaloid branchpoints and sprouts

formation showed that increased angiogenic vasculature induced by tt-DDE can be rescued by metformin, rosiglitazone and carnosine. One datapoint means one hyaloid per larva. The bars indicate mean ± SD values. Statistical analysis was performed by one-way ANOVA. *p < 0.05, **p < 0.01, ***p < 0.001, ****p < 0.0001. MF, metformin; RG, rosiglitazone; CAR, carnosine.

4. Discussion

In this study, we established an aldh9a1b knockout animal model for the first time and demonstrated that accumulation of tt-DDE leads to a decrease in insulin signaling, an increase in gluconeogenesis, a disorder of fatty acid metabolisms and consequently to a microvascular damage, which could be rescued by several drugs currently used to treat patients with diabetes. The study further proved that tt-DDE could elicit all the effects observed in the aldh9a1b knockout, further supporting the notion that this RCS is the main target of Aldh9a1b.

4.1 ALDH9a1b act as a novel detoxification system of tt-DDE

Aldehydes constitute a subgroup of RCS characterized by the presence of a carbonyl carbon atom bonded to at least one hydrogen atom and various additional functional groups. Aldehydes can be categorized into distinct subclasses, including: (i) short-chain aldehydes, such as formaldehyde and acetaldehyde; (ii) long-chain aldehydes, like hexanal and nonanal; (iii) aromatic aldehydes, for instance, cinnamaldehyde and benzaldehyde; (iv) α,β-unsaturated aldehydes, including tt-DDE and acrolein; and (v) α-oxoaldehydes, such as glyoxal and glycolaldehyde [30]. It is important to note that many aldehydes are inherently toxic due to their reactivity as electrophiles, leading to the formation of adducts with proteins or DNA, which impairs their biological functions. Consequently, understanding the intrinsic detoxification mechanisms for these aldehydes is crucial for maintaining normal physiological activities.

Specifically, in the case of α,β-unsaturated aldehydes, previous research has revealed that 4- HNE is metabolized by both phase I and phase II enzymes [106]. In more detail, HNE is efficiently detoxified through a Michael addition with glutathione, a reaction that can occur spontaneously but is catalyzed by glutathione S-transferases [106, 107]. Phase I metabolic reactions can involve either the reduction of the carbonyl group to an alcohol or its oxidation to an acid, mediated by alcohol dehydrogenase or AKR, ALDH, respectively [106, 108]. It is worth noting that these redox reactions can also involve glutathione (GSH) conjugates. The primary metabolite of HNE found in urine is the reduced mercapturic acid of HNE, known as 1,4-dihydroxynonane mercapturic acid [108].

The prominence of tt-DDE as a prevalent α,β-unsaturated aldehyde in the diet underscores the critical importance of comprehending its detoxification mechanisms[109, 110]. Previous reports have suggested potential detoxification pathways for tt-DDE, similar to those observed for other α,β-unsaturated aldehydes, involving GSH

conjugation and aldehyde oxidation[74, 111]. However, the exact pathway and specific ALDHs involved remain to be determined. In the present study, we introduce an innovative approach by utilizing an *aldh9a1b* knockout zebrafish model. This model, characterized by reduced ALDH enzyme activity in the context of tt-DDE exposure, has revealed significant findings. Specifically, elevated levels of cysteine conjugates (cys-con) and GSH-DDE were observed in zebrafish larvae, livers, and muscles, which correlate with *aldh9a1b* expression in these organs and suggest that ALDH9a1b is the specific enzyme responsible for tt-DDE detoxification. Furthermore, shared phenotypic and molecular changes resulting from both *aldh9a1b* knockout and in vitro tt-DDE exposure were observed. This study represents pioneering work in identifying ALDH9a1b as a pivotal component of the detoxification system for tt-DDE, providing valuable insights into the function of ALDH9a1b. Moreover, it also expands our knowledge of detoxification mechanisms for α,β-unsaturated aldehydes and offers a potential target for therapeutic interventions.

4.2 tt-DDE impairs glucose metabolism

A solitary prior study has indicated an association between tt-DDE and glucose metabolism. This particular investigation involved Sprague-Dawley (SD) rats that were administered a diet rich in tt-DDE for a duration of 28 days. The results of this study showed that an intake of 1000 mg tt-DDE/kg body weight led to an increase in fasting blood glucose levels, though the increase was not statistically significant (7.1 ± 0.51 mg/dl compared to 6.3 ± 0.47 mg/dl)[81]. Our research aligns with this pattern as it unveils heightened fasting blood glucose levels. Additionally, our study introduces novel findings, including a substantial rise in 2-hour postprandial glucose levels and a decrease in insulin sensitivity, which were substantiated through a combination of transcriptome and metabolomics analysis. Notably, our research reveals a reduction in insulin receptor levels (including *insra* and *insrb*) in zebrafish larvae, livers, and muscles, which corresponds with an increase in tt-DDE metabolites, namely cys-con and GSH-DDE. This points to a disruption in glucose metabolism. Intriguingly, different organs displayed distinct patterns in key processes of glucose metabolism. Genes associated with gluconeogenesis and glycogenesis, including *g6pc1a*.1, *pck1*, *ugp2a*, and *gys2*, exhibited significant changes, whereas in the livers, only gluconeogenesis, specifically *pck1*, was affected.

Furthermore, tt-DDE, recognized as a reactive Michael acceptor, can modify proteins and DNAs such as cytochrome c, apo-SOD1, and dGuo[112-119]. This modification

process can cause DNA damage, oxidative stress, and mitochondrial dysfunction, ultimately resulting in disordered energy metabolism. Specifically, tt-DDE preferred the residue of cysteine, histidine and lysine and formed covalent binding to disrupt the normal function of cytochrome c and apo-SOD1. In recent years, molecular docking has emerged as a leading technology to analyze the interaction between compounds and proteins [120]. Therefore, we performed a molecular docking analysis to investigate the potential interaction between tt-DDE and the insulin receptor. We focused on the intra-cellular tyrosine kinase domain, a functional domain in the insulin receptor, and explored the potential binding site in its activation loop (residues 1149–1170, which contain the phosphorylation sites Tyr1158, Tyr1162, and Tyr1163) [121]. Since tt-DDE undergoes Michael addition, with the reaction predominately occurring at CYS, HIS, and LYS residues and insulin receptor, being a tyrosine kinase, has fewer targeted residues, our investigation did not reveal any evidence of covalent binding within this specific loop. However, our docking analysis suggests a possible stable polar binding between tt-DDE and the insulin receptor via three hydrogen bonds, offering a different perspective of direct receptor modification by tt-DDE. However, the likelihood of a Michael adduct formation between tt-DDE and the insulin receptor remains plausible. A thorough comprehension of these mechanisms and further exploration of protein or DNA modifications, both in vivo and in vitro, necessitate the development of a tt-DDE probe.

4.3 tt-DDE was identified as a novel inducer of diabetic retinopathy

This study revealed impaired detoxification of tt-DDE led to hallmarks of diabetic retinopathy. tt-DDE has been recognized as a key contributor to various cardiovascular diseases, including endothelial dysfunction, atherosclerosis, and hypertension.[80, 81]. In comparison to other commonly encountered aldehydes such as acrolein, crotonaldehyde, and 4HNE, tt-DDE demonstrated the most detrimental effect on the viability of human umbilical vein endothelial cells (HUVEC) [80]. This is underscored by its capacity to induce substantial mitochondrial damage, characterized by a decrease in mitochondrial DNA copy number, ATP synthesis, mitochondrial membrane potential, elevated mitochondrial ROS production, and the release of cytochrome c from mitochondria [80]. Moreover, tt-DDE treatment leads to the obstruction of autophagic flux, resulting in the accumulation of autophagosomes and the initiation of apoptosis in endothelial cells, whether in vitro or in vivo [80, 81]. tt-DDE also downregulates the

expression of the TNF-alpha gene in THP-1 human macrophages, contributing to the progression of atherosclerosis [82]. Notably, dysregulation of eNOS is a central feature of endothelial cell dysfunction induced by tt-DDE. The reduction of eNOS is considered a major factor in vascular complications and is associated with insulin resistance in diabetes[122, 123]. Our research indicates a decrease in nos2b, an eNOS homolog, upon tt-DDE exposure, suggesting downstream alterations in insulin signaling.

Human exposure to tt-DDE is influenced by factors like cooking methods, cooking oils, and food types [68, 76]. Notably, tt-DDE is predominantly found in plant-derived oils, and it significantly contributes to the aroma of fried foods [76]. For instance, heated sunflower oil was demonstrates the highest tt-DDE concentration, ranging between 29-129 μg/g. Furthermore, during the frying process, the atmospheric tt-DDE concentrations fluctuated from 210-890 μg/m³ for potato chips and 476-698 μg/m³ for pork [77, 124-126]. This exposure pattern in our zebrafish model mirrors likely human exposure through both ingestion and inhalation. Although the lack of cellular or tissue-level tt-DDE measurements poses challenges for comprehensive human exposure comparisons, our developed tissue quantification method establishes a potential correlation between tt-DDE metabolites and insulin resistance. This approach serves as a robust foundation for future investigations.

Additionally, considering the documented adverse effects of tt-DDE on workers in specific occupations and the lack of clear legal regulations governing tt-DDE concentrations in cooking oil fumes, our study strongly advocates for the establishment of regulatory guidelines and the monitoring of occupational exposure to tt-DDE. Consequently, the observed development of diabetic retinopathy in the presence of widespread tt-DDE exposure suggests a novel link between tt-DDE and diabetic retinopathy, emphasizing the importance of appropriate pharmacological treatment and the measurement of endogenous tt-DDE as a potential individual therapeutic target for diabetic patients.

4.4 tt-DDE provides new insights in the exposure of omega-6 fatty acids

The implications of high omega-6 fatty acid intake for diabetic patients remain a subject of debate[61, 72, 127, 128]. Over recent years, vegetable oils that rich in omega-6 fatty acids have been positioned as protective to replace saturated fatty acids against cardiovascular disease, gaining endorsements from prominent health organizations

such as the American Diabetes Association, the National Institutes of Health, and the Global Burden of Disease Study [64-67]. Nevertheless, a significant surge of 1000-fold in vegetable oil consumption, primarily abundant in omega-6 fatty acids, has coincided with a substantial 12-fold increase in diagnosed diabetes prevalence and a 3-fold rise in obesity rates in the United States[63, 129, 130]. Pooled analysis findings have indicated that linoleic acid, a specific omega-6 fatty acid, exhibits a dose-dependent association with a reduced risk of [131, 132]. However, an alternate meta-analysis has suggested that omega-6 polyunsaturated fatty acids may serve more as markers of hyperinsulinemia and inducers of obesity, rather than being protective or risk factors for T2D [133, 134] The most comprehensive systematic review to date has yielded inconclusive outcomes regarding omega-6 fatty acids' impact on diabetes diagnosis, largely due to the limited quality of available evidence[61].

Our research sheds new light on the potential adverse effects of omega-6 fatty acid supplementation and its association with T2D, emphasizing the need for cautious consideration when implementing nutritional supplementation strategies. It is noteworthy that deep-fried cooking methods yield 2-3 times more tt-DDE in food and almost 5 times more in cooking oil fumes compared to the pan-fried food preparation method. Sunflower oil, which is commonly used, contributes 5-6 times more tt-DDE than olive oil. Hence, our study also suggests that, even though vegetable oils are an integral part of our daily life, the choice of cooking method and type of oil can significantly impact the risk of developing T2D. This underscores the importance of advocating a healthy dietary pattern for diabetic patients.

Furthermore, considering polymorphism in aldehyde dehydrogenase gene superfamily [135], tt-DDE might act as a significant inducer for specific populations, suggesting an individualized approach to omega-6 intake and T2D prevention strategy.

4.5 Reactive metabolites as upstream factors of glucose metabolism and microvascular complications in zebrafish

Majority of RCS are toxic during metabolic processes due to their capacity to modify and impair the function of biomolecules, including DNA, phospholipids, and proteins [16]. This modification and binding to biomolecules often lead to the production and accumulation of advanced lipoxidation and glycation end products (ALEs and AGEs), which are implicated in a wide array of pathogenic effects contributing to the development and progression of various diseases, such as diabetes mellitus,

neurological disorders, and cancer [16-18, 20, 136]. Beyond the general pathogenic effects of AGEs and ALEs, recent years have witnessed a heightened focus on specific RCS with subsequent downstream signaling in the progress of metabolic disease research. One such RCS, 4-HNE, is detoxified by ALDH3a1. Accumulation of 4-HNE can disrupt pancreatic development, eventually inducing a T1D phenotype along with vascular alterations [13]. MDA can influence collagen stiffness through the formation of sugar adducts, akin to ALEs and AGEs [137]. Accumulation of acrolein, which serves as a substrate for AKR1a1a, has been associated with T2D and insulin resistance [31].
Furthermore, elevated levels of acetaldehyde, in contrast to 4-HNE, acrolein, and MG, can lead to hypoglycemia by inhibiting glucose-6-phosphatase activity [14].
The present study is primarily focused on ALDH9a1b, as its expression was found to be upregulated in *glo1*$^{-/-}$ zebrafish mutants and exhibited a moderate increase in its RCS MG [15]. This suggests that ALDH9a1b may have compensatory RCS detoxification capabilities. Our data have shown that tt-DDE serves as a substrate for *ALDH9a1b in vivo*. Furthermore, external exposure to tt-DDE and the knockout of *aldh9a1b* induced similar alterations in glucose homeostasis and retinal abnormalities, further affirming ALDH9a1b as a specific detoxifying enzyme system for tt-DDE.

The findings put ALDH9a1b and its substrate tt-DDE in the center of microvascular disease associated with prediabetes and diabetes. tt-DDE is a naturally generated RCS in the metabolism that has been linked to a number of cardiovascular disorders [79-82]. Yet, a specific function of tt-DDE in diabetes and diabetes related diseases, in contrast to other RCSs, was largely unknown. Based on our and other data, a concept evolves indicating that different RCS, including 4-HNE, MDA, acrolein and acetaldehyde have distinct effects *in vivo* and in the context of diabetes [13, 14, 24, 31, 137-139]. The present data now identified tt-DDE as a new RCS inducing an altered glucose homeostasis and further improves our understanding how a distinct signature of RCS can cause an altered glucose homeostasis, diabetes and its organ complications [13, 14, 31]. Intriguingly, the studies have also proven for the first time that RCS act upstream of hyperglycemia and are not necessarily formed secondary upon hyperglycemic conditions. Instead, loss of distinct detoxification enzyme systems for different RCS leads to an accumulation of RCS, which are subsequently primary inducers of insulin deficiency and insulin resistance leading to hyperglycemia.

4.6 Conclusion and future perspectives

This study discusses the practical implications of findings in a clinical context, emphasizing potential therapeutic interventions and their application for diabetic patients. The establishment of diabetes related RCS concept fundamentally addresses the questions what and how environmental factors contribute to T2D. Their distinct function of these RCS make them as specific inducers of diabetes, thereby suggesting that a comprehensive evaluation of these RCSs in the context of diabetes could significantly enhance personalized therapeutic approaches for diabetic patients. Moreover, the identification of ALDH9a1b as a key detoxification system in tt-DDE metabolism opens avenues for targeted drug development. Drugs currently used in rescue experiment have shown efficacy in rescuing the observed effects, suggesting their potential repurposing for tt-DDE-induced complications. Additionally, the study's insights into omega-6 fatty acid exposure advocate for dietary recommendations tailored to individual needs, considering the potential risks associated with tt-DDE. The establishment of regulatory guidelines for tt-DDE concentrations, particularly in occupational settings, emerges as a crucial step for safeguarding public health.

Nevertheless, certain limitations persist within the scope of the current study. The lack of human-specific data and the reliance on a zebrafish model necessitate exploration of human *vivo* tt-DDE concentrations. Future research should focus on validating these findings in human cohorts and exploring the interindividual variability in response to tt-DDE exposure, considering genetic factors and environmental contexts.

Our research presents groundbreaking findings on the detoxification of tt-DDE by ALDH9a1b and its profound implications for glucose metabolism and microvascular complications. The *aldh9a1b* knockout zebrafish model serves as a valuable tool in uncovering the specific detoxification pathways for α,β-unsaturated aldehydes. The study establishes tt-DDE as a novel inducer of diabetic retinopathy, shedding light on its diverse effects on endothelial cells and mitochondrial function. The intricate interplay between tt-DDE, omega-6 fatty acids, and diabetes suggests a need for a specific approach to dietary recommendations.

In conclusion, this research significantly advances our understanding of the molecular mechanisms underlying tt-DDE toxicity and its role in diabetes-related complications. The identified detoxification enzyme, ALDH9a1b, emerges as a potential therapeutic target. These findings contribute significantly to the scientific understanding of reactive

metabolites in diabetes, offering immediate implications for clinical practice, public health policies, and the direction of future research endeavors.

5. Summary

Essential fatty acids, including both omega-3 and omega-6, are vital nutrients that can only be sourced from our diets. These fatty acids are crucial for health, with an ideal dietary ratio of omega-6 to omega-3 falling between 1:1 and 2:1 to prevent chronic illnesses. Unfortunately, modern dietary patterns, particularly in Western diets, have distorted this ratio to an unhealthy level of 15:1 to 16.7:1, mainly due to an overconsumption of linoleic acid, which constitutes over 90% of our polyunsaturated fatty acid intake. Omega-3 fatty acids supplementation is advocated for its beneficial cardiovascular effects, whereas omega-6 fatty acids exhibit a complex relationship with cardiovascular disease (CVD). They are known to contribute to inflammatory responses, vascular constriction, and platelet aggregation, which are crucial in the onset of atherosclerosis and subsequent acute CVD incidents. In contrast, omega-6 fatty acids are thought to reduce CVD risk by modulating serum lipid profiles and decreasing blood pressure. Linoleic acid, in particular, can be metabolized into cardioprotective agents like nitrated linoleic acid. However, there is a growing concern regarding the increased consumption of n-6 PUFAs, especially when exposed to oxidative conditions like heating, which give rise to exceedingly reactive RCS, with tt-DDE being the primary compound. Comparable to other RCSs such as 4-HNE, acrolein, acetaldehyde, and MG, the prompt and efficient neutralization of tt-DDE holds paramount importance in averting harm and its associated diseases.

ALDH9a1b, an enzyme linked to lipid metabolism, was found to be upregulated in *glo1* knockout zebrafish, suggesting its potential for compensatory RCS detoxification in the context of diabetes. Consequently, a zebrafish line with a knockout of *aldh9a1b* knockout zebrafish line was established with CRISPR/CAS9 technology, revealing the enzyme ALDH9a1b's proficiency in detoxifying tt-DDE. Loss of *aldh9a1b* increased tt-DDE and caused an abnormal retinal vasculature and glucose intolerance in *aldh9a1b*$^{-/-}$ zebrafish. Transcriptomic and metabolomic analyses revealed insulin resistance and disrupted glucose homeostasis induced by tt-DDE and *aldh9a1b* deficiency in both larval and adult zebrafish. Subsequently, hyaloid vasculature alterations in *aldh9a1b* knockout and by tt-DDE treatment can be rescued by insulin receptor sensitizers metformin and rosiglitazone.

In conclusion, this research underscores the pivotal function of ALDH9a1b in regulating reactive RCS deriving from omega-6 sources, particularly tt-DDE. Failure to

comprehensively detoxify tt-DDE could set off a sequence of events including insulin resistance, disordered gluconeogenesis, and altered fatty acid metabolism, consequently leading to microvascular disorders.

6. References

1. Jackson, B, Brocker, C, Thompson, DC, Black, W, Vasiliou, K, Nebert, DW, Vasiliou, V: Update on the aldehyde dehydrogenase gene (ALDH) superfamily. *Hum Genomics,* 5**:** 283-303, 2011. https://doi.org/10.1186/1479-7364-5-4-283
2. Shortall, K, Djeghader, A, Magner, E, Soulimane, T: Insights into Aldehyde Dehydrogenase Enzymes: A Structural Perspective. *Front Mol Biosci,* 8**:** 659550, 2021. https://doi.org/10.3389/fmolb.2021.659550
3. Vasiliou, V, Nebert, DW: Analysis and update of the human aldehyde dehydrogenase (ALDH) gene family. *Hum Genomics,* 2**:** 138-143, 2005. https://doi.org/10.1186/1479-7364-2-2-138
4. O'Brien, PJ, Siraki, AG, Shangari, N: Aldehyde sources, metabolism, molecular toxicity mechanisms, and possible effects on human health. *Crit Rev Toxicol,* 35**:** 609-662, 2005. https://doi.org/10.1080/10408440591002183
5. Marchitti, SA, Brocker, C, Stagos, D, Vasiliou, V: Non-P450 aldehyde oxidizing enzymes: the aldehyde dehydrogenase superfamily. *Expert Opin Drug Metab Toxicol,* 4**:** 697-720, 2008. https://doi.org/10.1517/17425255.4.6.697
6. Koncitikova, R, Vigouroux, A, Kopecna, M, Sebela, M, Morera, S, Kopecny, D: Kinetic and structural analysis of human ALDH9A1. *Biosci Rep,* 39, 2019. https://doi.org/10.1042/BSR20190558
7. Wyatt, JW, Korasick, DA, Qureshi, IA, Campbell, AC, Gates, KS, Tanner, JJ: Inhibition, crystal structures, and in-solution oligomeric structure of aldehyde dehydrogenase 9A1. *Arch Biochem Biophys,* 691**:** 108477, 2020. https://doi.org/10.1016/j.abb.2020.108477
8. Karan, BM, Little, K, Augustine, J, Stitt, AW, Curtis, TM: Aldehyde Dehydrogenase and Aldo-Keto Reductase Enzymes: Basic Concepts and Emerging Roles in Diabetic Retinopathy. *Antioxidants (Basel),* 12, 2023. https://doi.org/10.3390/antiox12071466
9. McDowell, RE, McGahon, MK, Augustine, J, Chen, M, McGeown, JG, Curtis, TM: Diabetes Impairs the Aldehyde Detoxifying Capacity of the Retina. *Invest Ophthalmol Vis Sci,* 57**:** 4762-4771, 2016. https://doi.org/10.1167/iovs.16-19424
10. Sato, W, Horie, Y, Kataoka, E, Ohshima, S, Dohmen, T, Iizuka, M, Sasaki, J, Sasaki, T, Hamada, K, Kishimoto, H, Suzuki, A, Watanabe, S: Hepatic gene expression in hepatocyte-specific Pten deficient mice showing steatohepatitis without ethanol challenge. *Hepatol Res,* 34**:** 256-265, 2006. https://doi.org/10.1016/j.hepres.2006.01.003
11. Matsunaga, A, Harita, Y, Shibagaki, Y, Shimizu, N, Shibuya, K, Ono, H, Kato, H, Sekine, T, Sakamoto, N, Igarashi, T, Hattori, S: Identification of 4-Trimethylaminobutyraldehyde Dehydrogenase (TMABA-DH) as a Candidate Serum Autoantibody Target for Kawasaki Disease. *PLoS One,* 10**:** e0128189, 2015. https://doi.org/10.1371/journal.pone.0128189
12. Henrion, MY, Purdue, MP, Scelo, G, Broderick, P, Frampton, M, Ritchie, A, Meade, A, Li, P, McKay, J, Johansson, M, Lathrop, M, Larkin, J, Rothman, N, Wang, Z, Chow, WH, Stevens, VL, Diver, WR, Albanes, D, Virtamo, J, Brennan, P, Eisen, T, Chanock, S, Houlston, RS: Common variation at 1q24.1 (ALDH9A1) is a potential risk factor for renal cancer. *PLoS One,* 10**:** e0122589, 2015. https://doi.org/10.1371/journal.pone.0122589
13. Lou, B, Boger, M, Bennewitz, K, Sticht, C, Kopf, S, Morgenstern, J, Fleming, T, Hell, R, Yuan, Z, Nawroth, PP, Kroll, J: Elevated 4-hydroxynonenal induces hyperglycaemia via Aldh3a1 loss in zebrafish and associates with diabetes

progression in humans. *Redox Biol,* 37**:** 101723, 2020. https://doi.org/10.1016/j.redox.2020.101723
14. Wohlfart, DP, Lou, B, Middel, CS, Morgenstern, J, Fleming, T, Sticht, C, Hausser, I, Hell, R, Hammes, HP, Szendrodi, J, Nawroth, PP, Kroll, J: Accumulation of acetaldehyde in aldh2.1(-/-) zebrafish causes increased retinal angiogenesis and impaired glucose metabolism. *Redox Biol,* 50**:** 102249, 2022. https://doi.org/10.1016/j.redox.2022.102249
15. Lodd, E, Wiggenhauser, LM, Morgenstern, J, Fleming, TH, Poschet, G, Buttner, M, Tabler, CT, Wohlfart, DP, Nawroth, PP, Kroll, J: The combination of loss of glyoxalase1 and obesity results in hyperglycemia. *JCI Insight,* 4, 2019. https://doi.org/10.1172/jci.insight.126154
16. Semchyshyn, HM: Reactive carbonyl species in vivo: generation and dual biological effects. *ScientificWorldJournal,* 2014**:** 417842, 2014. https://doi.org/10.1155/2014/417842
17. Mano, J: Reactive carbonyl species: their production from lipid peroxides, action in environmental stress, and the detoxification mechanism. *Plant Physiol Biochem,* 59**:** 90-97, 2012. https://doi.org/10.1016/j.plaphy.2012.03.010
18. Tian, CJ, Zhen, Z: Reactive Carbonyl Species: Diabetic Complication in the Heart and Lungs. *Trends Endocrinol Metab,* 30**:** 546-556, 2019. https://doi.org/10.1016/j.tem.2019.05.005
19. Zimniak, P: Relationship of electrophilic stress to aging. *Free Radic Biol Med,* 51**:** 1087-1105, 2011. https://doi.org/10.1016/j.freeradbiomed.2011.05.039
20. Pamplona, R: Advanced lipoxidation end-products. *Chem Biol Interact,* 192**:** 14-20, 2011. https://doi.org/10.1016/j.cbi.2011.01.007
21. Davies, SS, Zhang, LS: Reactive Carbonyl Species Scavengers-Novel Therapeutic Approaches for Chronic Diseases. *Curr Pharmacol Rep,* 3**:** 51-67, 2017. https://doi.org/10.1007/s40495-017-0081-6
22. Rodnick, KJ, Holman, RW, Ropski, PS, Huang, M, Swislocki, ALM: A Perspective on Reagent Diversity and Non-covalent Binding of Reactive Carbonyl Species (RCS) and Effector Reagents in Non-enzymatic Glycation (NEG): Mechanistic Considerations and Implications for Future Research. *Front Chem,* 5**:** 39, 2017. https://doi.org/10.3389/fchem.2017.00039
23. Chen, Y, Cong, Y, Quan, B, Lan, T, Chu, X, Ye, Z, Hou, X, Wang, C: Chemoproteomic profiling of targets of lipid-derived electrophiles by bioorthogonal aminooxy probe. *Redox Biol,* 12**:** 712-718, 2017. https://doi.org/10.1016/j.redox.2017.04.001
24. Conklin, DJ, Barski, OA, Lesgards, JF, Juvan, P, Rezen, T, Rozman, D, Prough, RA, Vladykovskaya, E, Liu, S, Srivastava, S, Bhatnagar, A: Acrolein consumption induces systemic dyslipidemia and lipoprotein modification. *Toxicol Appl Pharmacol,* 243**:** 1-12, 2010. https://doi.org/10.1016/j.taap.2009.12.010
25. Hecker, M, Wagner, AH: Role of protein carbonylation in diabetes. *J Inherit Metab Dis,* 41**:** 29-38, 2018. https://doi.org/10.1007/s10545-017-0104-9
26. Singh, RM, Waqar, T, Howarth, FC, Adeghate, E, Bidasee, K, Singh, J: Hyperglycemia-induced cardiac contractile dysfunction in the diabetic heart. *Heart Fail Rev,* 23**:** 37-54, 2018. https://doi.org/10.1007/s10741-017-9663-y
27. Chikezie, PC, Ojiako, OA, Ogbuji, AC: Oxidative stress in diabetes mellitus. *Int J Biol Chem,* 9**:** 92-109, 2015.
28. Yang, Z, Zhang, W, Lu, H, Cai, S: Methylglyoxal in the Brain: From Glycolytic Metabolite to Signalling Molecule. *Molecules,* 27, 2022. https://doi.org/10.3390/molecules27227905

29. Penning, TM, Jonnalagadda, S, Trippier, PC, Rizner, TL: Aldo-Keto Reductases and Cancer Drug Resistance. *Pharmacol Rev,* 73**:** 1150-1171, 2021. https://doi.org/10.1124/pharmrev.120.000122
30. Ahmed Laskar, A, Younus, H: Aldehyde toxicity and metabolism: the role of aldehyde dehydrogenases in detoxification, drug resistance and carcinogenesis. *Drug Metab Rev,* 51**:** 42-64, 2019. https://doi.org/10.1080/03602532.2018.1555587
31. Qi, H, Schmohl, F, Li, X, Qian, X, Tabler, CT, Bennewitz, K, Sticht, C, Morgenstern, J, Fleming, T, Volk, N, Hausser, I, Heidenreich, E, Hell, R, Nawroth, PP, Kroll, J: Reduced Acrolein Detoxification in akr1a1a Zebrafish Mutants Causes Impaired Insulin Receptor Signaling and Microvascular Alterations. *Adv Sci (Weinh),* 8**:** e2101281, 2021. https://doi.org/10.1002/advs.202101281
32. Ali, MK, Pearson-Stuttard, J, Selvin, E, Gregg, EW: Interpreting global trends in type 2 diabetes complications and mortality. *Diabetologia,* 65**:** 3-13, 2022. https://doi.org/10.1007/s00125-021-05585-2
33. Zheng, Y, Ley, SH, Hu, FB: Global aetiology and epidemiology of type 2 diabetes mellitus and its complications. *Nat Rev Endocrinol,* 14**:** 88-98, 2018. https://doi.org/10.1038/nrendo.2017.151
34. Sun, H, Saeedi, P, Karuranga, S, Pinkepank, M, Ogurtsova, K, Duncan, BB, Stein, C, Basit, A, Chan, JCN, Mbanya, JC, Pavkov, ME, Ramachandaran, A, Wild, SH, James, S, Herman, WH, Zhang, P, Bommer, C, Kuo, S, Boyko, EJ, Magliano, DJ: IDF Diabetes Atlas: Global, regional and country-level diabetes prevalence estimates for 2021 and projections for 2045. *Diabetes Res Clin Pract,* 183**:** 109119, 2022. https://doi.org/10.1016/j.diabres.2021.109119
35. Mortality, GBD, Causes of Death, C: Global, regional, and national age-sex specific all-cause and cause-specific mortality for 240 causes of death, 1990-2013: a systematic analysis for the Global Burden of Disease Study 2013. *Lancet,* 385**:** 117-171, 2015. https://doi.org/10.1016/S0140-6736(14)61682-2
36. Roglic, G, Unwin, N: Mortality attributable to diabetes: estimates for the year 2010. *Diabetes Res Clin Pract,* 87**:** 15-19, 2010. https://doi.org/10.1016/j.diabres.2009.10.006
37. Atlas, D: International diabetes federation. *IDF Diabetes Atlas, 7th edn Brussels, Belgium: International Diabetes Federation,* 33, 2015.
38. Ahlqvist, E, Storm, P, Karajamaki, A, Martinell, M, Dorkhan, M, Carlsson, A, Vikman, P, Prasad, RB, Aly, DM, Almgren, P, Wessman, Y, Shaat, N, Spegel, P, Mulder, H, Lindholm, E, Melander, O, Hansson, O, Malmqvist, U, Lernmark, A, Lahti, K, Forsen, T, Tuomi, T, Rosengren, AH, Groop, L: Novel subgroups of adult-onset diabetes and their association with outcomes: a data-driven cluster analysis of six variables. *Lancet Diabetes Endocrinol,* 6**:** 361-369, 2018. https://doi.org/10.1016/S2213-8587(18)30051-2
39. Global Burden of Disease Study, C: Global, regional, and national incidence, prevalence, and years lived with disability for 301 acute and chronic diseases and injuries in 188 countries, 1990-2013: a systematic analysis for the Global Burden of Disease Study 2013. *Lancet,* 386**:** 743-800, 2015. https://doi.org/10.1016/S0140-6736(15)60692-4
40. Avogaro, A, Fadini, GP: Microvascular complications in diabetes: A growing concern for cardiologists. *Int J Cardiol,* 291**:** 29-35, 2019. https://doi.org/10.1016/j.ijcard.2019.02.030
41. Salvotelli, L, Stoico, V, Perrone, F, Cacciatori, V, Negri, C, Brangani, C, Pichiri, I, Targher, G, Bonora, E, Zoppini, G: Prevalence of neuropathy in type 2 diabetic patients and its association with other diabetes complications: The Verona

Diabetic Foot Screening Program. *J Diabetes Complications,* 29**:** 1066-1070, 2015. https://doi.org/10.1016/j.jdiacomp.2015.06.014
42. Solini, A, Penno, G, Bonora, E, Fondelli, C, Orsi, E, Arosio, M, Trevisan, R, Vedovato, M, Cignarelli, M, Andreozzi, F, Nicolucci, A, Pugliese, G, Renal, I, Cardiovascular Events Study, G: Diverging association of reduced glomerular filtration rate and albuminuria with coronary and noncoronary events in patients with type 2 diabetes: the renal insufficiency and cardiovascular events (RIACE) Italian multicenter study. *Diabetes Care,* 35**:** 143-149, 2012. https://doi.org/10.2337/dc11-1380
43. Voigt, M, Schmidt, S, Lehmann, T, Kohler, B, Kloos, C, Voigt, UA, Meller, D, Wolf, G, Muller, UA, Muller, N: Correction: Prevalence and Progression Rate of Diabetic Retinopathy in Type 2 Diabetes Patients in Correlation with the Duration of Diabetes. *Exp Clin Endocrinol Diabetes,* 126**:** e2, 2018. https://doi.org/10.1055/a-0757-3796
44. Yau, JW, Rogers, SL, Kawasaki, R, Lamoureux, EL, Kowalski, JW, Bek, T, Chen, SJ, Dekker, JM, Fletcher, A, Grauslund, J, Haffner, S, Hamman, RF, Ikram, MK, Kayama, T, Klein, BE, Klein, R, Krishnaiah, S, Mayurasakorn, K, O'Hare, JP, Orchard, TJ, Porta, M, Rema, M, Roy, MS, Sharma, T, Shaw, J, Taylor, H, Tielsch, JM, Varma, R, Wang, JJ, Wang, N, West, S, Xu, L, Yasuda, M, Zhang, X, Mitchell, P, Wong, TY, Meta-Analysis for Eye Disease Study, G: Global prevalence and major risk factors of diabetic retinopathy. *Diabetes Care,* 35**:** 556-564, 2012. https://doi.org/10.2337/dc11-1909
45. Bhavsar, AR: Diabetic retinopathy: the latest in current management. *Retina,* 26**:** S71-79, 2006. https://doi.org/10.1097/01.iae.0000236466.23640.c9
46. Crasto, W, Patel, V, Davies, MJ, Khunti, K: Prevention of Microvascular Complications of Diabetes. *Endocrinol Metab Clin North Am,* 50**:** 431-455, 2021. https://doi.org/10.1016/j.ecl.2021.05.005
47. Lin, KY, Hsih, WH, Lin, YB, Wen, CY, Chang, TJ: Update in the epidemiology, risk factors, screening, and treatment of diabetic retinopathy. *J Diabetes Investig,* 12**:** 1322-1325, 2021. https://doi.org/10.1111/jdi.13480
48. Forbes, JM, Cooper, ME: Mechanisms of diabetic complications. *Physiol Rev,* 93**:** 137-188, 2013. https://doi.org/10.1152/physrev.00045.2011
49. Dubin, RF, Rhee, EP: Proteomics and Metabolomics in Kidney Disease, including Insights into Etiology, Treatment, and Prevention. *Clin J Am Soc Nephrol,* 15**:** 404-411, 2020. https://doi.org/10.2215/CJN.07420619
50. Cole, JB, Florez, JC: Genetics of diabetes mellitus and diabetes complications. *Nat Rev Nephrol,* 16**:** 377-390, 2020. https://doi.org/10.1038/s41581-020-0278-5
51. Brownlee, M: Biochemistry and molecular cell biology of diabetic complications. *Nature,* 414**:** 813-820, 2001. https://doi.org/10.1038/414813a
52. Alhusseiny, SM, El-Beshbishi, SN: Omega polyunsaturated fatty acids and parasitic infections: An overview. *Acta Trop,* 207**:** 105466, 2020. https://doi.org/10.1016/j.actatropica.2020.105466
53. Innis, SM: Omega-3 fatty acid biochemistry: perspectives from human nutrition. *Mil Med,* 179**:** 82-87, 2014. https://doi.org/10.7205/MILMED-D-14-00147
54. Khan, I, Hussain, M, Jiang, B, Zheng, L, Pan, Y, Hu, J, Khan, A, Ashraf, A, Zou, X: (Omega-3 long-chain polyunsaturated fatty acids: Metabolism and health implications). *Prog Lipid Res,* 92**:** 101255, 2023. https://doi.org/10.1016/j.plipres.2023.101255
55. Gregory, MK, Gibson, RA, Cook-Johnson, RJ, Cleland, LG, James, MJ: Elongase reactions as control points in long-chain polyunsaturated fatty acid synthesis. *PLoS One,* 6**:** e29662, 2011. https://doi.org/10.1371/journal.pone.0029662

56. Moore, SA, Hurt, E, Yoder, E, Sprecher, H, Spector, AA: Docosahexaenoic acid synthesis in human skin fibroblasts involves peroxisomal retroconversion of tetracosahexaenoic acid. *J Lipid Res,* 36**:** 2433-2443, 1995.
57. Egalini, F, Guardamagna, O, Gaggero, G, Varaldo, E, Giannone, B, Beccuti, G, Benso, A, Broglio, F: The Effects of Omega 3 and Omega 6 Fatty Acids on Glucose Metabolism: An Updated Review. *Nutrients,* 15, 2023. https://doi.org/10.3390/nu15122672
58. Kumar, M, Pal, N, Sharma, P, Kumawat, M, Sarma, DK, Nabi, B, Verma, V, Tiwari, RR, Shubham, S, Arjmandi, B, Nagpal, R: Omega-3 Fatty Acids and Their Interaction with the Gut Microbiome in the Prevention and Amelioration of Type-2 Diabetes. *Nutrients,* 14, 2022. https://doi.org/10.3390/nu14091723
59. Sala-Vila, A, Fleming, J, Kris-Etherton, P, Ros, E: Impact of alpha-Linolenic Acid, the Vegetable omega-3 Fatty Acid, on Cardiovascular Disease and Cognition. *Adv Nutr,* 13**:** 1584-1602, 2022. https://doi.org/10.1093/advances/nmac016
60. Jiang, H, Wang, L, Wang, D, Yan, N, Li, C, Wu, M, Wang, F, Mi, B, Chen, F, Jia, W, Liu, X, Lv, J, Liu, Y, Lin, J, Ma, L: Omega-3 polyunsaturated fatty acid biomarkers and risk of type 2 diabetes, cardiovascular disease, cancer, and mortality. *Clin Nutr,* 41**:** 1798-1807, 2022. https://doi.org/10.1016/j.clnu.2022.06.034
61. Brown, TJ, Brainard, J, Song, F, Wang, X, Abdelhamid, A, Hooper, L, Group, P: Omega-3, omega-6, and total dietary polyunsaturated fat for prevention and treatment of type 2 diabetes mellitus: systematic review and meta-analysis of randomised controlled trials. *BMJ,* 366**:** l4697, 2019. https://doi.org/10.1136/bmj.l4697
62. Innes, JK, Calder, PC: Omega-6 fatty acids and inflammation. *Prostaglandins Leukot Essent Fatty Acids,* 132**:** 41-48, 2018. https://doi.org/10.1016/j.plefa.2018.03.004
63. Blasbalg, TL, Hibbeln, JR, Ramsden, CE, Majchrzak, SF, Rawlings, RR: Changes in consumption of omega-3 and omega-6 fatty acids in the United States during the 20th century. *Am J Clin Nutr,* 93**:** 950-962, 2011. https://doi.org/10.3945/ajcn.110.006643
64. American Diabetes, A: 5. Lifestyle Management: Standards of Medical Care in Diabetes-2019. *Diabetes Care,* 42**:** S46-S60, 2019. https://doi.org/10.2337/dc19-S005
65. Collaborators, GBDD: Health effects of dietary risks in 195 countries, 1990-2017: a systematic analysis for the Global Burden of Disease Study 2017. *Lancet,* 393**:** 1958-1972, 2019. https://doi.org/10.1016/S0140-6736(19)30041-8
66. Harris, WS, Mozaffarian, D, Rimm, E, Kris-Etherton, P, Rudel, LL, Appel, LJ, Engler, MM, Engler, MB, Sacks, F: Omega-6 fatty acids and risk for cardiovascular disease: a science advisory from the American Heart Association Nutrition Subcommittee of the Council on Nutrition, Physical Activity, and Metabolism; Council on Cardiovascular Nursing; and Council on Epidemiology and Prevention. *Circulation,* 119**:** 902-907, 2009. https://doi.org/10.1161/CIRCULATIONAHA.108.191627
67. Sacks, FM, Lichtenstein, AH, Wu, JHY, Appel, LJ, Creager, MA, Kris-Etherton, PM, Miller, M, Rimm, EB, Rudel, LL, Robinson, JG, Stone, NJ, Van Horn, LV, American Heart, A: Dietary Fats and Cardiovascular Disease: A Presidential Advisory From the American Heart Association. *Circulation,* 136**:** e1-e23, 2017. https://doi.org/10.1161/CIR.0000000000000510
68. Andrikopoulos, NK, Chiou, A, Mylona, A, Boskou, G, Dedoussis, GVZ: Monitoring of 2,4-decadienal in oils and fats used for frying in restaurants in Athens, Greece.

Eur J Lipid Sci Tech, 106**:** 671-679, 2004. https://doi.org/10.1002/ejlt.200401001
69. Spiteller, P, Kern, W, Reiner, J, Spiteller, G: Aldehydic lipid peroxidation products derived from linoleic acid. *Biochim Biophys Acta,* 1531**:** 188-208, 2001. https://doi.org/10.1016/s1388-1981(01)00100-7
70. Weidong, B: The Progress on Study of the Mechanism of 2,4-Decadienal in Meat Flavor. *Flavour Fragrance Cosmetics*, 2011.
71. Akakabe, Y, Matsui, K, Kajiwara, T: 2,4-Decadienals are produced via (R)-11-HPITE from arachidonic acid in marine green alga Ulva conglobata. *Bioorg Med Chem,* 11**:** 3607-3609, 2003. https://doi.org/10.1016/s0968-0896(03)00364-x
72. Yamashima, T, Ota, T, Mizukoshi, E, Nakamura, H, Yamamoto, Y, Kikuchi, M, Yamashita, T, Kaneko, S: Intake of omega-6 Polyunsaturated Fatty Acid-Rich Vegetable Oils and Risk of Lifestyle Diseases. *Adv Nutr,* 11**:** 1489-1509, 2020. https://doi.org/10.1093/advances/nmaa072
73. Chan, PC: NTP toxicity studies of toxicity studies of 2,4-decadienal (CAS No. 25152-84-5) administered by gavage to F344/N Rats and B6C3F1 mice. *Toxic Rep Ser***:** 1-94, 2011.
74. Pan, KL, Huang, WJ, Hsu, MH, Lee, HL, Liu, HJ, Cheng, CW, Tsai, MH, Shen, MY, Lin, P: Identification of trans,trans-2,4-decadienal metabolites in mouse and human cells using liquid chromatography-mass spectrometry. *Chem Res Toxicol,* 27**:** 1707-1719, 2014. https://doi.org/10.1021/tx500199b
75. Wu, SC, Yen, GC: Effects of cooking oil fumes on the genotoxicity and oxidative stress in human lung carcinoma (A-549) cells. *Toxicol in Vitro,* 18**:** 571-580, 2004. https://doi.org/10.1016/j.tiv.2004.01.004
76. Boskou, G, Salta, FN, Chiou, A, Troullidou, E, Andrikopoulos, NK: Content of trans,trans-2,4-decadienal in deep-fried and pan-fried potatoes. *Eur J Lipid Sci Tech,* 108**:** 109-115, 2006. https://doi.org/10.1002/ejlt.200500236
77. Yang, HH, Chien, SM, Lee, HL, Chao, MR, Luo, HW, Hsieh, DPH, Lee, WJ: Emission of trans,trans-2,4-decadienal from restaurant exhausts to the atmosphere. *Atmospheric Environment,* 41**:** 5327-5333, 2007. https://doi.org/10.1016/j.atmosenv.2007.02.031
78. Goicoechea, E, Van Twillert, K, Duits, M, Brandon, ED, Kootstra, PR, Blokland, MH, Guillen, MD: Use of an in vitro digestion model to study the bioaccessibility of 4-hydroxy-2-nonenal and related aldehydes present in oxidized oils rich in omega-6 acyl groups. *J Agric Food Chem,* 56**:** 8475-8483, 2008. https://doi.org/10.1021/jf801212k
79. Wang, Y, Dattmore, DA, Wang, W, Pohnert, G, Wolfram, S, Zhang, J, Yang, R, Decker, EA, Lee, KSS, Zhang, G: trans, trans-2,4-Decadienal, a lipid peroxidation product, induces inflammatory responses via Hsp90- or 14-3-3zeta-dependent mechanisms. *J Nutr Biochem,* 76**:** 108286, 2020. https://doi.org/10.1016/j.jnutbio.2019.108286
80. Hu, Y, Zhao, G, Qin, L, Yu, Z, Zhang, M, Ma, X, Zhou, D, Shahidi, F, Zhu, B: trans,trans-2,4-Decadienal induces endothelial cell injury by impairing mitochondrial function and autophagic flux. *Food Funct,* 12**:** 5488-5500, 2021. https://doi.org/10.1039/d1fo00372k
81. Hu, Y, Yin, F, Yu, Z, Peng, Y, Zhao, G, Liu, Z, Zhou, D, Ma, X, Shahidi, F, Zhu, B: Trans, trans-2,4-decadienal impairs vascular endothelial function by inducing oxidative/nitrative stress and apoptosis. *Redox Biol,* 34**:** 101577, 2020. https://doi.org/10.1016/j.redox.2020.101577
82. Girona, J, Vallve, JC, Ribalta, J, Heras, M, Olive, S, Masana, L: 2,4-Decadienal downregulates TNF-alpha gene expression in THP-1 human macrophages.

Atherosclerosis, 158**:** 95-101, 2001. https://doi.org/10.1016/s0021-9150(01)00419-1
83. Kimmel, CB, Ballard, WW, Kimmel, SR, Ullmann, B, Schilling, TF: Stages of embryonic development of the zebrafish. *Dev Dyn,* 203**:** 253-310, 1995. https://doi.org/10.1002/aja.1002030302
84. Lawson, ND, Weinstein, BM: In vivo imaging of embryonic vascular development using transgenic zebrafish. *Dev Biol,* 248**:** 307-318, 2002. https://doi.org/10.1006/dbio.2002.0711
85. Hill, JT, Demarest, BL, Bisgrove, BW, Su, YC, Smith, M, Yost, HJ: Poly peak parser: Method and software for identification of unknown indels using sanger sequencing of polymerase chain reaction products. *Dev Dyn,* 243**:** 1632-1636, 2014. https://doi.org/10.1002/dvdy.24183
86. Wiggenhauser, LM, Kohl, K, Dietrich, N, Hammes, HP, Kroll, J: Studying Diabetes Through the Eyes of a Fish: Microdissection, Visualization, and Analysis of the Adult tg(fli:EGFP) Zebrafish Retinal Vasculature. *J Vis Exp*, 2017. https://doi.org/10.3791/56674
87. Wiggenhauser, LM, Metzger, L, Bennewitz, K, Soleymani, S, Boger, M, Tabler, CT, Hausser, I, Sticht, C, Wohlfart, P, Volk, N, Heidenreich, E, Buettner, M, Hammes, HP, Kroll, J: pdx1 Knockout Leads to a Diabetic Nephropathy- Like Phenotype in Zebrafish and Identifies Phosphatidylethanolamine as Metabolite Promoting Early Diabetic Kidney Damage. *Diabetes,* 71**:** 1073-1080, 2022. https://doi.org/10.2337/db21-0645
88. Morgenstern, J, Kliemank, E, Campos, MC, Nawroth, P, Fleming, T: Michaelis-Menten Kinetics Measurements of Aldo-Keto Reductases for Various Substrates in Murine Tissue. *STAR Protoc,* 1**:** 100206, 2020. https://doi.org/10.1016/j.xpro.2020.100206
89. Tabler, CT, Lodd, E, Bennewitz, K, Middel, CS, Erben, V, Ott, H, Poth, T, Fleming, T, Morgenstern, J, Hausser, I, Sticht, C, Poschet, G, Szendroedi, J, Nawroth, PP, Kroll, J: Loss of glyoxalase 2 alters the glucose metabolism in zebrafish. *Redox Biol,* 59**:** 102576, 2022. https://doi.org/10.1016/j.redox.2022.102576
90. Gegner, HM, Mechtel, N, Heidenreich, E, Wirth, A, Cortizo, FG, Bennewitz, K, Fleming, T, Andresen, C, Freichel, M, Teleman, AA, Kroll, J, Hell, R, Poschet, G: Deep Metabolic Profiling Assessment of Tissue Extraction Protocols for Three Model Organisms. *Front Chem,* 10**:** 869732, 2022. https://doi.org/10.3389/fchem.2022.869732
91. Pang, Z, Zhou, G, Ewald, J, Chang, L, Hacariz, O, Basu, N, Xia, J: Using MetaboAnalyst 5.0 for LC-HRMS spectra processing, multi-omics integration and covariate adjustment of global metabolomics data. *Nat Protoc,* 17**:** 1735-1761, 2022. https://doi.org/10.1038/s41596-022-00710-w
92. Eberhardt, J, Santos-Martins, D, Tillack, AF, Forli, S: AutoDock Vina 1.2.0: New Docking Methods, Expanded Force Field, and Python Bindings. *J Chem Inf Model,* 61**:** 3891-3898, 2021. https://doi.org/10.1021/acs.jcim.1c00203
93. Trott, O, Olson, AJ: AutoDock Vina: improving the speed and accuracy of docking with a new scoring function, efficient optimization, and multithreading. *J Comput Chem,* 31**:** 455-461, 2010. https://doi.org/10.1002/jcc.21334
94. Singh, R, Farooq, SA, Mannan, A, Singh, TG, Najda, A, Grazyna, Z, Albadrani, GM, Sayed, AA, Abdel-Daim, MM: Animal models of diabetic microvascular complications: Relevance to clinical features. *Biomed Pharmacother,* 145**:** 112305, 2022. https://doi.org/10.1016/j.biopha.2021.112305
95. Faselis, C, Katsimardou, A, Imprialos, K, Deligkaris, P, Kallistratos, M, Dimitriadis, K: Microvascular Complications of Type 2 Diabetes Mellitus. *Curr Vasc*

Pharmacol, 18**:** 117-124, 2020. https://doi.org/10.2174/1570161117666190502103733
96. Schalkwijk, CG, Stehouwer, CDA: Methylglyoxal, a Highly Reactive Dicarbonyl Compound, in Diabetes, Its Vascular Complications, and Other Age-Related Diseases. *Physiol Rev,* 100**:** 407-461, 2020. https://doi.org/10.1152/physrev.00001.2019
97. Armbruster, M, Grady, S, Agongo, J, Arnatt, CK, Edwards, JL: Neutron encoded derivatization of endothelial cell lysates for quantitation of aldehyde metabolites using nESI-LC-HRMS. *Anal Chim Acta,* 1190**:** 339260, 2022. https://doi.org/10.1016/j.aca.2021.339260
98. Sasson, S: Nutrient overload, lipid peroxidation and pancreatic beta cell function. *Free Radic Biol Med,* 111**:** 102-109, 2017. https://doi.org/10.1016/j.freeradbiomed.2016.09.003
99. Onyango, AN: Cellular Stresses and Stress Responses in the Pathogenesis of Insulin Resistance. *Oxid Med Cell Longev,* 2018**:** 4321714, 2018. https://doi.org/10.1155/2018/4321714
100. Lepiller, S, Franche, N, Solary, E, Chluba, J, Laurens, V: Comparative analysis of zebrafish nos2a and nos2b genes. *Gene,* 445**:** 58-65, 2009. https://doi.org/10.1016/j.gene.2009.05.016
101. Mulvihill, MJ, Cooke, A, Rosenfeld-Franklin, M, Buck, E, Foreman, K, Landfair, D, O'Connor, M, Pirritt, C, Sun, Y, Yao, Y, Arnold, LD, Gibson, NW, Ji, QS: Discovery of OSI-906: a selective and orally efficacious dual inhibitor of the IGF-1 receptor and insulin receptor. *Future Med Chem,* 1**:** 1153-1171, 2009. https://doi.org/10.4155/fmc.09.89
102. Zhao, F, Wang, H, Wei, P, Jiang, G, Wang, W, Zhang, X, Ru, S: Impairment of bisphenol F on the glucose metabolism of zebrafish larvae. *Ecotoxicol Environ Saf,* 165**:** 386-392, 2018. https://doi.org/10.1016/j.ecoenv.2018.09.017
103. Xie, F, Xu, S, Lu, Y, Wong, KF, Sun, L, Hasan, KMM, Ma, ACH, Tse, G, Manno, SHC, Tian, L, Yue, J, Cheng, SH: Metformin accelerates zebrafish heart regeneration by inducing autophagy. *NPJ Regen Med,* 6**:** 62, 2021. https://doi.org/10.1038/s41536-021-00172-w
104. Capiotti, KM, Antonioli, R, Jr., Kist, LW, Bogo, MR, Bonan, CD, Da Silva, RS: Persistent impaired glucose metabolism in a zebrafish hyperglycemia model. *Comp Biochem Physiol B Biochem Mol Biol,* 171**:** 58-65, 2014. https://doi.org/10.1016/j.cbpb.2014.03.005
105. Wiggenhauser, LM, Qi, H, Stoll, SJ, Metzger, L, Bennewitz, K, Poschet, G, Krenning, G, Hillebrands, JL, Hammes, HP, Kroll, J: Activation of Retinal Angiogenesis in Hyperglycemic pdx1 (-/-) Zebrafish Mutants. *Diabetes,* 69**:** 1020-1031, 2020. https://doi.org/10.2337/db19-0873
106. Aldini, G, Carini, M, Yeum, KJ, Vistoli, G: Novel molecular approaches for improving enzymatic and nonenzymatic detoxification of 4-hydroxynonenal: toward the discovery of a novel class of bioactive compounds. *Free Radic Biol Med,* 69**:** 145-156, 2014. https://doi.org/10.1016/j.freeradbiomed.2014.01.017
107. Balogh, LM, Atkins, WM: Interactions of glutathione transferases with 4-hydroxynonenal. *Drug Metab Rev,* 43**:** 165-178, 2011. https://doi.org/10.3109/03602532.2011.558092
108. Alary, J, Gueraud, F, Cravedi, JP: Fate of 4-hydroxynonenal in vivo: disposition and metabolic pathways. *Mol Aspects Med,* 24**:** 177-187, 2003. https://doi.org/10.1016/s0098-2997(03)00012-8
109. Association, AD: 5. Lifestyle management: standards of medical care in diabetes-2019. *Diabetes care,* 42**:** S46-S60, 2019.
110. England, PH: Government dietary recommendations. *Health Do, editor*, 2016.

111. Williamson, G, Ball, SK: Purification of glutathione S-transferase from lean pork muscle and its reactivity with some lipid oxidation products. *Journal of the Science of Food and Agriculture,* 44**:** 363-374, 1988.
112. Dantas, LS, Viviani, LG, Inague, A, Piccirillo, E, Rezende, L, Ronsein, GE, Augusto, O, Medeiros, MHG, Amaral, ATD, Miyamoto, S: Lipid aldehyde hydrophobicity affects apo-SOD1 modification and aggregation. *Free Radic Biol Med,* 156**:** 157-167, 2020. https://doi.org/10.1016/j.freeradbiomed.2020.05.011
113. Loureiro, AP, de Arruda Campos, IP, Gomes, OF, di Mascio, P, Medeiros, MH: Structural characterization of diastereoisomeric ethano adducts derived from the reaction of 2'-deoxyguanosine with trans,trans-2,4-decadienal. *Chem Res Toxicol,* 17**:** 641-649, 2004. https://doi.org/10.1021/tx034225+
114. Loureiro, AP, de Arruda Campos, IP, Gomes, OF, Possari, EP, Di Mascio, P, Medeiros, MH: Structural characterization of an etheno-2'-deoxyguanosine adduct modified by tetrahydrofuran. *Chem Res Toxicol,* 18**:** 290-299, 2005. https://doi.org/10.1021/tx0497494
115. Loureiro, AP, Di Mascio, P, Gomes, OF, Medeiros, MH: trans,trans-2,4-decadienal-induced 1,N(2)-etheno-2'-deoxyguanosine adduct formation. *Chem Res Toxicol,* 13**:** 601-609, 2000. https://doi.org/10.1021/tx000004h
116. Sigolo, CA, Di Mascio, P, Kowaltowski, AJ, Garcia, CC, Medeiros, MH: trans,trans-2,4-decadienal induces mitochondrial dysfunction and oxidative stress. *J Bioenerg Biomembr,* 40**:** 103-109, 2008. https://doi.org/10.1007/s10863-008-9137-y
117. Sigolo, CA, Di Mascio, P, Medeiros, MH: Covalent modification of cytochrome c exposed to trans,trans-2,4-decadienal. *Chem Res Toxicol,* 20**:** 1099-1110, 2007. https://doi.org/10.1021/tx700111v
118. Young, SC, Chang, LW, Lee, HL, Tsai, LH, Liu, YC, Lin, P: DNA damages induced by trans, trans-2,4-decadienal (tt-DDE), a component of cooking oil fume, in human bronchial epithelial cells. *Environ Mol Mutagen,* 51**:** 315-321, 2010. https://doi.org/10.1002/em.20550
119. Zhu, X, Tang, X, Zhang, J, Tochtrop, GP, Anderson, VE, Sayre, LM: Mass spectrometric evidence for the existence of distinct modifications of different proteins by 2(E),4(E)-decadienal. *Chem Res Toxicol,* 23**:** 467-473, 2010. https://doi.org/10.1021/tx900379a
120. Awoonor-Williams, E, Walsh, AG, Rowley, CN: Modeling covalent-modifier drugs. *Biochim Biophys Acta Proteins Proteom,* 1865**:** 1664-1675, 2017. https://doi.org/10.1016/j.bbapap.2017.05.009
121. Lawrence, MC: Understanding insulin and its receptor from their three-dimensional structures. *Mol Metab,* 52**:** 101255, 2021. https://doi.org/10.1016/j.molmet.2021.101255
122. Haeusler, RA, McGraw, TE, Accili, D: Biochemical and cellular properties of insulin receptor signalling. *Nat Rev Mol Cell Biol,* 19**:** 31-44, 2018. https://doi.org/10.1038/nrm.2017.89
123. Siragusa, M, Oliveira Justo, AF, Malacarne, PF, Strano, A, Buch, A, Withers, B, Peters, KG, Fleming, I: VE-PTP inhibition elicits eNOS phosphorylation to blunt endothelial dysfunction and hypertension in diabetes. *Cardiovasc Res,* 117**:** 1546-1556, 2021. https://doi.org/10.1093/cvr/cvaa213
124. Karademir, Y, Gokmen, V, Oztop, HM: Investigation of lipid-derived formation of decadien-1-amine, 2-pentylpyridine, and acrylamide in potato chips fried in repeatedly used sunflower oil. *Food Res Int,* 121**:** 919-925, 2019. https://doi.org/10.1016/j.foodres.2019.01.020
125. Klein, F, Pieber, SM, Ni, H, Stefenelli, G, Bertrand, A, Kilic, D, Pospisilova, V, Temime-Roussel, B, Marchand, N, El Haddad, I, Slowik, JG, Baltensperger, U,

Cao, J, Huang, RJ, Prevot, ASH: Characterization of Gas-Phase Organics Using Proton Transfer Reaction Time-of-Flight Mass Spectrometry: Residential Coal Combustion. *Environ Sci Technol,* 52**:** 2612-2617, 2018. https://doi.org/10.1021/acs.est.7b03960
126. Peng, CY, Lan, CH, Lin, PC, Kuo, YC: Effects of cooking method, cooking oil, and food type on aldehyde emissions in cooking oil fumes. *J Hazard Mater,* 324**:** 160-167, 2017. https://doi.org/10.1016/j.jhazmat.2016.10.045
127. Hamilton, JS, Klett, EL: Linoleic acid and the regulation of glucose homeostasis: A review of the evidence. *Prostaglandins Leukot Essent Fatty Acids,* 175**:** 102366, 2021. https://doi.org/10.1016/j.plefa.2021.102366
128. Jeppesen, C, Schiller, K, Schulze, MB: Omega-3 and omega-6 fatty acids and type 2 diabetes. *Curr Diab Rep,* 13**:** 279-288, 2013. https://doi.org/10.1007/s11892-012-0362-8
129. Centers for Disease, C, Prevention: Decline in deaths from heart disease and stroke--United States, 1900-1999. *MMWR Morb Mortal Wkly Rep,* 48**:** 649-656, 1999.
130. Hales, CM, Carroll, MD, Fryar, CD, Ogden, CL: Prevalence of Obesity and Severe Obesity Among Adults: United States, 2017-2018. *NCHS Data Brief***:** 1-8, 2020.
131. Mousavi, SM, Jalilpiran, Y, Karimi, E, Aune, D, Larijani, B, Mozaffarian, D, Willett, WC, Esmaillzadeh, A: Dietary Intake of Linoleic Acid, Its Concentrations, and the Risk of Type 2 Diabetes: A Systematic Review and Dose-Response Meta-analysis of Prospective Cohort Studies. *Diabetes Care,* 44**:** 2173-2181, 2021. https://doi.org/10.2337/dc21-0438
132. Wu, JHY, Marklund, M, Imamura, F, Tintle, N, Ardisson Korat, AV, de Goede, J, Zhou, X, Yang, WS, de Oliveira Otto, MC, Kroger, J, Qureshi, W, Virtanen, JK, Bassett, JK, Frazier-Wood, AC, Lankinen, M, Murphy, RA, Rajaobelina, K, Del Gobbo, LC, Forouhi, NG, Luben, R, Khaw, KT, Wareham, N, Kalsbeek, A, Veenstra, J, Luo, J, Hu, FB, Lin, HJ, Siscovick, DS, Boeing, H, Chen, TA, Steffen, B, Steffen, LM, Hodge, A, Eriksdottir, G, Smith, AV, Gudnason, V, Harris, TB, Brouwer, IA, Berr, C, Helmer, C, Samieri, C, Laakso, M, Tsai, MY, Giles, GG, Nurmi, T, Wagenknecht, L, Schulze, MB, Lemaitre, RN, Chien, KL, Soedamah-Muthu, SS, Geleijnse, JM, Sun, Q, Harris, WS, Lind, L, Arnlov, J, Riserus, U, Micha, R, Mozaffarian, D, Cohorts for, H, Aging Research in Genomic Epidemiology Fatty, A, Outcomes Research, C: Omega-6 fatty acid biomarkers and incident type 2 diabetes: pooled analysis of individual-level data for 39 740 adults from 20 prospective cohort studies. *Lancet Diabetes Endocrinol,* 5**:** 965-974, 2017. https://doi.org/10.1016/S2213-8587(17)30307-8
133. Muhlhausler, BS, Ailhaud, GP: Omega-6 polyunsaturated fatty acids and the early origins of obesity. *Curr Opin Endocrinol Diabetes Obes,* 20**:** 56-61, 2013. https://doi.org/10.1097/MED.0b013e32835c1ba7
134. Weir, NL, Nomura, SO, Steffen, BT, Guan, W, Karger, AB, Klein, R, Klein, BEK, Cotch, MF, Tsai, MY: Associations between omega-6 polyunsaturated fatty acids, hyperinsulinemia and incident diabetes by race/ethnicity: The Multi-Ethnic Study of Atherosclerosis. *Clin Nutr,* 39**:** 3031-3041, 2020. https://doi.org/10.1016/j.clnu.2020.01.003
135. Priyadharshini Christy, J, George Priya Doss, C: Single amino acid polymorphism in aldehyde dehydrogenase gene superfamily. *Front Biosci (Landmark Ed),* 20**:** 335-376, 2015. https://doi.org/10.2741/4313
136. Behl, T, Gupta, A, Chigurupati, S, Singh, S, Sehgal, A, Badavath, VN, Alhowail, A, Mani, V, Bhatia, S, Al-Harrasi, A, Bungau, S: Natural and Synthetic Agents Targeting Reactive Carbonyl Species against Metabolic Syndrome. *Molecules,* 27, 2022. https://doi.org/10.3390/molecules27051583

137. Slatter, DA, Bolton, CH, Bailey, AJ: The importance of lipid-derived malondialdehyde in diabetes mellitus. *Diabetologia,* 43**:** 550-557, 2000. https://doi.org/10.1007/s001250051342
138. Tsukahara, H, Sekine, K, Uchiyama, M, Kawakami, H, Hata, I, Todoroki, Y, Hiraoka, M, Kaji, M, Yorifuji, T, Momoi, T, Yoshihara, K, Beppu, M, Mayumi, M: Formation of advanced glycosylation end products and oxidative stress in young patients with type 1 diabetes. *Pediatr Res,* 54**:** 419-424, 2003. https://doi.org/10.1203/01.PDR.0000076662.72100.74
139. Daimon, M, Sugiyama, K, Kameda, W, Saitoh, T, Oizumi, T, Hirata, A, Yamaguchi, H, Ohnuma, H, Igarashi, M, Kato, T: Increased urinary levels of pentosidine, pyrraline and acrolein adduct in type 2 diabetes. *Endocr J,* 50**:** 61-67, 2003. https://doi.org/10.1507/endocrj.50.61

7. CURRICULUM VITAE

Personal Information

Name:	Xin Qian
Date of birth:	18.03.1994
Place of birth:	Jiangsu province, China

University Education

09.2012-06.2017	Bachelor of Medicine, Tongji Medical school, Huazhong University of Science and Technology, Wuhan, China
09.2017-06.2020	Master of Surgery, Medical School, Shanghai Jiao Tong University, Shanghai, China
11-2020-Present	Medical Faculty Mannheim, Heidelberg University, Germany

8. ACKNOWLEGEMENT

I extend my heartfelt gratitude to all those who played a pivotal role in the successful completion of this endeavor.

Foremost, my profound appreciation goes to Prof. Dr. Jens Kroll, my esteemed supervisor, who facilitated the realization of my MD/Dr.med study. His unwavering guidance, unwavering encouragement, and invaluable advice have been instrumental throughout my research journey.

I would also like to convey my sincerest thanks to the entire Kroll-Lab team, who have been my companions and pillars of support over the past years. My gratitude extends to Katrin Bennewitz, Dr. Bowen Lou, Dr. Haozhe Qi, Dr. Mike Boger, Dr.David Wohlfart, Huehn Bjoern, Shu Li, and all other individuals who have contributed to the vitality of the laboratory. Your contributions have been truly indispensable.

I am grateful to Dr. Gernot Poschet, Dr. Michael Buettner, Dr. Carsten Sticht, Dr. Thomas Flemming, Dr. Jakob Morgenstern, Dr. Ingrid Hausser, Dr. Stephan Klatt, Prof. Dr. Peter Paul Nawroth, Prof. Dr. Ingrid Fleming, Prof. Dr. Julia Szendroedi, and Live Cell Imaging Mannheim for their unwavering technical support, exceptional guidance, and seamless collaboration.

I also acknowledge with gratitude the support extended by CRC 1118, project 517361638, Deutsche Forschungsgemeinschaft (grant ZUK 40/2010–3009262) and the China Scholarship Council (CSC).

Finally, I would like to thank my friends and family, whose support has been irreplaceable over the past few years.